Reports on Progress in Physics

REVIEW

Hydrodynamic quantum analogs

To cite this article: John W M Bush and Anand U Oza 2021 *Rep. Prog. Phys.* **84** 017001

IOP Publishing Reports on Progress in Physics
Rep. Prog. Phys. **84** (2020) 017001 (41pp) https://doi.org/10.1088/1361-6633/abc22c

Review

Hydrodynamic quantum analogs

John W M Bush[1,*] **and Anand U Oza**[2]

[1] Department of Mathematics, Massachusetts Institute of Technology, Cambridge, MA, United States of America
[2] Department of Mathematical Sciences, New Jersey Institute of Technology, Newark, NJ, United States of America

E-mail: bush@math.mit.edu

Received 29 June 2020, revised 21 September 2020
Accepted for publication 16 October 2020
Published 21 December 2020

Abstract

The walking droplet system discovered by Yves Couder and Emmanuel Fort presents an example of a vibrating particle self-propelling through a resonant interaction with its own wave field. It provides a means of visualizing a particle as an excitation of a field, a common notion in quantum field theory. Moreover, it represents the first macroscopic realization of a form of dynamics proposed for quantum particles by Louis de Broglie in the 1920s. The fact that this hydrodynamic pilot-wave system exhibits many features typically associated with the microscopic, quantum realm raises a number of intriguing questions. At a minimum, it extends the range of classical systems to include quantum-like statistics in a number of settings. A more optimistic stance is that it suggests the manner in which quantum mechanics might be completed through a theoretical description of particle trajectories. We here review the experimental studies of the walker system, and the hierarchy of theoretical models developed to rationalize its behavior. Particular attention is given to enumerating the dynamical mechanisms responsible for the emergence of robust, structured statistical behavior. Another focus is demonstrating how the temporal nonlocality of the droplet dynamics, as results from the persistence of its pilot wave field, may give rise to behavior that appears to be spatially nonlocal. Finally, we describe recent explorations of a generalized theoretical framework that provides a mathematical bridge between the hydrodynamic pilot-wave system and various realist models of quantum dynamics.

Keywords: walking droplets, pilot-wave dynamics, quantum analogs

(Some figures may appear in colour only in the online journal)

1. Introduction

> 'A man may imagine things that are false, but he can only understand things that are true …'
> – Sir Isaac Newton

Pilot-wave hydrodynamics is the nascent field of study initiated in 2005 by the discovery of Yves Couder and Emmanuel Fort [1, 2] that a millimetric droplet may self-propel along the surface of a vibrating liquid bath through a resonant interaction with its own quasi-monochromatic wave field [3–5]. The compound object comprising the droplet and its guiding or 'pilot' wave is termed a walker (figure 1). Hydrodynamic quantum analogs is the subject dedicated to exploring the ability of this hydrodynamic pilot-wave system and related dynamical systems to exhibit behavior analogous to that arising in quantum systems. The walking-droplet system has led to hydrodynamic analogs of various microscopic quantum systems, to varying degrees of success, including tunneling [6–9], the quantum corral [10–14], the quantum mirage [13], Landau levels [15–17], Friedel oscillations [18], diffraction

* Author to whom any correspondence should be addressed.
'Corresponding Editor Professor Masud Mansuripur'

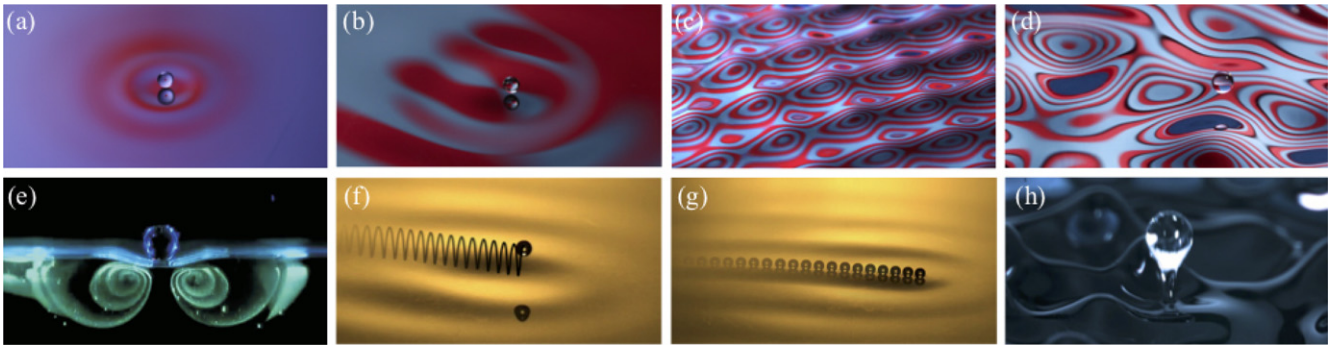

Figure 1. Image gallery. (a) A bouncing drop. (b) A walker. (c) Faraday waves apparent just above the Faraday threshold. (d) A droplet moves unpredictably on a bath forced above the Faraday threshold. (e) The subsurface vortical flow generated by a bouncing drop. (f) A walking droplet, with its trajectory indicated by the black line. (g) A strobed image of a walker surfing its pilot wave. (h) Well above the Faraday threshold, Faraday waves break, generating droplets. (a), (d) Reproduced from [159]. CC BY 3.0. (b), (c) Reprinted by permission from Springer Nature Customer Service Centre GmbH: Journal of Visualization. [161] © 2017. (e) Reprinted figure by permission from [61], Copyright (2014) by the American Physical Society. (f), (g) Reproduced with permission from [4].

from slits [2, 19–25], spin states [17, 26, 27], Zeeman splitting [27, 28], the quantum harmonic oscillator [26, 29–35], and the Hong–Ou–Mandel effect [36]. Assemblages of bouncing droplets have been shown to exhibit features characteristic of the microscopic realm, including quantized static and dynamic bound states [28, 37–50], crystal vibrations [51–53] and spin–spin correlations [54, 55]. Hydrodynamic analogs of various optical systems have also been explored with the walking-droplet system, including optical waveguides [56], Bragg scattering [57], optical ratcheting [58] and particle trapping with the Talbot effect [59, 60]. The walking-droplet system has suggested classical reinterpretations of a number of traditionally beguiling quantum notions, including wave–particle duality, wave function collapse, superposition of states, statistical projection effects, single-particle diffraction and interference, nonlocality, uncertainty and entanglement.

When successful, hydrodynamic quantum analogs provide a means of understanding emergent quantum phenomena from a classical, trajectory-based perspective. When unsuccessful, they demarcate the limits of the hydrodynamic system as a quantum analog, and suggest new directions to explore theoretically from a more general pilot-wave framework. The subject thus offers a mechanism for distinguishing between what can and cannot be understood about quantum systems from a classical perspective. In a field whose most distinguished practitioners have been known to glory in the inscrutability of their subject (for example, Feynman's dictum 'Nobody understands quantum mechanics'), this progressive approach should represent a welcomed change. The implications of the field of hydrodynamic quantum analogs for the state of quantum foundations has been the source of speculation among both physicists and philosophers [62–71].

Laplacian determinism postulates that, given the initial conditions and governing laws of a physical system, one can predict its evolution indefinitely. This simple state of affairs is lost for hereditary systems [72, 73], systems with 'memory', whose dynamics are non-local in time, with their evolution depending explicitly on their past. Locality is a feature of a physical theory of particle motion if the particle feels only forces acting locally upon it. Temporal locality requires that a body respond only to forces acting instantaneously upon it, while spatial locality forbids action at a distance. The apparent action at a distance implied by Coulomb's law of electrostatics was reconciled through the realization that the forces so defined are mediated by electromagnetic waves that propagate no faster than the speed of light. Pilot-wave hydrodynamics explores the possibility that the spatial nonlocality of quantum mechanics might likewise be rooted in a currently unresolved wave dynamics, that quantum non-locality might be a manifestation of spatially local hereditary pilot-wave dynamics.

Particle-wave interactions are common on the macroscopic scale. Familiar examples include a buoy floating on the surface of the sea, and a grain of sand moving in response to elastic waves induced on a Chladni plate [74]. In both, the particles move primarily in response to imposed waves rather than waves of their own creation. Conversely, in the hydrodynamic pilot-wave system, drop motion is driven entirely by the bouncing drop's interaction with its own wave field (figure 1). If the droplet were not present, there would be no pilot wave; if there were no pilot-wave, there would be no lateral drop motion. Identifying the droplet as a self-propelling wave source [40] differentiates the walker system from the great majority of classical wave–particle systems.

A key feature of the walking droplet system is that of 'path-memory' [15, 75]. At each impact, the drop responds to the wave field generated by some number of its previous bounces, the precise number being determined by the longevity of its pilot-wave field. The bath thus serves as the memory of the system, storing the information of the walker's past, specifically its path and its environment, in its wave field. The more persistent the waves generated by the bouncing drop, the longer the memory. The feature of path-memory is apparent in virtually all of the theoretical models developed to describe the walking droplets [76]. Specifically, there is a propulsive wave force proportional to the slope of the local wave field whose form must be deduced by integrating backwards in time in order to account for all the waves generated along the walker's path. The path memory renders the drop motion non-Markovian, its dynamics hereditary. Of course, the walker system is local in both space and time: the instantaneous force acting on the drop

is determined by the local form of its pilot-wave, and the pilot-wave field evolves in time through a local partial differential equation. However, the influence of its wave field renders the *droplet dynamics* non-local in time: the wave force depends on the droplet's history. This temporal non-locality in the drop dynamics can give rise to behavior that appears to be non-local in space. Several examples of the possible misinference of spatial nonlocality in the walker system will be reviewed in what follows.

The other critical ingredient for the emergent quantum-like behavior is resonance between the walker's bouncing motion and its wave field. The combination of the bath vibration and this resonance leads to a highly structured, quasi-monochromatic wave field that imposes a dynamic constraint on the walking droplet. The three established paradigms for the emergence of quantized dynamical states and quantum-like statistics from pilot-wave hydrodynamics, to be detailed in what follows and summarized in section 10.1, are all firmly rooted in the quasi-monochromatic form of the droplet's pilot wave.

The hydrodynamic pilot-wave system is a particular case of a more general classical pilot-wave dynamics, theoretical explorations of which have extended the range of quantum analogs, as reviewed in section 9. Such a generalized pilot-wave framework also provides a means of comparing pilot-wave hydrodynamics with its quantum predecessors, including de Broglie's double-solution pilot-wave theory [68, 77–80], Bohmian mechanics [81, 82], stochastic dynamics [70, 83, 84], and stochastic electrodynamics [85, 86]. It has also lead to the first tentative walker-inspired attempts to formulate a trajectory-based quantum mechanics [20, 70, 87–89].

Before proceeding, it is appropriate to define the limited scope of this review. Hydrodynamics has been a rich source of metaphor and physical analogy for microscopic physics [4], from Newton's description of photons as stones skipping through the ether [90] to Lord Kelvin's description of microscopic particles as vortical knots in the ether [91]. The walking-droplet system has a significant number of precursors in terms of hydrodynamic quantum analogs. These include Thomas Young's use of ripple-tank experiments to demonstrate the wave nature of light [92], hydrodynamic analogs of the Aharanov–Bohm [93] and Casimir [94] effects, and a classification of droplet vibration in terms of a dynamic periodic table [95]. The specific goal of this report is to review work done on the walking-droplet system since its discovery, and to outline its intriguing connections to existing realist models of quantum dynamics.

By way of providing both motivation and historical context, in section 2 we discuss the quantum predecessors of the hydrodynamic pilot-wave system. In section 3, we provide a brief overview of the walking-droplet system, and in section 4 detail the hierarchy of theoretical models developed to describe it. In section 5, we review experimental and theoretical studies of static and dynamic bound states formed from the interactions of multiple bouncing droplets. We devote section 6 to a review of orbital pilot-wave dynamics, as may arise when the walking droplet is subjected to an external force. In section 7, we review studies of walker motion in a confined corral geometry. More general walker-boundary interactions, including scattering and diffraction, are treated in section 8. Finally, in section 9 we review the explorations of a generalized pilot-wave framework in which the common features of de Broglie's quantum dynamics and the walking-droplet system are retained, but the limitations and shortcomings of both may be side-stepped. A summary is presented in section 10, along with projections for fruitful research directions.

2. Quantum pilot-wave theories

Quantum mechanics is a theory that describes the statistical behavior of microscopic particles. The absence of a satisfactory description of an underlying dynamics has left the field in a state comparable to that of thermodynamics prior to the development of statistical mechanics [96]. Moreover, it has left the door open to the proliferation of quantum interpretations, attempts to comprehend what the theory actually means [97–99]. Such interpretations have run the gamut from mystical to perfectly sensible. According to the Copenhagen interpretation, the statistical description provided by quantum mechanics is complete: there is no underlying physical reality, or notion of quantum particles following trajectories. The insistence on the completeness of the statistical description of quantum systems leads immediately to various difficulties, including superluminal wave-function collapse [100], the confounding notion of complementarity, and the paradox of Schrödinger's cat. The philosophical extravagance of the Copenhagen interpretation opened the door to equally untestable rivals, notable among them being the Many-Worlds interpretation [101], according to which the universe branches into copies of itself in response to any decoherence event such as the act of human observation.

Following the preeminence of the Copenhagen interpretation, a number of relatively commonsensical perspectives have emerged, and are evidently gaining ground. According to the statistical [102] or ensemble interpretation [103], quantum mechanics describes the statistical evolution of an ensemble of similarly prepared states. Consistent histories [104] dispenses with many of the difficulties of other interpretations, including wave function collapse and non-locality, and ensures a framework in which classical rules of probability are satisfied by formulating a self-consistent history of the system evolution. While undoubtedly improvements over their comparatively immoderate predecessors, these perspectives remain but interpretations, providing no physical picture as to what form the underlying quantum dynamics might take.

Virtually all attempts to envisage a realist quantum dynamics have involved particles interacting with a background field, either a coherent pilot wave as proposed by de Broglie [77–79] and Bohm [81, 82], or a stochastic vacuum field as posited in stochastic dynamics [83, 84] and stochastic electrodynamics [85, 86]. As we shall see, experimental and theoretical modeling of pilot-wave hydrodynamics has, in various parameter regimes, captured certain features of all such theories. Since these theories of quantum dynamics have yet to be satisfactorily completed, they remain classified as interpretations. However, it is worth noting that, if successful in providing a

dynamical picture that is consistent with the statistical predictions of standard quantum mechanics in all settings, they will leave no room for interpretation.

2.1. For whom the Bell does not toll

It is widely believed that the work of John Bell, specifically the derivation of Bell's inequality [105] and the experimental violation thereof [106–109], sounds the death knell for hidden variable theories. A more defensible inference is that experimental violation of Bell's inequality requires that any hidden variable theory be nonlocal in the quantum sense [110]. Morgan [111] and Vervoort [66, 67] assert that Bell's inequalities have no bearing on hidden-variable theories in which particles interact through a background wave field. Bell himself, who derived his inequality, then saw it violated by the experiments of Aspect [106–108], came to the conclusion that there must be a pilot-wave dynamics underlying quantum statistics [110, 112]. Specifically, he supported the de Broglie–Bohm theory, according to which particles interact with a nonlocal quantum potential [112]. Readers who believe that they understand Bell's work better than Bell himself are invited to revisit his original writings [110], along with a recent account of the systematic misinterpretation thereof [98].

Any theory, hidden variable or otherwise, must answer to the same experimental data. All features of quantum mechanics must be captured by a successful hidden variable theory, including quantum non-locality. In the absence of a hidden variable theory, the quantum non-locality inferred by the quantum correlations measured experimentally [106–108] requires superluminal signaling, 'spooky action at a distance.' A successful theory would provide a rational explanation for such correlations based on the particle dynamics, thereby obviating the need for superluminal signaling.

2.2. The Madelung transformation

The original hydrodynamic interpretation of quantum mechanics follows directly from the Madelung transformation [113], which allows the linear Schrödinger equation (LSE) to be recast in hydrodynamic form. Consider the standard quantum mechanical description of a particle of mass m in the presence of a potential $V(\boldsymbol{x}, t)$. The particle's wave function $\Psi(\boldsymbol{x}, t)$ evolves according to the LSE:

$$i\hbar\Psi_t = \left(-\frac{\hbar^2}{2m}\boldsymbol{\nabla}^2 + V\right)\Psi, \tag{1}$$

where $\hbar$ is the reduced Planck's constant. Expressing the wave function in polar form, $\Psi(\boldsymbol{x}, t) = R(\boldsymbol{x}, t)\,\mathrm{e}^{\mathrm{i}S(\boldsymbol{x},t)/\hbar}$, and substituting into (1) yields

$$\frac{D\rho_\mathrm{q}}{Dt} + \rho_\mathrm{q}\boldsymbol{\nabla}\cdot\boldsymbol{v}_\mathrm{q} = 0, \qquad \frac{\partial S}{\partial t} + \frac{1}{2}m\boldsymbol{v}_\mathrm{q}^2 + Q + V = 0, \tag{2}$$

where $\boldsymbol{v}_\mathrm{q}(\boldsymbol{x}, t) = \boldsymbol{\nabla}S(\boldsymbol{x}, t)/m$ is the quantum velocity of probability, $D/Dt = \partial_t + \boldsymbol{v}_\mathrm{q}\cdot\boldsymbol{\nabla}$ the material derivative, $S(\boldsymbol{x}, t)$ the action, $\rho_\mathrm{q}(\boldsymbol{x}, t) = R^2$ the probability density, and $Q(\boldsymbol{x}, t) = -\frac{\hbar^2}{2m}\frac{1}{R}\boldsymbol{\nabla}^2 R$ the quantum potential. The first equation in (2) expresses the conservation of probability. Taking the gradient of the second yields the evolution equation for the quantum velocity of probability $\boldsymbol{v}_\mathrm{q}$:

$$m\frac{D\boldsymbol{v}_\mathrm{q}}{Dt} = -\boldsymbol{\nabla}Q - \boldsymbol{\nabla}V. \tag{3}$$

From the perspective of the fluid mechanician, the Madelung formulation [113] has two attractive features [114]. First, it consigns Planck's constant $\hbar$ to a single term, the coefficient on the quantum potential. Second, the system corresponds to that describing the evolution of a shallow, inviscid fluid layer if one associates ρ_q with the fluid depth, and $\boldsymbol{v}_\mathrm{q}$ with the depth-averaged fluid velocity. When Q is linearized about a state of uniform ρ_q, it assumes the form of the surface-tension-induced curvature pressure in shallow-water hydrodynamics [115]. One thus sees the first tentative relation between the roles of $\hbar$ in quantum statistics and surface tension σ in hydrodynamics, a relation that has been deepened by a comparison between the walker system and de Broglie's physical picture [3] (see section 2.4).

The hydrodynamic formulation that follows from the Madelung transformation is the standard approach to describing a number of quantum systems, including Bose–Einstein condensates [116]. As it represents no more than a mathematical reformulation of the Schrödinger equation, it adds no new physics, only a means of interpreting the evolution of the statistics of a quantum system in terms of fluid flow. The walking-droplet system suggests a much richer hydrodynamic interpretation of quantum mechanics, a physical picture replete with the notion of particles generating waves and moving in response to them [3–5], a dynamics evocative of de Broglie's original pilot-wave theory (see section 2.4).

2.3. Bohmian mechanics

Bohmian mechanics [81, 82] was formulated by David Bohm in 1952 in an attempt to reintroduce the notion of particle trajectory to quantum mechanics. It is briefly reviewed here in order to distinguish it from the relatively rich double-solution pilot-wave theory of de Broglie, which the walking droplet system more closely resembles [3, 117]. Unlike de Broglie's mechanics, Bohmian mechanics was not rooted in relativity: its starting point was the linear Schrödinger equation (1). The basic assertion of Bohmian mechanics is that the particle velocity $\dot{\boldsymbol{x}}_\mathrm{p}$ is identical to the quantum velocity of probability $\boldsymbol{v}_\mathrm{q}$; consequently, the trajectory of the particle is prescribed by equation (3). The particle thus moves in response to the classical and quantum potentials. Notably, Bohmian mechanics posits no mechanism for wave generation. The only wave in Bohmian mechanics is the wavefunction of the standard quantum formulation, as necessarily satisfies Schrödinger's equation (1) and prescribes the statistical behavior of the system.

Bohmian mechanics immediately drew criticism from several circles, a common objection being to the nonlocal form of the quantum potential [118]. In response to these criticisms, Bohm and Vigier [119] invoked a stochastic background field. They then viewed the Bohmian trajectories as streamlines in a gas flow, but imagined that the real particles would stray from

these streamlines in response to stochastic fluctuations, just as dust particles in an air flow stray from streamlines in response to Brownian motion [3, 117].

Particle diffraction from slits is treated in Bohmian mechanics by solving Schrödinger's equation for the wavefunction, from which the form of the quantum potential is calculated. The Bohmian particle paths are then computed via (3) using an ensemble of initial conditions corresponding to a Gaussian beam. Philippidis [120] thus deduced a self-consistent result, specifically, particle paths consistent with the wavefunction used to derive them. Recent advances in weak measurement have reported that mean particle paths in the single and double slit experiments are consistent with the predictions of Bohmian mechanics [121]. Given that Bohmian mechanics can be seen as a dynamical reformulation of a statistical theory, it would seem optimistic to imagine that it might describe anything more than a mean dynamics. Of course, a description of the mean dynamics is an improvement over no description at all; thus, Bohmian mechanics has found wide application in both optics [122] and physical chemistry [123, 124]. Moreover, as noted by Bell [110, 112], workers in Bohmian mechanics [71, 96, 125–128] have provided a valuable perspective that has acted to counter the prevailing complacency surrounding the meaning of quantum mechanics.

The walking droplet system demonstrates how quantum-like statistics may, in certain circumstances, emerge from classical pilot-wave dynamics. It is significantly richer than Bohmian mechanics, replete with a mechanism for particle-induced wave generation, and with a real, particle-centered wave to complement the statistical wave form. While these added complexities of the walker system make it a more challenging dynamical system to analyze, it allows one to see the manner in which one might circumvent the difficulties inherent in Bohmian mechanics, namely the need to invoke a nonlocal quantum potential and a stochastic background field. The manner in which the hydrodynamic pilot-wave system does so is evocative of a predecessor of Bohmian mechanics, de Broglie's double-solution pilot-wave theory.

2.4. de Broglie's matter waves

de Broglie's double-solution pilot-wave program [77–80, 129, 130] was an attempt to reconcile quantum mechanics with relativity [68]. His basic premise was that there are two things in the Universe, light and matter. Since light was then known to have both wave and particle natures, he proposed that so too must matter, hence de Broglie's matter waves. He posited that particles have an internal vibration, and move in concert with their matter waves. On the basis of his physical picture, de Broglie predicted electron diffraction, the experimental confirmation of which [131, 132] earned him the Nobel Prize in physics in 1929.

Relativity requires that a particle of rest mass m_0 have energy $E = m_0c^2$, while quantum mechanics requires that $E = \hbar\omega$. Equating these two equations, referred to by Wilczek [133] as a 'poem in two lines', yields the Einstein–de Broglie relation, $m_0c^2 = \hbar\omega$, as defines the Compton frequency, $\omega_c = m_0c^2/\hbar$. According to de Broglie, quantum particles are oscillators exchanging their rest mass energy m_0c^2 with field energy $\hbar\omega$ at the Compton frequency. In a manner left unspecified by de Broglie, the particle vibration generates a pilot wave with the de Broglie wavelength λ_B that guides the particle. The synchrony of the particle's internal oscillation with its pilot wave in all reference frames, as follows from relativistic considerations [68, 88], was referred to by de Broglie as the 'harmony of phases', and considered to be a key feature of his pilot-wave mechanics, '*une grand loi de la nature*' [134]. Notably, synchrony between the droplet and its pilot wave is also critical to the emergent quantum-like behavior of the hydrodynamic pilot-wave system.

de Broglie envisioned a quantum particle as having an internal vibration, with the Compton frequency, that creates a pilot-wave field satisfying the Klein–Gordon equation [130, 135],

$$\phi_{tt} - c^2\Delta\phi + \omega_c^2\phi = 0. \tag{4}$$

The particle thus excites a field of monochromatic waves and moves in response to the gradient of the wave phase (see table 3). The de Broglie wavelength, $\lambda_B = 2\pi/k_B$, represents the wavelength of the monochromatic wave form whose group speed corresponds to the particle speed: $\frac{d\omega}{dk}(k_B) = v$. The de Broglie relation $p = \gamma_L m_0 v = \hbar k_B$, where $\gamma_L = \left[1 - (v/c)^2\right]^{-1/2}$ is the Lorentz factor, follows directly from the dispersion relation of the Klein–Gordon equation: $\omega^2 = \omega_c^2 + k^2c^2$. The resulting physical picture is that of a particle being propelled by a monochromatic wave form that dresses the particle, an image manifest in the walking droplet system.

While there are similarities between de Broglie's conception and the hydrodynamic pilot-wave system, there are also a number of qualitative differences. First and foremost, de Broglie did not specify the manner in which the particle vibration generates the wave: equation (4) is unforced. Second, the Klein–Gordon equation is undamped, while the waves accompanying the walking drop are damped by viscous effects. Third, de Broglie's trajectory equation posits that the particle responds to gradients in the phase of its pilot-wave field: particle inertia plays no role. As we shall see in what follows, there is accumulating evidence that the low-drop-inertia, undamped wave limit is that in which the quantum-like behavior of the walking droplets is most pronounced.

De Broglie's greatest obstacle was identifying the form of his pilot wave ϕ. While he asserted that the particle vibration was responsible for wave generation, he did not express mathematically the manner in which this generation arose. He stated that the pilot wave satisfied the Klein–Gordon equation (4), but did not demonstrate the manner in which a particle vibrating at the Compton frequency would generate such a waves, or the form that it would take. Several possibilities were thus explored. First, he assumed that ϕ was monochromatic, from which $p = \hbar k_B$ follows directly from his trajectory equation (table 3). Following the work of Bohm [81, 82], he proposed that ϕ took the same form as the Ψ wave of equation (1), apart from a nonlinearity in the vicinity of the particle [80, 130]. With this concession, $\Psi \propto \phi$, de Broglie's double-solution theory effectively merges with Bohmian mechanics, hence the

so-called de Broglie–Bohm pilot-wave theory, which is effectively Bohmian mechanics [136]. The hydrodynamic pilot-wave system presents an example where the instantaneous pilot wave differs substantially from the emergent statistical form [10, 13], which is more in line with de Broglie's original conception [3, 117]. A recent attempt to extend de Broglie's double-solution mathematical program, informed by the walking-droplet system [88, 89], will be described in section 9.3.

de Broglie presented an early form of his theory at the Solvay conference of 1927, but drew criticism from several circles, and his theory was not thereafter widely accepted [137]. Indeed, de Broglie himself abandoned it for a time before returning to it following the work of Bohm [81, 82]. Nevertheless, it provided a number of the cornerstones of quantum theory. In addition to inspiring the de Broglie relation, $p = \hbar k_{\mathrm{B}}$, and the Einstein–de Broglie relation, $m_0 c^2 = \hbar\omega$, his physical picture suggested that many of the quantum mysteries may be rooted in an unresolved dynamics on the Compton scale, the scale of particle vibration [138]. His physical picture inspired Schrödinger to develop both the Klein–Gordon and Schrödinger equations in order to describe the pilot wave [139]. Subsequently, these wave equations were adopted to describe the wavefunction, and so only the statistical behavior of quantum systems, a development to which Schrödinger himself objected [140]. The physical picture that had inspired the development of the principal governing equations of quantum mechanics was thus abandoned in favor of …no physical picture.

Compelling as de Broglie's double-solution theory may seem in light of a number of the alternatives, it was never completed. In particular, because the generation mechanism and form of the pilot-wave field ϕ were not specified, it was not possible to demonstrate that the proposed pilot-wave dynamics would give rise to statistical behavior described by the Ψ wave. Furthermore, the physical origin of the pilot wave field was not specified. In his later works, de Broglie [80] sought its origins in a stochastic background field, the modern equivalent of which would be the quantum vacuum [141]. While the electromagnetic vacuum field has been most thoroughly investigated as a potential pilot-wave field [85, 86], other possibilities exist. Notably, the wave equation (4) considered by de Broglie is precisely that describing the Higgs field [88].

Before proceeding, it is worth enumerating the many lines of evidence supporting de Broglie's proposal of associating a quantum particle with a high frequency oscillation at the Compton frequency ω_{c}. First, it is required from dimensional analysis if one assumes that the relevant fundamental constants are $\hbar$, c and m_0. Second, it provides the means by which to connect solutions ϕ of the Klein–Gordon equation (4) to solutions Ψ of the linear Schrödinger equation (1). Specifically, if $\phi(\boldsymbol{x}, t) = \Psi(\boldsymbol{x}, t)\mathrm{e}^{\mathrm{i}\omega_{\mathrm{c}} t}$ is a solution of the Klein–Gordon equation, then $\Psi(\boldsymbol{x}, t)$ satisfies the LSE provided the particle speed $v \ll c$ [142]. Zitterbewegung was a feature of early models of quantum theory taken to indicate a high-frequency jitter of microscopic particles at ω_{c} [143]. The classical model of the electron is that of a charge orbiting the Compton radius, $\lambda_{\mathrm{c}} = h/(mc)$ at the Compton frequency [144]. Particle vibration at ω_{c} plays a critical role in both Hestenes' Zitterbewegung interpretation of quantum mechanics [145] and in stochastic electrodynamics [85, 86]. Notably, Compton frequencies are not yet observable experimentally for most particles; for example, the Zitter frequency of the electron is $1.6 \times 10^{21}\ \mathrm{s}^{-1}$. Nevertheless, some evidence of Zitterbewegung has recently been reported in Bose–Einstein condensates [146] and trapped ion systems [147].

2.5. Stochastic dynamics

While the pilot-wave theories of de Broglie and Bohm rely on a particle being guided by a coherent wave form, either the Ψ wave in Bohm's mechanics or the unspecified ϕ wave in de Broglie's, stochastic dynamics posits that microscopic particles are propelled by a stochastic background field associated with the quantum vacuum. Nelson [83, 84] introduced the stochastic interpretation of quantum mechanics. Starting with the linear Schrödinger equation (1), he argued that the evolution of the quantum statistics of a microscopic particle of mass m may be understood in terms of a diffusive process characterized by diffusivity $\hbar/(2m)$. If one asserts that a microscopic particle has momentum $p = \hbar k_{\mathrm{B}}$, then this diffusivity may be reexpressed as $D \sim v\lambda_{\mathrm{B}}$, as one expects to arise from a random walk of a particle with mean speed v and step length λ_{B}. As will be seen in what follows, similar random walks have been found in a number of theoretical models of pilot-wave hydrodynamics.

A modern extension of de Broglie's double-solution pilot-wave theory has emerged from the field of stochastic electrodynamics, according to which the pilot wave is electromagnetic in origin [86]. A number of lines of evidence suggest that, even at zero Kelvin, there is electromagnetic energy in the quantum vacuum field [141]. Consistency with the requirement of Lorentz invariance and experiments on the Casimir effect indicates that this zero-point field has a particular spectral form: the vacuum mode with frequency ω has energy $U(\omega) = \hbar\omega/2$ [148]. Notably, the quantum vacuum thus provides a natural means by which to introduce Planck's constant $\hbar$ into a classical theory. The successes and limitations of stochastic electrodynamics in rationalizing quantum phenomena have been recently reviewed by Boyer [149].

In de la Peña and Cetto's conception of stochastic electrodynamics [85, 86], the stochastic background field excites the vibration of the particle at its natural frequency. The particle then interacts with resonant vacuum modes: the resulting pilot-wave is thus an electromagnetic wave with the Compton frequency and Compton wavelength in the particle frame of reference. The de Broglie wave arises due to the particle motion [86], and represents the envelope of this Doppler-shifted, Lorentz-transformed pilot wave [85]. As posited, stochastic electrodynamics provides alternative rationale for a number of quantum phenomena [150–152], but its ability to capture diffraction from slits has been questioned [153, 154]. The relation between stochastic dynamics and stochastic electrodynamics has recently been reviewed by de la Peña *et al* [155].

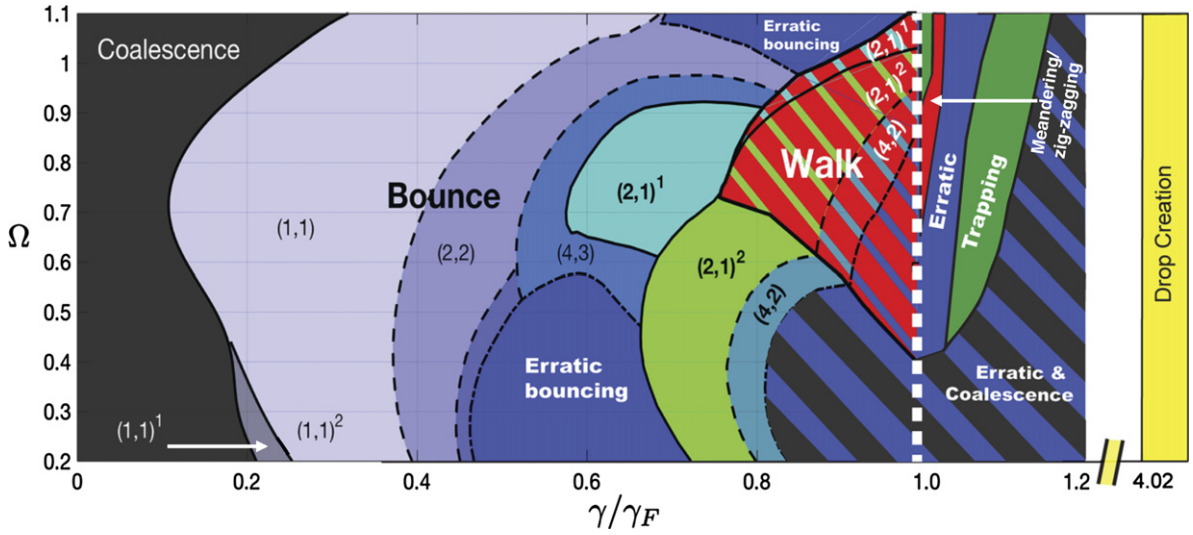

Figure 2. Regime diagram indicating the dependence of the drop's bouncing behavior on the dimensionless vibrational acceleration of the bath, γ/γ_F, and vibration number, $\Omega = \omega/\sqrt{\sigma/\rho a^3}$, for a bath with viscosity 20 cS driven at $\omega/(2\pi) = 80$ Hz. Drop dynamics both below [156] and above [157] the Faraday threshold, $\gamma/\gamma_F = 1$, are shown. Reprinted from [157], with the permission of AIP Publishing.

3. The walking droplet system

The hydrodynamic pilot-wave system consists of a millimetric drop placed on the surface of a vibrating liquid bath (figure 1). The walking droplet system is visually striking, its aesthetic appeal evident even with a simple classroom demonstration [158–161]. Quantitative experiments are typically performed on a fluid bath of silicone oil with viscosity between 20 and 100 cS vibrating at 20–100 Hz. While all are based on the original design of Couder and Fort's experiments [2, 38, 162], a number of refinements have improved precision and repeatability [25, 49, 163–165]. The drop behavior is known to depend critically on both drop size and driving acceleration [38, 41, 156, 166–168]; consequently, the generation of reproducible data requires precise control of both. Based on the drop-generator designs of Terwagne *et al* [169] and Yang *et al* [170], Harris *et al* [165, 171] thus developed a device to produce uniform droplets with diameters ranging from 0.5 to 1.4 mm (accurate to $\pm 1\%$). A number of experiments have indicated the importance of isolating the walkers from air currents with a lid [13, 23]. This requirement has prompted the development of launchers that allow for the experiments to run continuously, even with a lid [18, 23, 45, 46, 172]. Most recently, Ellegaard and Levinsen [25] achieved temperature control of the bath, thereby eliminating spurious effects associated with drift of the ambient room temperature.

3.1. Faraday waves

Consider a horizontal liquid bath of depth H, density ρ, surface tension σ and kinematic viscosity ν subjected to a vertical vibration of amplitude A_0, frequency ω and acceleration $\gamma \sin \omega t$ (where $\gamma = A_0\omega^2$), in the presence of a gravitational acceleration g. Faraday waves [173] develop on the surface when a critical vibrational acceleration, the Faraday threshold γ_F, is exceeded [174–176] (figure 1(c)). The system vibration has the feature of naturally imposing a quantization on the resulting waves; specifically, the Faraday waves always have an oscillation frequency that is an integer multiple of $\omega/2$. In all cases considered to date in the context of pilot-wave hydrodynamics, the most unstable mode is subharmonic, with half the frequency of the bath's vibrational forcing. The wavelength λ_F of the resulting Faraday wave field is then prescribed by the water-wave dispersion relation, which relates the Faraday wavenumber $k_F = 2\pi/\lambda_F$ to the frequency of vibrational forcing ω and the wave frequency ω_w:

$$(\omega/2)^2 = \omega_w^2(k_F) \equiv \left(gk_F + \frac{\sigma k_F^3}{\rho}\right) \tanh\ k_F H. \qquad (5)$$

The form taken by the Faraday wave field may be influenced by the bounding geometry for small domains, but a square planform is the norm in sufficiently large domains.

Beyond the Faraday instability threshold, $\gamma > \gamma_F$, the Faraday wave system has a number of curious features, including some common to quantum systems and quantum chaos [177]. In certain parameter regimes, the most unstable wave pattern is a mixed state consisting of two distinct wavelengths, the result being a quasi-crystalline wave structure [176, 178]. In the chaotic wave regime arising for $\gamma \gg \gamma_F$, 'scars' emerge [179, 180], corresponding to regions of anomalous wave energy. Scars are also prominent features of quantum billiards, which describe the wavefunction of a particle confined to a domain and colliding perfectly elastically against the domain's boundary [181]. Finally, there is a critical vibrational acceleration $\gamma_R \sim (\sigma/\rho)^{1/3}\omega^{4/3}$ above which the vibration prompts interfacial fracture: surface tension is incapable of stabilizing the wave, whose crests pinch off into drops with size comparable to λ_F (figure 1(h)) [182, 183].

3.2. Bouncing and walking drops

A fluid drop of radius a, density ρ, mass $m = 4\pi a^3\rho/3$ and surface tension σ is an oscillator with a natural frequency $\omega_d \sim \sqrt{\sigma/m}$ prescribed by a balance between fluid

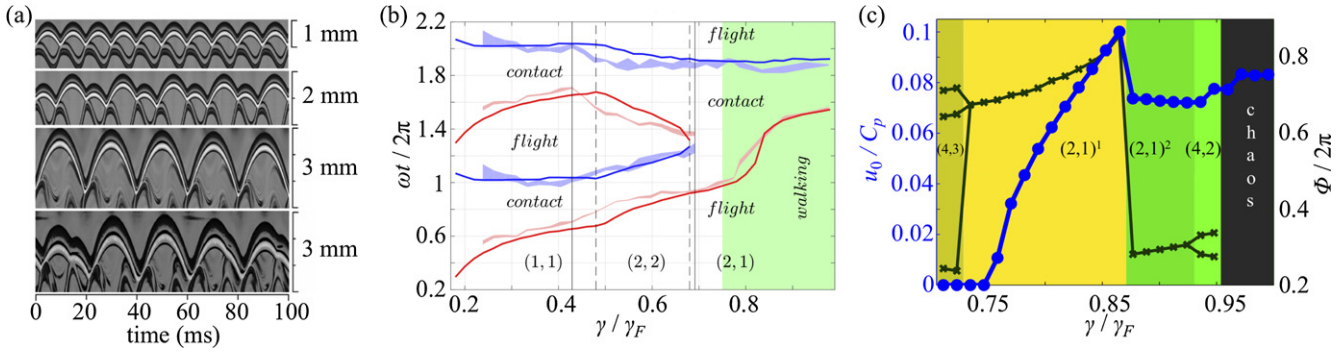

Figure 3. Vertical dynamics of bouncing and walking droplets. (a) Kymographs, deduced by juxtaposing a vertical array of pixels through the droplet's centerline, illustrate the drop's bouncing [167] and walking [156] modes: in order, $(1, 1)$ bouncing, $(2, 2)$ bouncing, $(2, 1)^2$ walking and chaotic walking. (b) Dependence of a bouncing droplet's touch-down (red) and take-off (blue) times on the bath's vibrational acceleration γ/γ_F. The kinematic-match model of the droplet's vertical dynamics (curves) [193] (see section 4.4) is compared with experiments (shaded regions) [194]. The vertical lines indicate the transitions between different bouncing modes in experiment (solid) and simulations (dashed). (c) The dependence of the impact phase Φ (black lines) and horizontal speed u_0 (blue line) on the vibrational forcing γ/γ_F, as predicted by the theoretical model of Milewski *et al* [44] (see section 4.4). The droplet speed u_0 is nondimensionalized by the phase speed, C_p, of a wave with the Faraday wavelength. Background colors denote different bouncing and walking modes. The impact phase necessarily takes multiple values in regimes with more than one impact per bouncing cycle. The abrupt jump in both phase and speed indicates the transition between the $(2, 1)^1$ and $(2, 1)^2$ walking modes. (a) Reproduced with permission from [156, 167]. © Cambridge University Press. (b) Adapted with permission from [193]. © Cambridge University Press. (c) Reproduced with permission from [44]. © Cambridge University Press.

inertia and curvature forces induced by surface tension [184, 185]. When a millimetric fluid drop is placed on the surface of a vibrating bath, it may be levitated on the bath surface, either hovering or bouncing [186]. The criterion for non-coalescence is that the air layer between bath and drop maintain a critical thickness (of order 100 nm) during the course of each impact; otherwise, van der Waals forces acting between the two liquid phases initiate coalescence [162, 187, 188]. When the drop bounces, its distortion into an oblate spheroid during impact increases the surface area of the underlying air film, thereby discouraging coalescence. When the drop bounces at its natural frequency, there is a resonance in the system. Hydrodynamic quantum analogs arise when there is an additional resonance, between the bouncing and the resulting subthreshold Faraday waves. Because the Faraday waves are viscously damped, the system may then be viewed as a damped oscillator forced at its resonant frequency. For a bath of a given viscosity, the longevity of the waves generated by the droplet impact, as determines the system's 'path-memory', increases with the vibrational acceleration. The terms 'memory' and vibrational acceleration are thus used interchangeably henceforth.

The evolution of the bouncing droplet system with increasing vibrational acceleration at a fixed frequency has been characterized experimentally in a number of studies [37, 38, 156, 167, 168, 189]. The system behavior depends on the chosen fluid, as well as the vibrational frequency. The most extensive walking regime arises with the 20 cS–80 Hz combination [41, 156, 168], the behavior of which is summarized in figure 2. The horizontal axis indicates the magnitude of the vibrational acceleration, while the vertical axis indicates the vibration number, $\Omega = \omega/\omega_d = \omega/\sqrt{\sigma/\rho a^3}$, which indicates the relative magnitudes of the bath's vibrational frequency and the drop's natural frequency, and serves as a proxy for drop size [167, 190, 191]. Different periodicities are evident in the vertical dynamics of both bouncing and walking states. In the bouncing mode $(i, j)^p$, a droplet bounces j times over i vibration periods [167, 192]. The subscript p orders different modes with the same bouncing periodicity according to their mechanical energies, with large p denoting bouncers with larger bouncing amplitude.

Consider a drop of radius $a = 0.4$ mm, and viscosity $\nu = 20$ cS forced at $\omega/(2\pi) = 80$ Hz, corresponding to a horizontal line in figure 2 with vibration number $\Omega = 0.87$. Just above the coalescence threshold, the drop bounces with the same period as the bath vibration, in a $(1, 1)$ mode (figure 3(a)). The amplitude of the bouncing droplet then generally increases progressively with driving acceleration and the impact phase shifts until the period of the bouncing reaches twice that of the vibrational forcing, and so becomes commensurate with the subharmonic Faraday waves favored by the bath vibration. Figures 3(b) and (c) illustrate the evolution of the bouncing dynamics during this progression. Drops in the resulting resonant $(2, 1)$ bouncing states may have one of two impact phases relative to the bath vibration, and so be either in-phase or out-of-phase with respect to other droplets. The transition to the resonant $(2, 1)$ state coincides with a substantial increase in the bouncer's wave energy, and is soon followed by the onset of horizontal droplet motion, the transformation from bouncing to walking.

In the walking state, a droplet self-propels in a straight line through a resonant interaction with its own wave field. A variety of walking states exist. Resonant $(2, 1)$ walkers arise when the bouncing frequency matches the Faraday frequency. In the parameter regime reported in figure 2, two different resonant walking states are possible, characterized by different impact phase and denoted by $(i, j) = (2, 1)^1$ or $(2, 1)^2$ [156]. In the $(2, 1)^1$ and $(2, 1)^2$ modes, the drop is in contact with the bath for approximately $T_F/2$ and $T_F/4$, respectively, where $T_F = 4\pi/\omega$ is the Faraday period [38, 44, 50, 156, 167, 195]

(figures 3(a) and (b)). In the high-memory limit, $\gamma \to \gamma_F^-$, this resonance may be lost, and the bouncing may become chaotic; nevertheless, the drop walks in a straight line [168]. The range of drop sizes over which walking arises for a particular fluid and vibrational frequency is limited. For example, in figure 2, the smallest walkers have a radius of 0.25 mm and the largest, 0.47 mm. It is thus, presumably, that this hydrodynamic pilot-wave system was not discovered until 2005 [1].

A striking feature of the walking droplets is the stability of the free walking state; indeed, in the absence of interactions with boundaries or other walkers, the walkers self-propel along a straight line. This stability is all the more beguiling when one considers that the drop is riding on the crest of its pilot wave field (see figures 1(b) and (g)). The simplest intuitive argument suggests that such an arrangement should be unstable. If the drop is perturbed backwards, it will receive a relatively small kick from its wave field at impact, so slow down; if perturbed forward, it will receive a relatively large kick, so speed up. What this reasoning fails to take into account is the stabilizing influence of the system memory. When the drop decelerates or accelerates, the effective density of wave sources along its path [196] increases or decreases, respectively, thereby increasing or decreasing the amplitude of the local wave field in such a way as to stabilize the walking state. The robust stability of the free walking state should thus remind us not only of the importance of memory in pilot-wave hydrodynamics, but of the subtlety of hereditary systems.

Tambasco and Bush [157] explored the behavior of the walker system just above the Faraday threshold, and reported a number of new dynamical states, characterized by zig-zagging and meandering motion, as well as a diffusive regime arising at high memory. Higher resonances in the drop oscillation may also be excited. Gilet *et al* [190] and Dorbolo *et al* [191] examined the bouncing of relatively large oil drops of radii $a \sim 0.75$ mm and viscosity $\nu < 100$ cS on a highly viscous bath ($\nu = 1000$ cS). Levitation criteria were deduced, and nonaxisymmetric modes of droplet vibration excited, leading to drop propulsion via tumbling. Hubert *et al* [197] examined the dependence of the bouncing threshold on the forcing frequency with a similar arrangement. They found that the bouncing threshold exhibits a minimum when the vibration number $\Omega \approx 1$ and a maximum when $\Omega \approx 3$, which correspond respectively to the drop's principal modes of deformation acting in resonance and antiresonance with the bath vibration. Most recently, it has been shown that bouncing droplets may be achieved with liquid metals, specifically, an alloy of gallium and indium [198]. While walking states have yet to be achieved with these liquids, this discovery may further extend the dynamical range of hydrodynamic pilot-wave systems.

Novel phenomena have also been observed by modulating either the phase or frequency of the vibrational forcing. Perrard *et al* [199] showed that, when a walker is subjected to an abrupt increase in the forcing acceleration, it may exhibit a π-shift in its bouncing phase, and so encounter a perfectly reversed wave field at impact. It thus reverses direction, retracing its trajectory for a time that increases as the forcing acceleration approaches the Faraday threshold, $\gamma \to \gamma_F$, effectively erasing its wave field in the process. Sampara and Gilet [200] examined the behavior of the walker system driven with two commensurate frequencies. A number of novel behaviors were reported, including chaotic walking near the Faraday threshold marked by a stop-and-start dynamics. Valani *et al* [201] recently showed that such a two-frequency forcing may give rise to a new class of walkers dubbed 'superwalkers', which are twice the size of the traditional walkers and self-propel at up to four times the speed owing to their relatively prolonged impact with the bath and the concomitant lateral acceleration induced by impact (figures 5(c) and (d)). The superwalkers open the door to a new parameter regime for pilot-wave hydrodynamics and invite further explorations of the role of multiple-frequency vibrational driving.

3.3. Pilot-wave field measurements

The novelty of the walking-droplet system lies in the subtle interplay between the droplet and its guiding wave. It thus behooves us to understand the precise form of the wave field generated by the drop impact on a free surface. The pilot-wave field in the walking droplet experiment has a characteristic amplitude of 1–20 microns and wavelength $\lambda_F \sim 4.8$ mm (figure 4). Its duration on the free surface can be as long as several seconds in the high-memory limit ($\gamma \to \gamma_F$). Visualization with a semi-reflective mirror [175] allows one to see its form. Moisy *et al* [202] developed a robust means of quantitative measurement of the pilot wave field, the free-surface synthetic Schlieren technique, which deduces the surface topography from the apparent distortion of a background image. The resulting quantitative measurements of the wave-field have been used to characterize walker interactions with boundaries [24, 172, 203] and to benchmark both theoretical models and numerical simulations [75, 204].

Each time the drop impacts the surface, it generates a transient wave front with a characteristic amplitude of 1–20 microns that propagates radially with a speed of 5–20 cm s^{-1} [44, 75, 204]. Behind this front, a quasi-monochromatic wave form persists with a wavelength λ_F prescribed by the surface wave dispersion equation (5). The superposition of many such waves yields the wave field of a stationary resonant bouncer, as illustrated in figure 4(a). While slow outward propagation of the zeros of this wave field indicate a weak traveling component [44, 204], the waves may in many instances be adequately described in terms of a quasi-monochromatic standing Faraday wave field [75]. The form of the walker wave field is illustrated in figure 4(b). Experimental measurements and simulations both indicate its characteristic horseshoe-like form [38, 44, 75, 204, 205]. As the walker is a moving source of waves, the Doppler effect is evident in its wavefield, the apparent wavelength decreasing and increasing, respectively, up- and downstream of the walker [75].

Tadrist *et al* [49] brought unprecedented experimental precision to bear on the walker system. Specifically, they developed an experimental technique for inferring the precise time and location of each drop impact by visualizing the outward propagating transient wave front generated at impact. Their

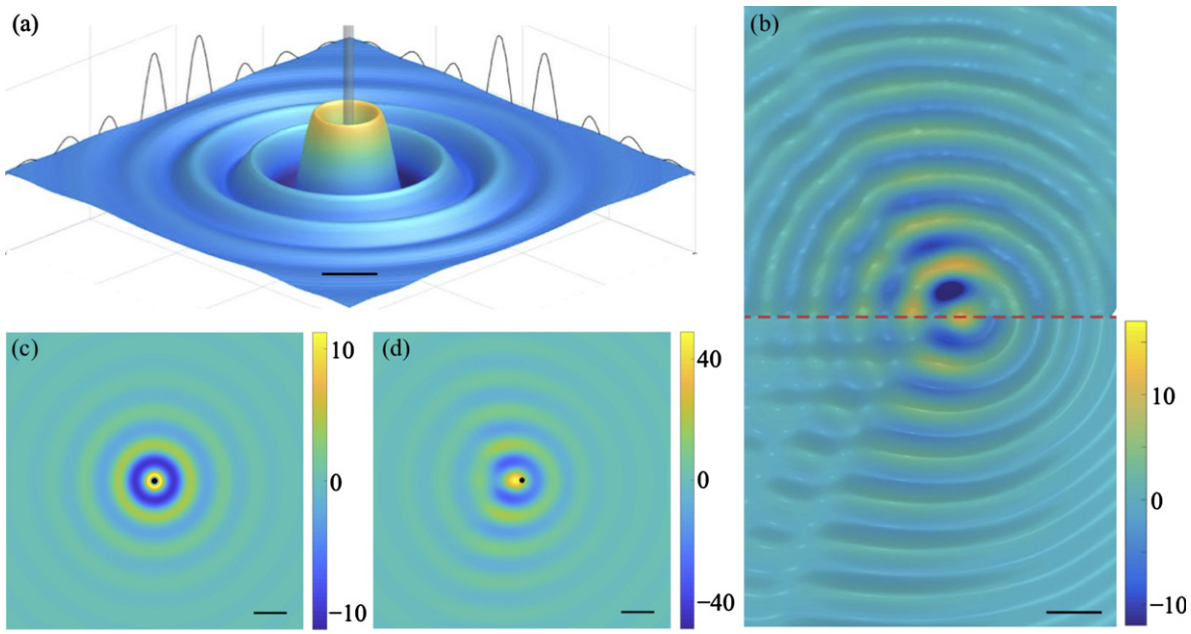

Figure 4. Bouncer and walker wave fields ($a = 0.38$ mm, $f = 80$ Hz). (a) Measured wave field of a period-doubled bouncer ($\gamma/\gamma_F = 0.77$) [204]. The gray curve shows a projection of the cross-section of the wave field passing through the droplet's center. The gray cylinder indicates the droplet's projected shadow. (b) Comparison between experimental measurements (top) and simulation (bottom) of the walker wave field ($\gamma/\gamma_F = 0.966$) [204]. The wave fields of (c) bouncing ($\gamma/\gamma_F = 0.73$) and (d) walking ($\gamma/\gamma_F = 0.9$) drops, as predicted by Milewski *et al* [44]. Color bars indicate the wave height in microns. Scale bars denote $\lambda_F \backsim 4.8$ mm. In panels (b) and (d), the walkers move to the right. (a), (b) Reprinted by permission from Springer Nature Customer Service GmbH: Experiments in Fluids. [194] © 2016. (c), (d) Reproduced with permission from [44]. © Cambridge University Press.

technique allows for resolution of the fast vertical dynamics responsible for wave generation, the uncertainty in which they identified as a source of chaos in the walker system [49].

Early studies of pilot-wave hydrodynamics were undertaken in relatively deep fluid layers, for which the Faraday wavelength $\lambda_F \ll 2\pi H$, which requires bath depths of $H > 5$ mm for the range of frequencies (50–80 Hz) typically considered. The resulting Faraday waves then decay before reaching the lower boundary, so the bottom topography has a negligible influence on the walker. Recent studies have shown that drops may also achieve a robust walking state in shallow water; specifically, Sáenz *et al* [13, 18] demonstrated that drops may walk in layers as thin as 1.6 mm. Chu *et al* [61] and Tsai *et al* [206] visualized the vortical flows beneath relatively large ($a \sim 1$ mm) bouncing droplets, and proposed that asymmetry in these vortices, induced either by a partner droplet or a weakly sloping bottom topography, could lead to propulsion. Finally, in many hydrodynamic quantum analogs, the boundaries of the fluid bath are generally marked by shallow 'beach' regions of typical depth 0.1 mm. While this geometry serves to locally damp the drop's pilot wave, it introduces uncertainty in the form of the interfacial boundary condition to be applied in theoretical models, which is necessarily neither Dirichlet (zero amplitude) nor Neumann (zero-slope) [11, 12, 21, 22, 56, 204, 207–209].

4. Theoretical modeling

The first theoretical treatment of parametric instability in a continuum system was Benjamin and Ursell's [210] description of inviscid Faraday waves, which was subsequently built upon to incorporate the role of fluid viscosity [211, 212]. Müller *et al* [213] presented a model for Faraday waves valid in the weak dissipation limit $\nu/\omega\lambda_F^2 \ll 1$, wherein the viscous boundary layers are small relative to the Faraday wavelength. Through a systematic asymptotic expansion of the linear water-wave dispersion relation with viscous corrections, they obtained an integro-differential Mathieu-type equation for the time evolution of the wave height. These models of Faraday waves have provided valuable touchstones for the development of the hierarchy of theoretical models describing resonant walkers, specifically, the motion of a droplet in response to the sub-threshold Faraday pilot-wave field that it generates by bouncing at the Faraday frequency. The models for resonant walkers can be roughly divided into two classes, those that approximate the wave field as the sum of monochromatic waves (sections 4.1–4.3), and those that solve the relevant partial differential equations for the evolution of the free surface (sections 4.4–4.5).

Because the Weber number characterizing the droplet motion is typically small, $\mathrm{We} = \rho v_z^2 a/\sigma \sim 0.1$, with v_z being the droplet's impact speed, the drops are only weakly perturbed by impact on the surface. Moreover, since the intrusion depth of the drop into the bath is small, the hydrostatic pressures generated during this impingement are negligible relative to the surface-tension-induced curvature pressures. Thus, the dominant physics of drop impact on a bath is captured by considering drop impact on a soap film, a problem examined experimentally and theoretically by Gilet and Bush [192, 214]. They demonstrated that, provided the film deflection

is sufficiently small, the soap film acts on the drop like a linear spring with a spring constant proportional to the surface tension σ. Such linear spring models also satisfactorily describe the vertical motion of a stationary drop bouncing in place on a liquid bath at low memory [167]. However, at high memory the bouncing state is affected by the drop's relic wave field [50, 156]. Describing the emergent walking state requires a description of the horizontal force balance, which in turn requires a model for the pilot-wave form generated by successive impacts.

4.1. Path-memory model

Emmanuel Fort developed the first theoretical model of walking droplets, a discrete-time model for a period-doubled resonant walker [2, 15, 26, 42]. The drop is modeled as a point particle and the impacts as instantaneous, occurring at times $t_n = nT_\mathrm{F}$. The vertical dynamics is assumed to be decoupled from the horizontal. The walker is subject to two forces in the horizontal direction: a linear drag force, and a propulsive force proportional to the gradient of the wave height $\tilde{h}$ at the walker's position. The walker's horizontal velocity is updated at each impact according to these two forces, and the horizontal position evolved accordingly. The model thus assumes the form of an iterated map in the walker's horizontal position $\boldsymbol{x}_n$ and velocity $\boldsymbol{v}_n$ at time $t = t_n$:

$$\begin{aligned}\boldsymbol{x}_{n+1} &= \boldsymbol{x}_n + \boldsymbol{v}_{n+1}T_\mathrm{F},\\ \boldsymbol{v}_{n+1} &= \mathrm{e}^{-Dt_s/m}\left(\boldsymbol{v}_n - |v_z|\boldsymbol{\nabla}\tilde{h}(\boldsymbol{x}_n, t_n)\right).\end{aligned} \tag{6}$$

Approximate values for the drop's vertical velocity v_z, drag coefficient D and contact time t_s are deduced from experiments. The form of the wave field taken in their path-memory model has been successively refined over time [26, 75, 196]. Most recently, the time-averaged wave height $\tilde{h}$ is given by time-averaging equation (9) (to be developed in section 4.2) over the impact time, with the $\sqrt{t}$-term removed for the sake of analytical convenience [26]. This model has successfully rationalized the emergent quantum behavior in a number of settings [15, 26, 29, 42, 117, 215, 216] to be detailed in sections 5–8.

4.2. Pilot-wave hydrodynamic models

Moláček and Bush [156, 167] developed a hydrodynamically consistent model for bouncer and walker motion based on a reduction of the Navier–Stokes equations. They demonstrated that the droplet's vertical position $z(t)$ on a vibrating fluid bath may be described to leading order in terms of a linear spring model:

$$m\ddot{z} + \mathcal{H}(-z)\,(c_1\dot{z} + c_2 z) = -mg(t), \tag{7}$$

where $g(t) = g + \gamma\sin\omega t$ is the effective gravity in the vibrating bath frame of reference and $\mathcal{H}$ is the Heaviside function, that ensures that the bath-induced spring force acts only during impact. Here, $z = 0$ at the point where the drop's lowermost extremity impacts the unperturbed bath surface. Implicit in this model is the assumption that the drop impacts an unperturbed interface, that the waves generated by prior impacts have decayed to zero, an assumption known to break down as γ approaches γ_F. Moláček and Bush [167] experimentally characterized the dependence of the droplet's coefficient of restitution and contact time with the bath on the Weber number, $\mathrm{We} = \rho\dot{z}^2 a/\sigma$, and the resulting empirical relations allowed them to express c_1 and c_2 in terms of We. Due to discrepancies between the experimentally measured bouncing mode transitions and those predicted by equation (7) at high memory, Moláček and Bush [167] developed a logarithmic spring model to account for the effect of bath and drop deformations on the vertical dynamics. Their model successfully rationalized the regime diagrams that detail the dependence of the bouncing behavior on the dimensionless vibrational acceleration and vibration number [156, 167, 168] (see figure 2).

To describe the walking state, Moláček and Bush [156] derived a trajectory equation for the droplet's horizontal displacement $\boldsymbol{x}_\mathrm{p}(t)$:

$$m\ddot{\boldsymbol{x}}_\mathrm{p} + D(t)\dot{\boldsymbol{x}}_\mathrm{p} = -F(t)\boldsymbol{\nabla}h(\boldsymbol{x}_\mathrm{p}, t). \tag{8}$$

Here, $F(t) = m(\ddot{z} + g(t))$ is the normal force exerted by the drop on the bath, and $D(t) = 6\pi a_0\mu_a + C\sqrt{\rho a/\sigma}F(t)$ is the time-dependent drag coefficient, which accounts for both the aerodynamic drag imparted during flight and the momentum transfer from drop to bath during impact. The constant C was shown to lie in the range $0.17 \leqslant C \leqslant 0.33$ in the parameter regime of interest, using measurements of the walker's coefficient of tangential restitution. The form of the wave field $h(\boldsymbol{x},t)$ was deduced using a quasi-potential formulation for the evolution of the free surface, assuming that the bath is forced near the Faraday threshold, $\gamma \lesssim \gamma_\mathrm{F}$, and that the walker's impact on the bath is point-like in both space and time:

$$\begin{aligned}h(\boldsymbol{x}, t) = \sum_{n=-\infty}^{\lfloor t/T_\mathrm{F}\rfloor} \frac{\tilde{A}\mathcal{S}}{\sqrt{t - nT_\mathrm{F}}} J_0(k_\mathrm{F}|\boldsymbol{x} - \boldsymbol{x}_\mathrm{p}(t_n)|)\\ \times \cos\frac{\omega t}{2}\,\mathrm{e}^{-(t-t_n)/T_\mathrm{M}}.\end{aligned} \tag{9}$$

Here, $\mathcal{S}$ is one of two parameters that characterize the droplet's impact phase:

$$\mathcal{S} = \frac{\int_0^{T_\mathrm{F}} F(\tau)\sin(\omega\tau/2)\,\mathrm{d}\tau}{\int_0^{T_\mathrm{F}} F(\tau)\,\mathrm{d}\tau}, \qquad \mathcal{C} = \frac{\int_0^{T_\mathrm{F}} F(\tau)\cos(\omega\tau/2)\,\mathrm{d}\tau}{\int_0^{T_\mathrm{F}} F(\tau)\,\mathrm{d}\tau}. \tag{10}$$

Moláček and Bush [156] derived an expression for $\tilde{A}$ in terms of the fluid parameters, and showed that the memory time T_M is related to the forcing acceleration γ through $T_\mathrm{M} = T_\mathrm{d}(1 - \gamma/\gamma_\mathrm{F})^{-1}$, where $T_\mathrm{d} \approx (2k_\mathrm{F}^2\nu)^{-1}$ is the viscous decay time of waves in the absence of vibrational forcing, a scaling derived previously by Eddi *et al* [75] using a multiple-scale perturbation expansion. The dimensionless memory parameter $M_e = T_\mathrm{M}/T_\mathrm{F}$ prescribes the number of prior bounces that influence the walker [75]. In typical experiments, M_e is in the range 3–400, and quantum-like features tend to emerge for $M_e > 10$. The fact that M_e diverges as $\gamma \to \gamma_\mathrm{F}$ simply reflects the shortcomings of the linear wave approximation in this limit, where the waves are expected to become nonlinear: the system behavior is not singular at the Faraday threshold, but the linear wave models used to describe it are.

Note that the walker's vertical and horizontal dynamics are coupled in equation (8), owing to the dependence of $F(t)$ and $D(t)$ on the walker's vertical position $z(t)$. Predictions made on the basis of the trajectory equation (8) and wave model (9) exhibited good agreement with experimental data on the walking threshold, and the dependence of the walking speed on drop size and forcing acceleration. Moreover, these equations form the basis for the stroboscopic models to be discussed in section 4.3. The primary shortcoming of the model is that the phase parameters $\mathcal{S}$ and $\mathcal{C}$ were not resolved, so were instead combined into a single fitting parameter $\mathcal{SC}$ constrained by experiments to lie in the range 0.1–0.3 [50].

An improvement to the wave form (9) was derived by Tadrist *et al* [217], whose developments were based on Müller *et al*'s [213] linear Faraday wave model:

$$h(\boldsymbol{x},t)=\sum_{n=-\infty}^{\lfloor t/T_{\mathrm{F}}\rfloor}\frac{\tilde{A}\mathcal{S}}{\sqrt{t-nT_{\mathrm{F}}}}J_0(k_{\mathrm{F}}|\boldsymbol{x}-\boldsymbol{x}_{\mathrm{p}}(t_n)|)\cos\ \frac{\omega t}{2}\times\exp\left[-\frac{\alpha|\boldsymbol{x}-\boldsymbol{x}_{\mathrm{p}}(t_n)|^2}{t-t_n}-\frac{t-t_n}{T_{\mathrm{M}}}\right],\qquad(11)$$

where $1/\alpha\approx 2c_{\mathrm{g}}^2/\nu k_{\mathrm{F}}^2$ has the units of diffusivity and c_{g} is the group velocity of waves with wavenumber k_{F}. This wave form incorporates a Gaussian kernel that accounts for spatial damping, the inclusion of which brings predictions for the standing wavefield generated by a bouncer in line with experimental measurements [204]. Equation (11) indicates that the wavefield of a bouncer decays exponentially over a characteristic lengthscale $\sqrt{T_{\mathrm{M}}/\alpha}$ [204]; thus, the spatial and temporal decay rates of sub-threshold Faraday waves are simply related. Tadrist *et al* [217] also calculated the wave field generated by a rectilinear walker, and found that it exhibited a Doppler shift similar to that reported in experiments [38, 75], a feature not captured by the waveform (9). Moreover, they found that the decay length δ of the wavefield in the wake of a rectilinear walker has an angular dependence, $\delta\to(4\alpha u_0(1+\cos\ \theta))^{-1}$ in the limit $\gamma\to\gamma_{\mathrm{F}}$, where u_0 is the walking speed and θ the angle with respect to the walking direction.

The bouncing drop models of Terwagne *et al* [218] and Blanchette [209] also incorporate the deformation of the droplet, and reproduce many features of the bouncing drop, including the period-doubling transition between bouncing modes as the vibrational acceleration is increased progressively. In a recent study of droplet pairs, Couchman *et al* [50] found that when the influence of the relic surface waves generated by prior impacts is considered, the linear spring model (7) is preferable to its logarithmic counterpart [156]: not only can it be solved analytically, but it improves the agreement between theory and experiment. They thus reverted to the simpler linear spring model (7), but explicitly modeled the influence of the relic surface waves on the drop's vertical dynamics. Their model will be further discussed in section 5.2.

4.3. The stroboscopic model

In the stroboscopic model of Oza *et al* [205], the drop's vertical dynamics is eliminated from consideration: the walker is modeled as a continuous source of standing waves. The drop is assumed to be in resonance with its Faraday wavefield, bouncing at the subharmonic frequency $\omega_{\mathrm{F}}=\omega/2$. Oza *et al* [205] approximated the sum in equation (9) by an integral, an approximation valid provided the timescale of the walker's horizontal motion is long relative to the bouncing period, $\lambda_{\mathrm{F}}/|\dot{\boldsymbol{x}}_{\mathrm{p}}|\gg T_{\mathrm{F}}$. Time-averaging equation (9) over the bouncing period then yields the trajectory equation

$$m\ddot{\boldsymbol{x}}_{\mathrm{p}}+D\dot{\boldsymbol{x}}_{\mathrm{p}}=-\frac{2mgA\mathcal{SC}}{T_{\mathrm{F}}}\nabla\left(\int_{-\infty}^{t}J_0(k_{\mathrm{F}}|\boldsymbol{x}-\boldsymbol{x}_{\mathrm{p}}(s)|)\times\mathrm{e}^{-(t-s)/T_{\mathrm{M}}}\,\mathrm{d}s\right)\Bigg|_{\boldsymbol{x}=\boldsymbol{x}_{\mathrm{p}}(t)},\qquad(12)$$

where $D=Cmg\sqrt{\rho a/\sigma}+6\pi a\mu_a$ is the drag coefficient averaged over the Faraday period and $A=\tilde{A}/2\sqrt{T_{\mathrm{F}}}$. Note that the $t^{-1/2}$-temporal decay evident in equation (9) was removed from the wave kernel for the sake of analytical expediency, on the grounds that it is subdominant to the exponential decay term.

Equation (12) represents an integro-differential equation for the walker's horizontal trajectory. The product of phase parameters $\mathcal{SC}$ is again taken to be a constant in the range 0.1–0.3, chosen to best match experimental data on the free walking speed [156]. The simplicity of the stroboscopic model (12) makes it amenable to mathematical analysis and numerical simulation. The authors showed that a bouncer transitions to a walker via a supercritical pitchfork bifurcation as the forcing acceleration is progressively increased. They concluded that the walking state is stable to in-line perturbations and neutrally stable to lateral perturbations in the parameter regime accessible in the laboratory. The stroboscopic model has been used to study the walker's complex nonlinear dynamics in a number of settings [17, 27, 31, 32, 34, 36, 45, 46, 48, 205, 219–221] to be detailed in sections 5–8.

4.4. Partial differential equations for the fluid interface

The wave generated by a single impact is dominated by the Faraday wavelength, which corresponds to the slowest decaying Faraday wave mode [156, 167]. In the models described so far, the wave field has thus been expressed as a sum (9) or integral (12) of monochromatic waveforms generated along the walker's path. A more sophisticated class of theoretical models expresses the wave height as the solution to a partial differential equation describing the free surface evolution. While the capillary waves generated on the surface of a quiescent bath by both moving [222–224] and oscillating [225] point sources have been characterized theoretically, the sub-threshold waves generated by a small source oscillating in resonance with a vibrating liquid bath have only been studied recently, in the context of pilot-wave hydrodynamics.

Milewski *et al* [44] developed a quasi-potential wave model consisting of partial differential equations for the velocity potential $\phi(\boldsymbol{x},z,t)$ and wave height $h(\boldsymbol{x},t)$. They considered the linearized Navier–Stokes equations for an incompressible, weakly viscous fluid, and employed the formulation of Lamb [226] and Dias *et al* [227], who derived viscous corrections to the free surface boundary conditions by accounting for the

vortical boundary layer at the free surface. Provided the fluid is irrotational and quiescent at infinity, the velocity potential satisfies

$$(\Delta + \partial_{zz})\,\phi = 0 \quad \text{for } z < 0,\ \phi \to 0 \text{ as } z \to -\infty, \tag{13}$$

where $\Delta = \partial_{xx} + \partial_{yy}$ is the 2D Laplacian. The boundary conditions applied on the interface $z = 0$ are

$$h_t = \phi_z + 2\nu\Delta h,$$
$$\phi_t = -g(t)h + \frac{\sigma}{\rho}\Delta h + 2\nu\Delta\phi - \frac{1}{\rho}P_{\mathrm{D}}(\boldsymbol{x} - \boldsymbol{x}_{\mathrm{p}}(t), t). \tag{14}$$

The pressure force P_{D} exerted by the drop on the bath is assumed to be nonzero and uniform over an area of radius $R(t)$:

$$P_{\mathrm{D}}(\boldsymbol{x}, t) = \frac{F(t)}{\pi R(t)^2}, \quad \text{where } F(t) = \max(m\ddot{z} + mg(t), 0) \tag{15}$$

and $R(t)$ is related to the drop size. The drop's vertical position $z(t)$ is assumed to evolve according to the logarithmic spring model of Moláček and Bush [156]. The model predictions for a bouncer's wave field compare well with experimental measurements [204]. The model captures both the Doppler shift in the walker wavefield [38, 75] and the transient wave propagating radially outwards following impact [75, 204], features not captured by the purely monochromatic wave models discussed in sections 4.1–4.3.

Galeano-Rios *et al* [193, 195] considered the impact of a small non-wetting rigid sphere on a quiescent bath, and demonstrated that the contact force between the sphere and bath emerges naturally from a kinematic match condition between the bath and sphere surface. They employed the wave model (13) and (14), but replaced the ad hoc pressure forcing with two kinematic constraints. First, the free surface was required to conform to the sphere surface beneath it. Second, the free surface was required to be tangent to the sphere surface at their line of convergence. These conditions are sufficient to determine the air pressure beneath the sphere, without the need to assume a specific form for either the spatial pressure distribution or the contact area, as was required in equation (15). Their framework was used to model bouncing drops, walkers and superwalkers, and lead them to conclude that drop deformation plays a significant role only for superwalkers [201]. While the model exhibited good agreement with the bouncing regime diagram reported by Wind-Willassen *et al* [168], it predicts the onset of chaotic bouncing at vibrational accelerations slightly below those reported in experiments, and wave amplitudes slightly larger than those reported by Damiano *et al* [204]. The authors attribute these relatively minor shortcomings to the limitations of the quasi-potential wave approximation (13) and (14).

4.5. Discrete-time model

Durey and Milewski [33] employed the wave model in equations (13) and (14) to simulate the dynamics of a resonant walker. They neglected consideration of the walker's vertical dynamics and instead assumed the walker to execute instantaneous point-like impacts at times $t_n = nT_{\mathrm{F}}$ and positions $\boldsymbol{x}_n = \boldsymbol{x}_{\mathrm{p}}(t_n)$, so the applied pressure is $P_{\mathrm{D}} = mgT_{\mathrm{F}}\sum_n \delta(\boldsymbol{x} - \boldsymbol{x}_n)\delta(t - t_n)$. This simplification allowed the wave model to be solved semi-analytically, through a decomposition of the wave field into the eigenmodes of the Laplacian, $\Phi_m(\boldsymbol{x}; k) = J_m(kr)\cos m\theta$ and $\Psi_m(\boldsymbol{x}; k) = J_m(kr)\sin m\theta$:

$$h(\boldsymbol{x}, t) = \sum_{m=0}^{\infty}\int_0^{\infty}\left[a_m(t; k)\Phi_m(\boldsymbol{x}; k) + b_m(t; k)\Psi_m(\boldsymbol{x}; k)\right] k\ \mathrm{d}k. \tag{16}$$

The authors showed that the mode amplitudes a_m and b_m both satisfy the Mathieu equation for $t \neq t_n$,

$$\ddot{a}_m + 4\nu k^2\dot{a}_m + \left[4\nu^2k^4 + \omega_{\mathrm{w}}^2(k) + k\gamma\ \sin(\omega t + \beta)\right] a_m = 0, \tag{17}$$

where β is the phase difference between the drop bouncing and bath vibration. During flight, the drop's inertia is balanced by a drag force $-D\dot{\boldsymbol{x}}_{\mathrm{p}}$ and any applied force $\boldsymbol{F}$:

$$m\ddot{\boldsymbol{x}}_{\mathrm{p}} = -D\dot{\boldsymbol{x}}_{\mathrm{p}} + \boldsymbol{F}(\boldsymbol{x}_{\mathrm{p}}), \quad t \neq t_n. \tag{18}$$

The drop impact results in a force being applied to the bath, consideration of which yields jump conditions on a_m and b_m. Similarly, the drop receives a propulsive force from the bath during impact, $-mgT_{\mathrm{F}}\delta(t - t_n)\nabla h(\boldsymbol{x}_n, t_n)$, which yields a jump condition on its velocity. These jump conditions may be expressed as

$$\begin{aligned}[\dot{a}_m(t_n; k)]_-^+ &= -\frac{mgk_{\mathrm{F}}T_{\mathrm{F}}}{\rho W_m}\Phi_m(\boldsymbol{x}_n; k),\\ \left[\dot{b}_m(t_n; k)\right]_-^+ &= -\frac{mgk_{\mathrm{F}}T_{\mathrm{F}}}{\rho W_m}\Psi_m(\boldsymbol{x}_n; k),\end{aligned} \tag{19}$$

$$\left[\dot{\boldsymbol{x}}_{\mathrm{p}}(t_n)\right]_-^+ = -\left(1 - \mathrm{e}^{-DT_{\mathrm{F}}/m}\right)\left(\frac{mg}{D}\nabla h(\boldsymbol{x}_{\mathrm{p}}(t_n), t_n) + \dot{\boldsymbol{x}}_{\mathrm{p}}(t_n^-)\right), \tag{20}$$

where $[f(t_n)]_-^+$ denotes the jump in f at time t_n, and $W_m = \pi$ for $m > 0$ and $W_0 = 2\pi$.

Using fundamental matrices to evolve the system between successive impacts, the authors recast equations (16)–(20) as an iterated map that evolves the wave field and walker position between impacts. By neglecting the details of the drop-bath impact, this formulation is more computationally efficient than Milewski *et al*'s [44] model (equations (13) and (14)) and so better suited to simulating the walker's long-time dynamics. It is also analytically tractable, permitting stability analysis of both bouncing and walking states. The energy of a walker's wave field was shown to be less than that of a bouncer provided $\gamma > \gamma_{\mathrm{W}}$, which suggests an energetic rationale for the transition from bouncing to walking [33].

4.6. Low-memory limits of the trajectory equation

The theoretical models for the walker dynamics may be simplified substantially in the low-memory limit. Protière *et al* [38] proposed a model that only considered the influence of a single

prior impact, and used it to qualitatively capture the dynamics of single and interacting walkers near the walking threshold. Filoux *et al* [43] and Rahman [228] used similar models to examine the dynamics of trains of walkers in a circular annulus (see section 5.1).

Starting from the stroboscopic model (section 4.3), Bush *et al* [229] derived a trajectory equation valid in the asymptotic limit of weak acceleration, $|\ddot{\boldsymbol{x}}_\mathrm{p}|T_\mathrm{M}/|\dot{\boldsymbol{x}}_\mathrm{p}| \ll 1$:

$$\frac{\mathrm{d}}{\mathrm{d}t}\left(m_\mathrm{w}(v)\boldsymbol{v}\right) + D_\mathrm{w}(v)\boldsymbol{v} = \boldsymbol{F}. \tag{21}$$

Here $m_\mathrm{w}(v)$ and $D_\mathrm{w}(v)$ prescribe, respectively, the dependence of the walker's effective mass and drag force on its speed $v = |\dot{\boldsymbol{x}}_\mathrm{p}|$, and $\boldsymbol{F}$ is an externally imposed force. The nonlinear drag force acts always to restore the walker to its free walking speed, u_0. Since $m_\mathrm{w}(v) > m$, the wavefield effectively imparts an added mass to the walker, an effect responsible for the anomalously large circular orbits observed in a rotating frame [15, 16] and harmonic potential [29, 220] in the low-memory regime (see section 6). Equation (21) is referred to as the 'boost model', as it indicates the role of the pilot-wave in increasing the walker mass relative to the droplet mass by a boost factor $m_\mathrm{w}(v)/m > 1$, a development inspired by those in stochastic electrodynamics suggesting that interaction with the electromagnetic quantum vacuum may alter a microscopic particle's inertial mass [230, 231]. Labousse and Perrard [232] proposed a Rayleigh oscillator-type model for the walker dynamics in which $D_\mathrm{w}(v)$ is proportional to $\left[(v/u_0)^2 - 1\right]$, which may be seen as a special case of equation (21) valid in the low-speed ($\lambda_\mathrm{F}/u_0 \gg T_\mathrm{M}$), low-memory limit [233].

4.7. Modeling boundary interactions

A number of important hydrodynamic quantum analogs involve the interaction of walkers with submerged topography or boundaries. To address this class of problems, a number of theoretical models have been developed since that of Couder and Fort [2, 117]. Nachbin *et al* [8] introduced a model allowing for consideration of one-dimensional walker motion above a two-dimensional fluid region in the (x, z)-plane with discontinuous bottom topography $z = -H(x)$. The authors built upon Milewski *et al*'s [44] quasi-potential wave model (section 4.4). Specifically, they augmented equations (13) and (14) with the no-penetration boundary condition $\partial\phi/\partial\boldsymbol{n} = 0$ on $z = -H(x)$, $\boldsymbol{n}$ being the unit normal to the boundary, and used conformal mapping to solve numerically the resulting elliptic boundary-value problem. The model has been used to investigate both unpredictable walker tunneling (section 8.1) and the role of wave-mediated coupling in inducing distant walker–walker correlations [234]. The approach of Nachbin *et al* [8] was extended to two dimensions by Durey *et al* [207] using a different computational method based on domain decomposition.

Faria [22] extended Milewski *et al*'s [44] quasi-potential model to simulate the motion of a resonant walker above a bath with a piecewise-linear depth profile $H(\boldsymbol{x})$, specifically, deep and shallow regions separated by discrete steps. The kinematic boundary condition in equation (14) was approximated by

$$h_t = -\boldsymbol{\nabla}\cdot\left(b(\boldsymbol{x})\boldsymbol{\nabla}\phi\right) + 2\nu\Delta h, \tag{22}$$

where $b(\boldsymbol{x}) = \tanh(k(\boldsymbol{x})H(\boldsymbol{x}))/k(\boldsymbol{x})$, and $k(\boldsymbol{x})$ satisfies the water-wave dispersion relation (5) in each region. Changes in topography were thus modeled through changes in the local phase speed of the Faraday waves through the function $b(\boldsymbol{x})$. As in Durey and Milewski [33], the pressure forcing in equation (14) was assumed to be point-like in both space and time. Faria's model [22] has been used successfully to rationalize a number of walker-boundary interactions detailed in section 8, including wall reflection [203], diffraction by slits [23], and scattering by submerged pillars [172] and wells [18].

4.8. Summary

The theoretical models for the dynamics of free walking droplets described in this section are listed in table 1. Some have been as faithful as possible to the hydrodynamic system; others have simply captured its essential features. Still others, developed to elucidate specific walker behavior, will be discussed in what follows. They can be categorized according to whether they account for the walker's vertical dynamics. Models that neglect the vertical dynamics [33, 205, 235] are more amenable to mathematical analysis and more numerically tractable, making them well-suited to characterizing a walker's long-time dynamics and emergent statistical behavior. However, these models have the impact phase as a free parameter, and do not satisfactorily capture the interactions between walkers. Conversely, models that consider the full vertical dynamics [44, 156, 193, 195] capture variations in bouncing phase but are computationally intensive. Couchman *et al*'s [50] variable-phase model (see section 5.2) plays an intermediate role by accounting for slow variations in the walker's vertical dynamics while remaining mathematically and computationally tractable [76].

5. Multiple droplet interactions

Bouncing droplets may interact through their mutual wave field to form a variety of bound states, either stationary or dynamic (figure 5). These bound states invariably exhibit a form of quantization; specifically, there are a finite number of preferred arrangements whose relative stability is prescribed by the system parameters. In addition to providing insight into the manner in which classical resonant wave sources interact [38, 40, 236], characterizing these bound states has lead to progressive refinement of the theoretical models of pilot-wave hydrodynamics. Specifically, examining their stability has elucidated the influence on the drop dynamics of spatial damping and the propagating transient on the pilot-wave field, and the effects of variations in the vertical bouncing [45–47, 50].

Protière *et al* [38] considered the collisions of two walking droplets, demonstrating that the pair may either scatter or lock into an orbiting pair [1] (figure 5(a)). For the case of

Table 1. Summary of theoretical models of walker dynamics. Computational times are given as orders of magnitude of time taken to simulate the motion of a single (2, 1) droplet on a desktop computer (with a 2.7 GHz Intel Core i5 processor), relative to real time in the experiments.

Model and authors	Vertical dynamics	Wave model	Comp. time/real time
Path-memory model (Fort *et al* [15])	Uncoupled from horizontal dynamics	Bessel functions generated by point impacts	$O(1)$
Pilot-wave hydrodynamic model (Moláček and Bush [156])	Logarithmic spring		
Stroboscopic model (Oza *et al* [205])	Constant bouncing phase	Bessel functions generated continuously along trajectory	
	Variable bouncing phase (Couchman *et al* [50])	Bessel functions with spatial damping [50, 76, 217]	
Rayleigh oscillator model (Labousse and Perrard [232])	No vertical dynamics	Wave effects enter through nonlinear drag	$O(10^{-3})$
Boost model (Bush *et al* [229])		Wave effects enter through nonlinear drag, added mass	
Faraday pilot-wave model (Milewski *et al* [44])	Logarithmic spring	Quasi-potential, weakly viscous	$O(10^{2})$
Discrete Faraday pilot-wave model (Durey and Milewski [33])	Discrete, instantaneous impacts		$O(10^{-1})$
Kinematic match pilot-wave model (Rios *et al* [193, 195])	Kinematic match of drop and bath surface		$O(10^{4})$

drops of different size, more complex orbital motions arose, including wobbling circular orbits and epicycles [40, 236]. The problem of walker collisions was revisited experimentally and theoretically by Tadrist *et al* [49]. By resolving the fast dynamics associated with the droplet bouncing, they concluded that, in the high-memory regime, the outcome of a walker collision cannot be predicted simply on the basis of the horizontal impact geometry. Rather, the system is chaotic, the origins of the unpredictability being uncertainty in the vertical bouncing dynamics. The validity of this conclusion in other settings is currently being explored.

5.1. Dynamic bound states: orbiting, promenading and ratcheting pairs, droplet strings

For identical drops, Protière *et al* [38] showed that circular orbits with quantized orbital radii arose, with different sets of radii accessible to pairs bouncing in-phase and out-of-phase. The orbital quantization was rationalized in terms of the assumed undulatory form of the pilot wave field. They also noted that the speed of the orbiting pairs is generally less than that of a free walker: the smaller the orbits, the slower the drops. The problem of identical orbiting droplet pairs was revisited by Oza *et al* [45], who characterized the influence of memory on the stability of the quantized orbital states. By categorizing the possible orbital states and the dependence of their stability on memory, their study prompted the refinement of the stroboscopic model, making clear the importance of spatial damping of the pilot wave field on the stability of orbiting pairs. The authors incorporated the effects of spatial damping [217] by replacing the wave kernel $J_0(k_F r)$ in the stroboscopic model (12) with that in (11), thereby substantially improving the agreement between theory and experiment.

Borghesi *et al* [42] presented a combined experimental and theoretical study of promenading pairs, the dynamic bound state arising when two droplets walk side by side with their separation distance either constant or oscillating periodically in time (figure 5(b)). They reported quantized interdrop distances, and demonstrated that such pairs move slower than their free counterparts. The system behavior was described theoretically in terms of a wave interaction energy. Arbelaiz *et al* [46] revisited the promenade mode in order to characterize the dependence of the stability of these dynamic bound states on the system memory.

In their studies of orbiting and promenading walker pairs, respectively, Oza *et al* [45] and Arbelaiz *et al* [46] found that a straightforward generalization of the stroboscopic model to multiple walkers failed to capture the detailed stability characteristics of these bound states. Specifically, the model predicted the onset of instability at forcing accelerations considerably below those observed experimentally. The source of this discrepancy was deduced to be the assumption of constant impact phase $\mathcal{SC}$; thus, the authors inferred an empirical functional form for the dependence of the phase on the forcing acceleration γ and the local wave height at the walker's position. The resulting stroboscopic model with phase adaptation thus indirectly accounted for slow variations in the walker's vertical dynamics without explicitly modeling them. Inclusion of this ad hoc model for phase adaptation substantially improved the match between theory and experiment. Together, these studies motivated the development of the variable-phase

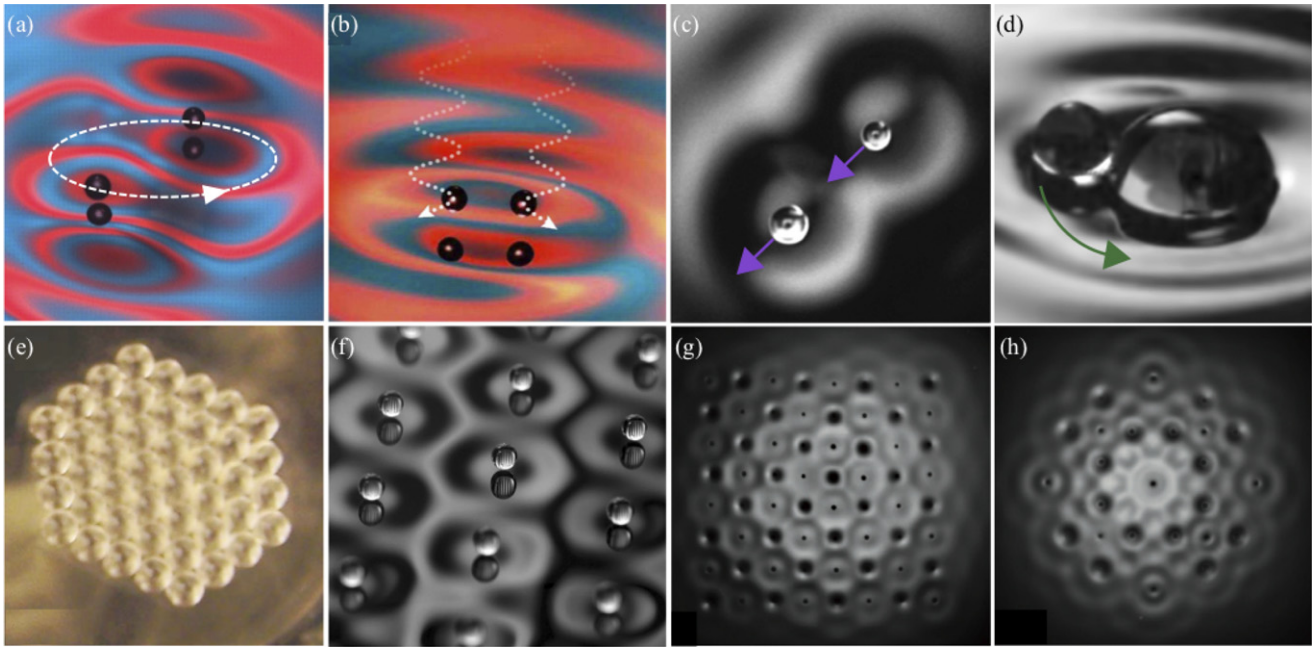

Figure 5. Bound states of bouncing droplets. (a) An orbiting pair [161]. (b) A promenading pair [159]. A superwalking pair in (c) chasing and (d) orbiting modes [201]. (e) Densely [39] and (f) loosely [165] packed lattices. (g) A square lattice achieved with two square sub-lattices bouncing out-of-phase [51]. (h) A more exotic Archimedean tiling [51] stabilized by the droplet in the center. (a) Reprinted by permission from Springer Nature Customer Service Centre GmbH: Journal of Visualization. [161] © 2017. (c), (d) Reprinted figure with permission from [201], Copyright (2019) by the American Physical Society. (e) Reprinted figure with permission from [39], Copyright (2007) by the American Physical Society. (f) Reprinted by permission from Springer Nature Customer Service Centre GmbH: Experiments in Fluids. [165] © 2015. (g), (h) Reproduced from [51]. © IOP Publishing Ltd. All rights reserved.

stroboscopic model of Couchman *et al* [50], to be described in section 5.2.

Drafting pairs or strings of walking droplets arise when a succession of identical droplets walk in the direction of the line joining them with a fixed distance between successive droplets. These dynamic bound states were first examined experimentally by Filoux *et al* [43, 237], who reported that strings confined to a circular annulus may walk at speeds exceeding that of individual walkers at the same memory. The observed behavior of drafting pairs of walkers was captured by the simulations of Durey and Milewski [33], who also examined their stability.

Eddi *et al* [41] demonstrated that when two bouncing drops of unequal size are placed nearby, they interact through their common wave field in such a way as to self-propel, with the inter-drop distance fixed, and assuming one of a discrete set of values. Owing to the asymmetry in the wave field along their line of centers, the pair propagates through a ratcheting mechanism. Ratcheting pairs of bouncing droplets were examined by Tang *et al* [58] using the liquid metal arrangement of Zhao *et al* [198]. The authors drew the physical analogy with optical ratcheting, as arises when dielectric nanoparticles of unequal size form optically bound states in a highly focused laser beam, leading to both self-propulsion and a discrete set of separation distances [238, 239].

Galeano-Rios *et al* [47] revisited ratcheting droplet pairs both experimentally and numerically. Their experiments demonstrate that the quantized inter-drop distances of a ratcheting pair depend on the vibrational acceleration, and that as the memory is increased progressively, the direction of the ratcheting motion may reverse up to four times. Their simulations, based on the model of Milewski *et al* [44] (section 4.4), highlighted the critical influence on the ratcheting motion of both the variations in the vertical bouncing dynamics and the traveling wave fronts generated by each impact. The transient wave generated by the partner drop creates a time-dependent force that changes from repulsive to attractive as the transient sweeps past. The reversal in the direction of motion of the ratcheting pairs may arise due to either changes in bouncing mode, as hypothesized by Eddi *et al* [41], or the subtle interplay between the traveling wave fronts and the droplet's vertical dynamics. Valani *et al* [201] demonstrated that unequal pairs of superwalkers may give rise to relatively high-speed ratcheting (figure 5(c)) or a symbiosis in which a small drop circles a large drop and so prevents the coalescence of its partner (figure 5(d)).

5.2. Static bound states: identical pairs, rings and crystal lattices

Crystalline structures may form from aggregates of identical or nearly identical bouncers (figures 5(e)–(h)). Protière *et al* [37], Lieber *et al* [39] and Eddi *et al* [41] reported both stationary and spontaneously spinning droplet lattices. Eddi *et al* [51] achieved eight of the eleven Archimedean tilings of the plane with static bouncer arrays. Doing so required control of the droplets' relative bouncing phase: while some arrangements were possible with all drops bouncing in phase (figures 5(e) and (f)), others required that neighboring drops be out of phase, so could only be achieved with resonant (2, 1) bouncers

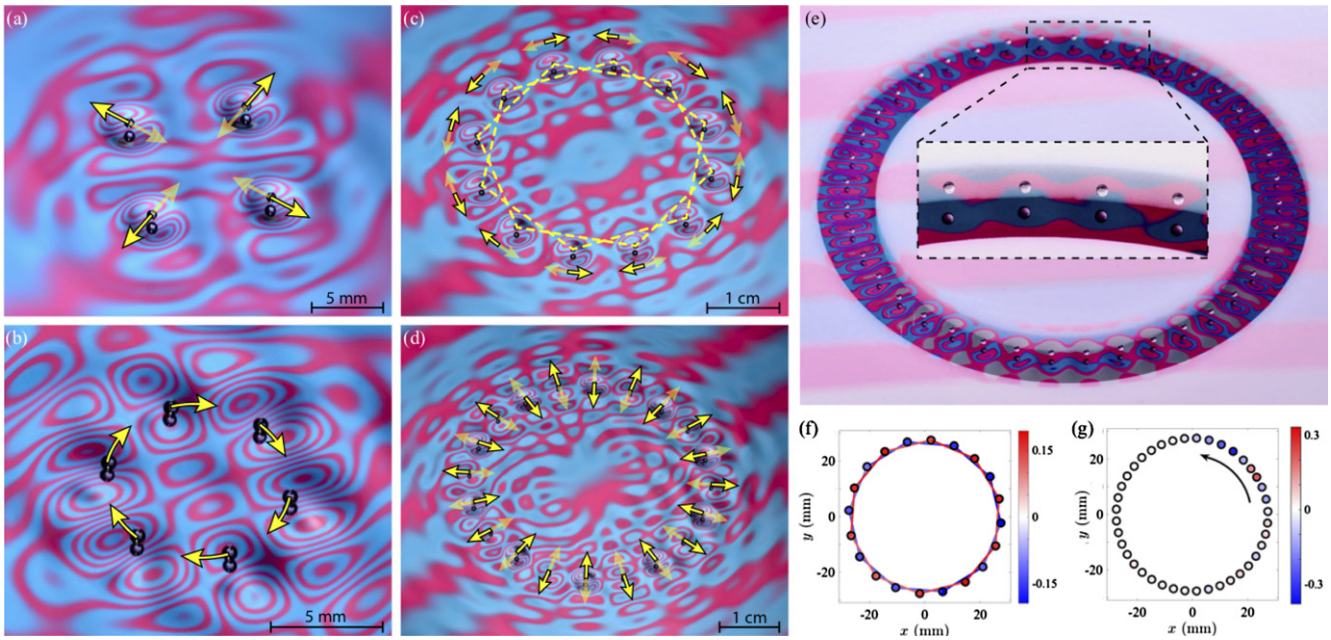

Figure 6. Free and confined rings of bouncing droplets. Free rings exhibit a number of instabilities [240], including: (a) in-phase radial oscillations, (b) orbital motion, (c) out-of-phase azimuthal oscillations and (d) out-of-phase radial oscillations. (e) 40 identical droplets confined to a circular annulus [53]. The chain may destabilize to either (f) optical oscillations or (g) a propagating solitary wave. In (f) and (g), colors denote the droplets' instantaneous angular velocity in rad s^{-1} and the inner ring radius is 24 mm. (a)–(d) Adapted with permission from [240]. © Cambridge University Press. (e) Reprinted figure with permission from [53], Copyright (2020) by the American Physical Society. (f), (g) Adapted figure with permission from [53], Copyright (2020) by the American Physical Society.

(figures 5(g) and (h)). Eddi *et al* [52] were the first to examine the destabilization of crystal lattices in response to increasing memory, and demonstrated that in both square and triangular lattices, instability sets in through a small oscillation of the individual drops that may then propagate through the crystal lattice like a phonon. As memory is increased progressively, these oscillations grow until the lattice rearranges and eventually collapses into an irregular form. An accompanying theoretical model of a one-dimensional crystal lattice was used to examine the onset of instability.

Couchman *et al* [50] examined the interaction of a pair of identical bouncing droplets, and characterized the dependence of the system behavior on memory. At sufficiently low memory, the inter-pair spacing is arbitrary; however, at a critical memory, this distance becomes quantized. As the memory is increased progressively, the interdrop distance changes weakly until the static state gives way to a dynamic state characterized by either colinear oscillations, promenading or orbital motion. The presence of the partner drop can be either stabilizing or destabilizing, depending on the droplet size. Larger drops went unstable to collinear oscillations below the walking threshold for a single drop γ_W. Smaller drops went unstable above γ_W to either orbital motion or side-by-side promenading motion, depending on the initial interdrop distance.

Attempts to rationalize the behavior of identical pairs prompted theoretical progress in the form of a variable-phase stroboscopic model [50]. The predicted pair stability changed qualitatively through consideration of the variable phase: constant-phase models always predict the onset of motion for $\gamma < \gamma_W$. The authors used a quasi-static approximation of the wave field of a stationary bouncer to derive a waveform with a purely spatial damping factor that is consistent with the far-field behavior of the wavefield defined in (11). They measured directly the dependence of bouncing phase on forcing acceleration γ, drop radius R and local wave height h_p. By measuring the time-dependent vertical acceleration of a bouncing droplet, they inferred the contact force $F(t)$ imparted from bath to drop, and thus the phase parameters $\mathcal{S}$ and $\mathcal{C}$ defined in equation (10). They then used Moláček and Bush's [167] linear spring model (7), augmented by a term to account for the relic surface waves, in order to determine the dependence of $\mathcal{S}$ and $\mathcal{C}$ on γ, R and h_p. The resulting physical picture is that the bouncing phase varies weakly with γ and h_p so as to maintain a roughly constant net upwards force, as required for periodic bouncing. Their study highlights the fact that drops may interact through altering either the local gradient or amplitude of their neighbor's wave field. Through altering the wave amplitude at impact, they change the impact phase, and so the evolution of both drop and wave. Consideration of phase modulations is similarly critical in modeling the dynamics of free circular rings of bouncing droplets, whose rich stability behavior has been characterized experimentally and theoretically by Couchman and Bush [240]. In addition to the oscillations shown in figures 6(a)–(d), they reported rearrangement of the circular ring into regular polygonal forms, including squares and pentagons.

Barnes *et al* [241] examined theoretically the resonant oscillations excited in a chain of bouncers when the drop at one end is subjected to periodic forcing in the horizontal direction. They demonstrated that, at relatively high memory, the

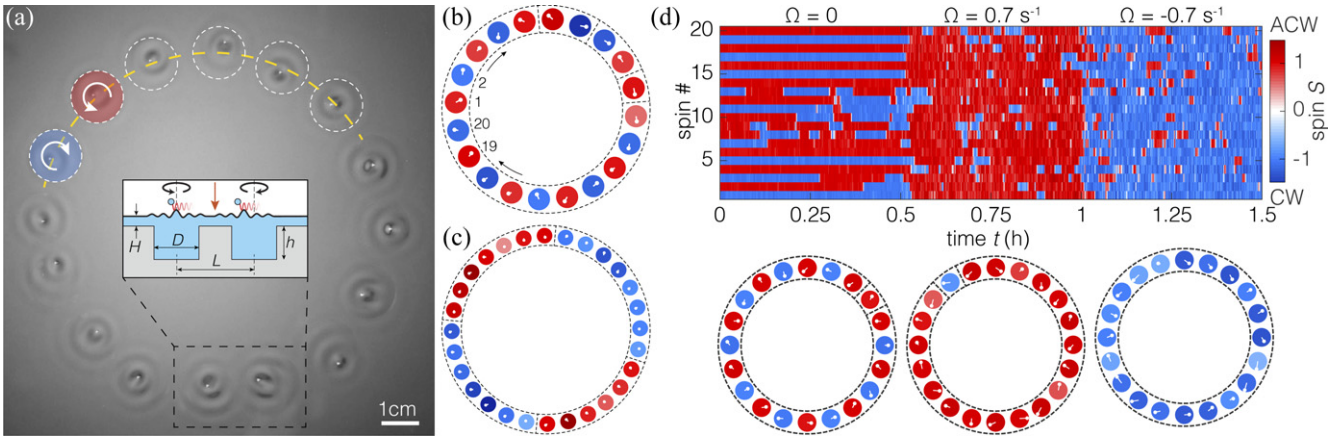

Figure 7. The hydrodynamic spin lattice [54, 55]. (a) Plan view and schematic cross section of a ring of submerged circular wells, each containing a single drop executing clockwise (blue) or anti-clockwise (red) motion on the surface of a vibrating fluid bath. A thin fluid layer between wells enables wave-mediated interactions between neighboring droplets and the emergence of global order. Snapshots showing collective (b) anti-ferromagnetic and (c) ferromagnetic order for different lattice spacings. (d) Rotating the system about a vertical axis with angular frequency Ω prompts a transition from antiferromagnetic to ferromagnetic states. Reproduced with permission from [55].

drops may oscillate with an amplitude larger than that prescribed, suggesting that the drops effectively extract energy from the collective wave field. They also found that dynamic stabilization of the chain could be achieved by sufficiently high-frequency forcing.

Thomson *et al* [53] considered the instability of a ring of bouncing droplets confined to a circular annulus (figure 6(e)). Owing to the annular bounding geometry, the drops were effectively confined to a circle. For 20 drops, the onset of instability was marked by small-amplitude optical oscillations of the droplets, wherein adjacent pairs move azimuthally out of phase (figure 6(f)). For 40 drops, a solitary wave sweeps through the array (figure 6(g)). At higher memory, counter-propagating waves arose; as additional wave modes appeared, the ring packing collapsed and dislocations appeared in the lattice. The observed dependence of the form of instability on the droplet number was rationalized theoretically [53, 242]. The annular ring system exhibits several features of the Toda lattice [243], a canonical theoretical model of crystal vibrations [53], and so forges new links with solid-state physics.

5.3. Coupled oscillators

Confining drops with bottom topography has allowed for the study of wave-mediated interactions giving rise to synchronization and long-range order in walker lattices. Nachbin [234] used his two-dimensional, variable-topography model (section 4.7) to consider theoretically the one-dimensional motion of a pair of walkers trapped in separate cavities. Between them, deep empty cavities facilitated wave-mediated communication between the pair. Depending on the system memory, geometry and drop size, different correlations could be induced between the pair. First, as observed in experiments [244], the drops could become perfectly synchronized, moving horizontally back and forth in tandem, in- or out-of-phase. A second regime was reported in which the droplets were not synchronized, but were statistically indistinguishable, with virtually identical signatures in position-momentum space. Finally, Nachbin [234] noted that the wave-mediated coupling between the droplets is much richer than that posited in the canonical Kuramoto model for coupled oscillators [245].

Sáenz *et al* [54, 55] introduced an analog of an electronic spin system, the hydrodynamic 'spin lattice', wherein walking droplets are confined by an array of circular wells submerged in a relatively shallow bath (figure 7). Each drop executes circular motion within its own well, spinning either clockwise or counterclockwise with equal probability. When the vibrational forcing is sufficiently weak, each droplet's wave is confined to its own well. At higher memory, however, the waves extend substantially beyond the well boundaries, resulting in wave-mediated interactions between neighboring drops. To explore whether such wave-mediated spin–spin interactions can induce coherent collective order, Sáenz *et al* [55] considered a number of lattice geometries, and demonstrated that three modes of analog 'magnetization' emerged according to the lattice geometry and memory. Disordered paramagnetic states arise when the spins of neighboring drops are uncorrelated. Antiferromagnetic or ferromagnetic order emerges when neighboring droplets tend to have, respectively, opposite or equal spin.

In the ring geometry (figure 7), Sáenz *et al* [55] found an optimal parameter regime in which the walker interactions generate large-scale collective order. At sufficiently low memory, the walker wave fields were too weak for neighbors to communicate effectively, corresponding to a disordered paramagnetic state. As memory was increased, the influence of the waves from the neighboring wells prompted the development of either antiferromagnetic (figure 7(b)) or ferromagnetic (figure 7(c)) order. Just as an antiferromagnetic material may be transformed into a ferromagnetic state by imposing a uniform magnetic field, a global transition from antiferromagnetic to ferromagnetic order was induced by applying system rotation (figure 7(d)). Consideration of the wave-mediated inter-drop forces allowed the authors to describe the system mathematically in terms of a generalized Kuramoto model for

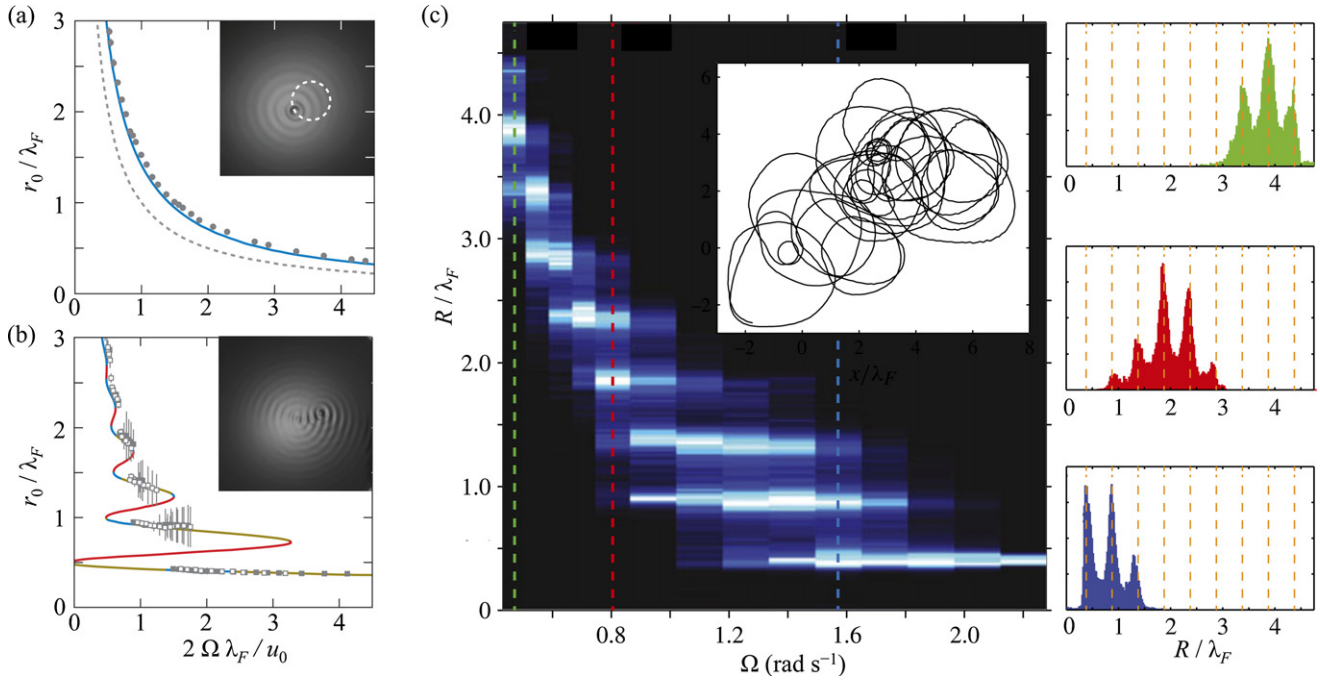

Figure 8. Orbital quantization [15] and chaotic pilot-wave dynamics [16] in a rotating frame. (a) Dependence of the orbital radius r_0 on the bath's rotation rate Ω at low memory ($\gamma/\gamma_F = 0.822$), obtained both experimentally (dots, [16]) and theoretically (curve, [17]). The dotted curve indicates the standard classical prediction for inertial orbits, $r_0 = u_0/2\Omega$, the offset from which has been rationalized with the boost model [229] (section 4.6). (b) At higher memory ($\gamma/\gamma_F = 0.971$), orbital quantization emerges. The orbits are color-coded according to their stability, as assessed using the stroboscopic model [17] (section 4.3). Blue indicates stable orbits, green and red indicate orbits that destabilize via oscillatory and non-oscillatory instabilities, respectively. (c) In the high-memory limit ($\gamma/\gamma_F = 0.988$), trajectories (inset) become chaotic and are characterized by intermittent switching between weakly unstable orbits. Colormap: the probability distribution of the radius of curvature R as a function of the rotation rate Ω. Bright segments indicate radii with high probability. Vertical dashed lines correspond to the three probability distributions shown at right [16]. (a)–(c) Adapted with permission [16, 17]. © Cambridge University Press.

coupled oscillators [245]. One thus expects that the hydrodynamic spin lattice will be a rich analog system capable of capturing many features of electronic spin systems and coupled oscillators, including spin waves [246].

6. Orbital pilot-wave systems

Studies of the motion of walkers under the influence of externally imposed forces have allowed for an examination of orbital pilot-wave dynamics. Such studies have collectively provided the first established paradigm for the emergence of quantum-like statistical behavior from classical pilot-wave dynamics, which is rooted in the chaotic switching between weakly unstable quantized orbital states [5].

6.1. Analog Landau levels

Fort *et al* [15] were the first to consider the dynamics of walkers in a rotating frame (figure 8), a problem that has subsequently been revisited both experimentally [16] and theoretically [17, 219, 247]. When an object of mass m moves at uniform speed u in a horizontal plane in a frame rotating uniformly with angular speed Ω about a vertical axis, it executes an anticyclonic inertial orbit with radius $u/2\Omega$, at which the radially outwards centripetal force is balanced by the inwards Coriolis force. So it is for walkers at low memory (figure 8(a)). However, as the memory is increased, the walker begins to interact with its own wake, whose time-averaged form corresponds to circularly polarized Faraday waves centered at the orbital center (figure 8(b)). Fort *et al* [15] demonstrated both experimentally and numerically with the path-memory model (section 4.1) that the result is the emergence of quantized orbits of radii $R_n \sim n\lambda_F/2$, where $n \in \mathbb{N}$. Owing to the analogous form of the Coriolis force acting on a mass in a rotating frame and the Lorentz force acting on a charge in a uniform magnetic field, the authors drew the physical analogy between the quantized inertial orbits arising in the walker system and Landau levels. Eddi *et al* [28] examined the influence of rotation on a pair of orbiting walkers, showing that the inter-drop distance was increased or decreased according to their sense of rotation relative to the ambient rotation, a hydrodynamic analog of Zeeman splitting.

Walkers in a rotating frame were revisited experimentally by Harris and Bush [16]. In addition to characterizing the onset of quantization at intermediate memory reported by Fort *et al* [15], they examined the onset of instability of the orbital states, as well as the complex chaotic behavior emerging in the high-memory limit. Stable circular orbits were seen to give way to wobbling orbits, then chaotic trajectories. The observed stability of the circular orbits was rationalized theoretically by Oza *et al* [17] via a linear stability analysis based on the stroboscopic model (section 4.3). A number of complex periodic

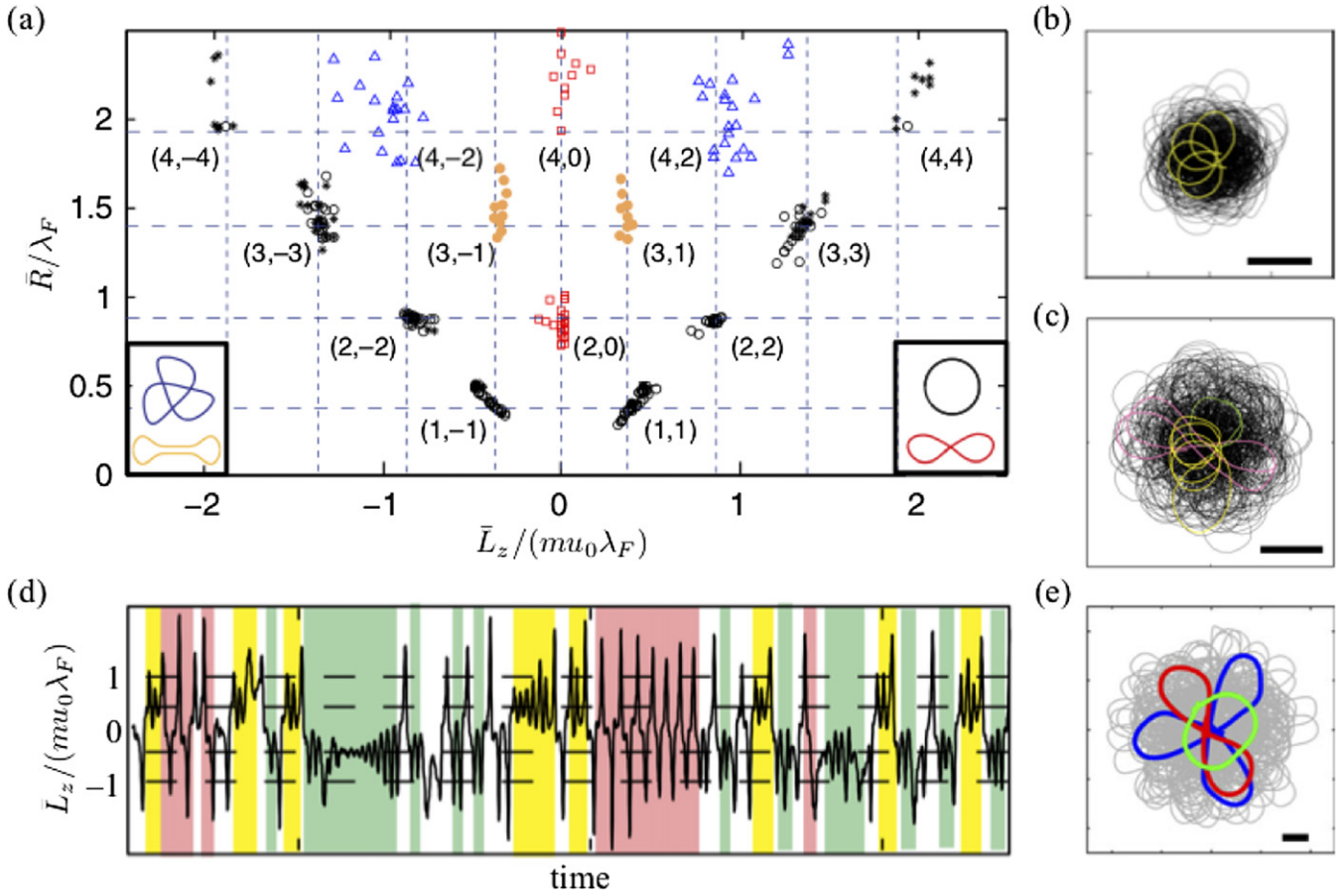

Figure 9. Double quantization of orbits and chaos in a central spring force $\boldsymbol{F} = -k\boldsymbol{x}$. (a) The mean radius $\bar{R}$ and angular momentum $\bar{L}_z$ of periodic orbits captured over a range of γ/γ_F and k [29]. Data points are color-coded according to the orbits shown in the legend. (b), (c) Chaotic trajectories observed in experiments [34] at $\gamma/\gamma_F = 0.98$ with (b) $\sqrt{k/m} = 4.44$ s^{-1} and (c) $\sqrt{k/m} = 3.58$ s^{-1}. (d) Time-evolution of $\bar{L}_z$ for the chaotic trajectory shown in (c). Colors correspond to sub-trajectories with $(\bar{R}/\lambda_F, \bar{L}_z/mu_0\lambda_F) \approx (1, 1)$ (yellow, clockwise circular orbit), $(1, -1)$ (green, counterclockwise circular orbit) and $(2, 0)$ (pink, lemniscate). (e) A chaotic trajectory (gray) obtained using the discrete-time model of Durey *et al* [33] contains the colored sub-trajectories shown. In (b), (c) and (e), scale bars denote λ_F. (a) Adapted by permission from Springer Nature Customer Service Centre GmbH: Nature Communications. [29] © 2014.

and aperiodic dynamical states arising at high memory were captured by their simulations [219]. In the chaotic regime, the walker motion is characterized by a chaotic switching between weakly unstable circular orbits (figure 8(c)). The walker thus has preferred radii of curvature; consequently, the histogram of the radius of curvature takes a peaked multimodal form reminiscent of that arising in the analogous quantum system. What would be considered a superposition of statistical states in quantum mechanics may here be viewed, with the added benefit of observable trajectories, as a superposition of weakly unstable, quantized periodic orbital states.

6.2. Walkers in a simple harmonic potential

Perrard *et al* [29, 248] developed an experimental technique for encapsulating a drop of ferrofluid within a droplet, which enabled them to impart external forces to walkers directly. By applying a vertical magnetic field with a radial gradient, they were able to examine walker motion in a central harmonic potential. The system was characterized in terms of the system memory and the equivalent spring constant k of the linear spring force, as determines the effective range of the walker, $L \sim u_0\sqrt{m/k}$, where u_0 is the walker's free speed. At moderate memory and over a range of spring constants, a variety of periodic and quasi-periodic states arose, including circles, lemniscates, trefoils and papillons (figure 9(a)). These periodic orbits were characterized in terms of their mean radius and angular momentum, and found to be roughly quantized in both quantities. In the high-memory regime, the walker was seen to switch intermittently between a number of these weakly unstable periodic orbits (figures 9(b)–(e)). At any given point in parameter space, typically two or three such states would be accessible: in this sense, the chaotic motion could be considered as a superposition of periodic states. The physical picture of a walker carving out then navigating its own slowly varying topography was developed by Labousse *et al* [31], and applies quite generally when the walker motion is confined.

The stability of circular orbits in a central force was treated theoretically by Labousse *et al* [220] using the constant-phase stroboscopic model (section 4.3). While qualitative agreement was obtained, the circular orbits were predicted to be more unstable than those observed. This observed mismatch between theory and experiment, also evident in the analysis

of circular orbits in the rotating frame [17], is now thought to be associated with the stabilizing influence of bouncing phase modulations on the wobbling orbits [50]. Durey and Milewski [33] used their Faraday-wave model (16)–(20) to simulate the long-time chaotic dynamics of a walker in a harmonic potential. They found that the walker's chaotic dynamics resulted from an intermittent switching between quasiperiodic trajectories consisting of ovals, lemniscates and trefoils (figure 9(e)), as in the original experiments [29]. They subdivided the walker trajectory into segments between successive radial maxima, then computed the time-averaged mean radius $\bar{R}$ and angular momentum $\bar{L}_z$ of each sub-trajectory. Using the K-means method to cluster the resulting data in the $(\bar{R}, \bar{L}_z)$ plane, they obtained a double quantization of $\bar{R}$ and $\bar{L}_z$ similar to that reported in the experiments of Perrard *et al* [29]. A similar double quantization was evident in the simulations of Kurianski *et al* [32], who noted that the double quantization arises when the crossing time L/u_0 is less than the memory time, and so relies on the walker interacting continuously with its self-generated potential.

Durey *et al* [35] used the discrete-time model (section 4.4) to simulate a walker confined to a line in the presence of a linear spring force. They showed that the walker's dynamics become chaotic as the forcing acceleration is progressively increased, and that the route to chaos resembles the Ruelle–Takens–Newhouse scenario. The authors also investigated the points where the drop reversed direction, and showed that the statistical distribution of these turning points was peaked at the minima of $J_0(k_F x)$. Through a statistical analysis, the authors showed that the walker's long-time trajectory may be interpreted as a random walk between these discrete turning points. While a multimodal statistical signature reminiscent of that arising in the one-dimensional quantum harmonic oscillator emerges at intermediate time, the small variability in the step length of this random walk leads to a smearing of this signature in the long-time limit.

6.3. Chaos in orbital pilot-wave hydrodynamics

Chaos, specifically, sensitivity to initial conditions and the resulting lack of predictability, is evident in virtually all orbital walker systems at high memory [5]. Chaos in hereditary systems is a subtle concept [249], and its possible significance to quantum mechanics has been suggested previously [250]. While one usually characterizes chaos in terms of sensitivity to initial conditions, in order to prescribe the evolution of a hereditary system, one must specify not only its initial conditions, but its history. In the walker system, one must prescribe not only the initial conditions of the drop, but those of its spatially extended wave field, the form of which depends on the drop's history. While Tadrist *et al* [49] demonstrate that the lack of predictability in the walker system may be rooted in uncertainty of the fast timescale responsible for wave generation, chaos would seem to be a more generic feature, as it also appears in stroboscopic models.

Tambasco *et al* [221] characterized theoretically the onset of chaos through the destabilization of circular orbits in orbital pilot-wave dynamics using the stroboscopic model (section 4.3). The authors considered the dynamics of walking droplets acted upon by external forces, specifically Coriolis, Coulomb, and linear spring forces. Initial conditions for the drop and accompanying waveform were taken as those arising for steady circular orbits. For each external force considered, an increase in γ destabilized circular orbits into wobbling and eventually chaotic orbits. The authors demonstrated that the route to chaos following the destabilization of circular orbits depends on the form of the external force. For the case of Coulomb and Coriolis forces, chaos sets in via a classic period-doubling cascade [251]. In the case of a central harmonic potential, the route to chaos is reminiscent of the Ruelle–Takens–Newhouse scenario, whereby the temporal power spectrum exhibits the successive appearance of incommensurate frequencies with increasing memory, leading to the broadening of the spectrum characteristic of chaos [252–254].

Using numerical simulations of the stroboscopic model, Budanur and Fleury [255] characterized the chaotic attractor of a walker moving in a central harmonic potential and showed that it is composed of distinct regions corresponding to different unstable periodic orbits. They also showed that distinct chaotic attractors merge via a global bifurcation as the memory is progressively increased. Rahman and Blackmore [256] review the walking-droplet system from the perspective of the dynamical-systems-theory community. It is noteworthy that attempts to characterize transitions to chaos experimentally face the difficulty that the transition typically happens abruptly; for example, in the case of a walker in a simple harmonic potential, over a span of $\Delta\gamma/\gamma_F \sim 0.004$ [221]. Perrard and Labousse [34] drew a distinction between the chaotic dynamics observed just at the onset of chaos, and the intermittency observed in the high-memory limit. Specifically, they showed that the former exhibits characteristics of low-dimensional chaos, as the dominant contributions to the wave field may be expressed using only a few modes. The latter exhibits features reminiscent of noise-driven chaos: once the system departs a stable region of phase space, a rapid transition drives it to another attractor.

Chaotic pilot-wave dynamics for drop motion in a rotating frame and a simple harmonic potential have key common features. The form of fully chaotic walker motion appears to be new for classical systems, and has provided the first important paradigm for the emergence of quantum-like statistics in hydrodynamic quantum analogs [5]. At relatively low memory, the drop executes one of several periodic orbits. At high memory, these periodic states all destabilize, and the drop switches between some number of them. One may thus view the chaotic states observed in orbital pilot-wave dynamics as a superposition of weakly unstable, quantized periodic orbits. While in quantum mechanics, systems are described in terms of a superposition of statistical eigenstates, pilot-wave hydrodynamics suggests that these states are not incompatible with the notion of particle trajectories in the form of unstable periodic orbits. Furthermore, the emergent statistics are a reflection of the relative instability of these weakly unstable orbits. The system thus has features of the periodic orbit theory proposed by Gutzwiller [257], who analyzed orbital

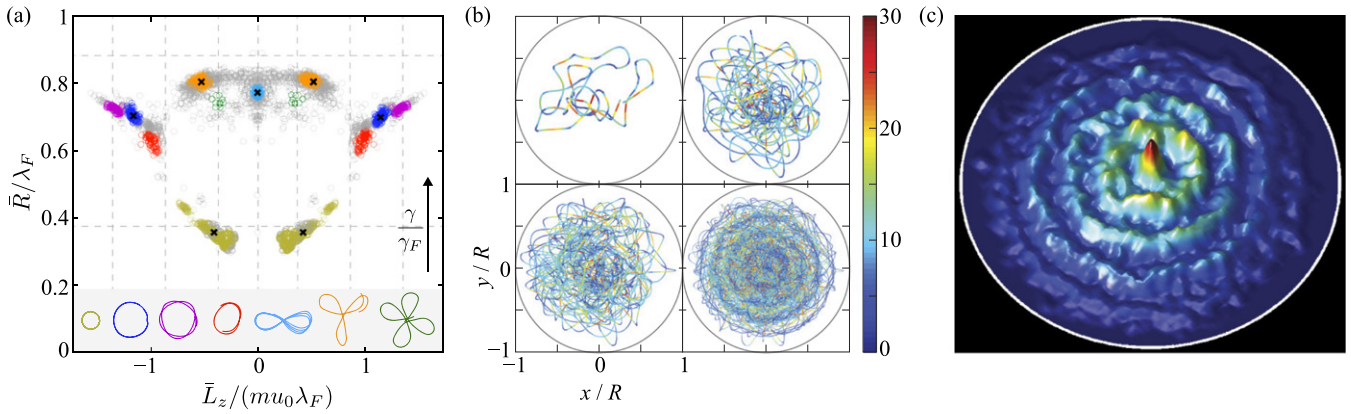

Figure 10. Dynamics and statistics of a drop in a circular corral. (a) In a corral of radius $R_c = 10.1$ mm $= 2\lambda_F$, double quantization of angular momentum $\bar{L}_z$ and mean orbital radius $\bar{R}$ emerges in the intermediate memory regime ($\gamma/\gamma_F = 0.87$–0.95) [14]. Gray circles indicate sub-trajectories obtained by segmenting long trajectories between successive radial maxima [33], and periodic trajectories are color-coded according to the legend. The black crosses are the centroids found via K-means clustering. (b) In a corral of radius $R_c = 14.3$ mm $= 4.5\lambda_F$, chaos ensues in the high-memory regime ($\gamma/\gamma_F = 0.989$). Trajectories of increasing length are color-coded according to droplet speed (in mm s^{-1}) [10]. (c) The corresponding histogram of the walker's position exhibits a multimodal statistical pattern reminiscent of the quantum corral [259, 260], with oscillations on the Faraday wavelength λ_F. (a) Reprinted from [14], with the permission of AIP Publishing. (b), (c) Reproduced figure with permission from [10], Copyright (2013) by the American Physical Society.

instabilities in the classical electrostatic n-body problem and used the computed classical trajectories to approximate energy spectra. Similar approaches have been advanced in attempts to characterize turbulence in terms of periodic subcomponents [258].

7. Analog quantum corrals

The quantum corral consists of a number of electrons (typically 60–80) moving on the surface of a metal, trapped by an array of positively charged copper ions that serve as the fence around the corral and discourage the electrons from escaping [259, 260]. Using a scanning tunneling microscope, the voltage of the system may be measured, serving as a proxy for the probability distribution function of the electrons. The corral is appealing in that it represents a quantum system in which the wave function may thus be directly measured. The observed statistical behavior is rationalized in terms of solutions of the time-independent Schrödinger equation with suitable boundary conditions. The observed wave forms can be reproduced by superposition of several cavity modes whose relative magnitudes are treated as fitting parameters [261].

7.1. Circular corrals

Harris *et al* [10] presented the results of an experimental investigation of a droplet walking in a circular corral, a deep liquid region surrounded by a confining shallow layer. At the lowest memories considered, the drop followed the outer boundary, executing circular trajectories. As the memory was increased progressively, the circular orbits began to wobble, then gave way to more complex periodic or aperiodic orbits such as stationary or drifting lemniscates or trefoils. This class of periodic and weakly aperiodic orbits, prevalent in relatively small corrals, was classified in greater detail by Cristea-Platon *et al* [14], who noted that they exhibit a double quantization in mean radius and angular momentum, reminiscent of walkers in a simple harmonic potential [29] (figure 10(a)). They rationalized this similarity on the grounds that the boundaries act effectively as a confining potential. They further examined the form of the mean wave field, noting that the symmetries of the periodic orbits were reflected in those of the associated mean wave fields. The physical picture emerging from these studies of small corrals is similar to that arising in the orbital pilot-wave systems discussed in section 6.

The most striking behavior in the hydrodynamic corral experiments arose in relatively large corrals in the high memory limit, at memories within 0.2% of the Faraday threshold [10]. Here, the droplet follows a complex path marked by frequent changes of direction prompted by interaction with its pilot-wave field (figure 10(b)). Despite this erratic drop motion, a robust statistical behavior emerged after approximately 30 min (figure 10(c)). The histogram of the drop position was comparable in form to the magnitude of the cavity's most unstable Faraday mode. The roots of this statistical signature were apparent in the speed map, which showed alternating concentric rings of anomalously high and low speed (figure 10(b)), which corresponded, respectively, to regions of low and high probability in the droplet's position histogram. The striking similarities between the quantum and hydrodynamic corral experiments are remarkable given the vast disparity of scales between the two (table 2).

The robust statistical forms emerging in the experiments of Harris *et al* [10] motivated a number of theoretical studies of walker dynamics in bounded domains [11, 12, 207, 247]. While certain features of the corral experiments have been captured, none of the theoretical models has satisfactorily captured its emergent dynamics and statistics. Gilet [11, 12] considered the discrete-time walker dynamics in a cavity with eigenmodes $\Psi_k(\boldsymbol{x})$ satisfying a Neumann condition on the boundary of the cavity. He considered the limit of zero drop

Table 2. The characteristic scales of the quantum and hydrodynamic corral experiments indicate the remarkable range of the physical analogy.

	Particle radius (m)	Corral diameter (m)	Particle frequency (s^{-1})	Particle speed (m s^{-1})	Statistical wavelength (m)
Quantum corral [259, 260]	2.80×10^{-18}	7.5×10^{-9}	$\omega_c = 1.60 \times 10^{21}$	10^6	10^{-9}
Hydrodynamic corral [10, 13]	3×10^{-4}	2.86×10^{-2}	50	2×10^{-2}	4.75×10^{-3}

inertia, and proposed the iterated map

$$\boldsymbol{x}_{n+1} = \boldsymbol{x}_n - K\sum_k a_{k,n}\nabla\Psi_k(\boldsymbol{x}_n),$$
$$a_{k,n+1} = \mu_k\left[\Psi_k^*(\boldsymbol{x}_n) + a_{k,n}\right], \tag{23}$$

where $0 < \mu_k < 1$ plays the role of the memory parameter for mode k, and $K > 0$ is a constant that prescribes the strength of the wave–particle coupling. Gilet [11] first restricted his attention to the 1D motion of a walker in a cavity with a single mode $\Psi(x)$. At low memory, the walker either settled into a stable fixed point or executed a periodic orbit about a fixed point. The periodic orbits destabilized as the memory was progressively increased, and the resulting chaotic trajectory could be decomposed into a sequence of intermittent jumps between unstable states. Gilet found that the probability distribution of the walker position approximately satisfies $\sim 1/|\Psi'(x)|$. Rahman and Blackmore [262] proved that the fixed points in Gilet's [11] model destabilized via supercritical or subcritical Neimark–Sacker (discrete-time Hopf) bifurcations as the memory parameter is progressively increased. They also proved that, as K is increased progressively, a periodic orbit may destabilize due to the appearance of a chaotic strange attractor [263, 264].

Subsequently, Gilet [12] conducted numerical simulations of equation (23) in a circular domain. Circular orbits stable at low memory destabilized via a Neimark–Sacker bifurcation as the memory was progressively increased. At high memory, there were no stable periodic attractors, and the walker explored the entire cavity in a chaotic fashion. While the emergent statistics were qualitatively similar to those reported by Harris *et al* [10], they differed quantitatively, presumably owing to the neglect of particle inertia, and differences between the theoretical and experimental wave forms and boundary conditions. Gilet's [12] simulations revealed that chaotic walker trajectories were ballistic on short timescales and diffusive on long timescales. The coherence distance, the length scale beyond which the walker's behavior was diffusive, was roughly $\lambda_F/2$. Gilet argued that the walker's effective diffusion coefficient then plays the role of $\hbar/2m$ in quantum mechanics, evoking Nelson's Stochastic Dynamics [83, 84]. He further compared his model predictions for the momentum and kinetic energy to the analogous quantum observables, and suggested new links with experiments employing weak measurement in quantum systems [121].

Durey *et al* [207] simulated the pilot-wave dynamics of a resonant walker in a circular corral, using the wave model in equations (13) and (14) augmented by a no-penetration boundary condition on the corral's edge. Building upon their discrete-time model [33] (section 4.5), the authors derived a map for the coupled evolution of the wave mode amplitudes, drop position and velocity. They found that quantized circular orbits destabilize into precessing loops, rectilinear oscillations, and off-center lemniscates, comparable to those reported experimentally in small corrals [10, 14], as the vibrational acceleration is increased progressively. At high memory, the drop switches intermittently between these weakly unstable orbital states. Although their model captured the reported form of the droplet dynamics at high-memory in relatively large corrals [10, 13], it did not capture the emergent wavelike pattern in the walker histogram (figure 10(c)). The authors attribute this shortcoming to their assumption that the walker's vertical dynamics is perfectly periodic, and conjecture that a model that accounts for modulations in vertical phase might better capture the walker's observed statistical behavior.

7.2. Elliptical corrals: mode superposition and statistical projection effects

Our understanding of the hydrodynamic corrals was advanced considerably by the experimental study of Sáenz *et al* [13], who considered walker motion in an elliptical corral (figure 11). In the high memory limit, a robust statistical form again emerged (figure 11(d)) from the correlation between speed and position (figure 11(b)). However, two important new inferences were made as to its form. First, while the instantaneous wave field is relatively complex (figure 11(a)), the mean pilot-wave field (figure 11(c)) takes a simple form that is strikingly similar to the droplet histogram (figure 11(d)). Second, the emergent statistical form need not correspond to the most unstable Faraday mode of the cavity, as was the case in the circular corral [10]. In the elliptical corral, the walker histogram was expressible as a linear superposition of a small number of modes: the presence of the drop could introduce additional modes that were the most unstable at nearby frequencies.

The study of Sáenz *et al* [13] was also important in demonstrating that pilot-wave hydrodynamics was viable in shallow water; thus, variations in bottom topography can be used to influence the walkers. The concurrence of several statistical modes thus allowed for the possibility of using variations in bottom topography to induce statistical projection effects. Figure 11 indicates that the particle histogram (figure 11(d)) and the mean wave field (figure 11(c)) in an elliptical corral both take a form that may be deduced by superposing two distinct cavity modes, as is suggestive of a superposition of statistical states. Adding a well at an arbitrary position only introduced a localized perturbation to the histogram (figure 11(e));

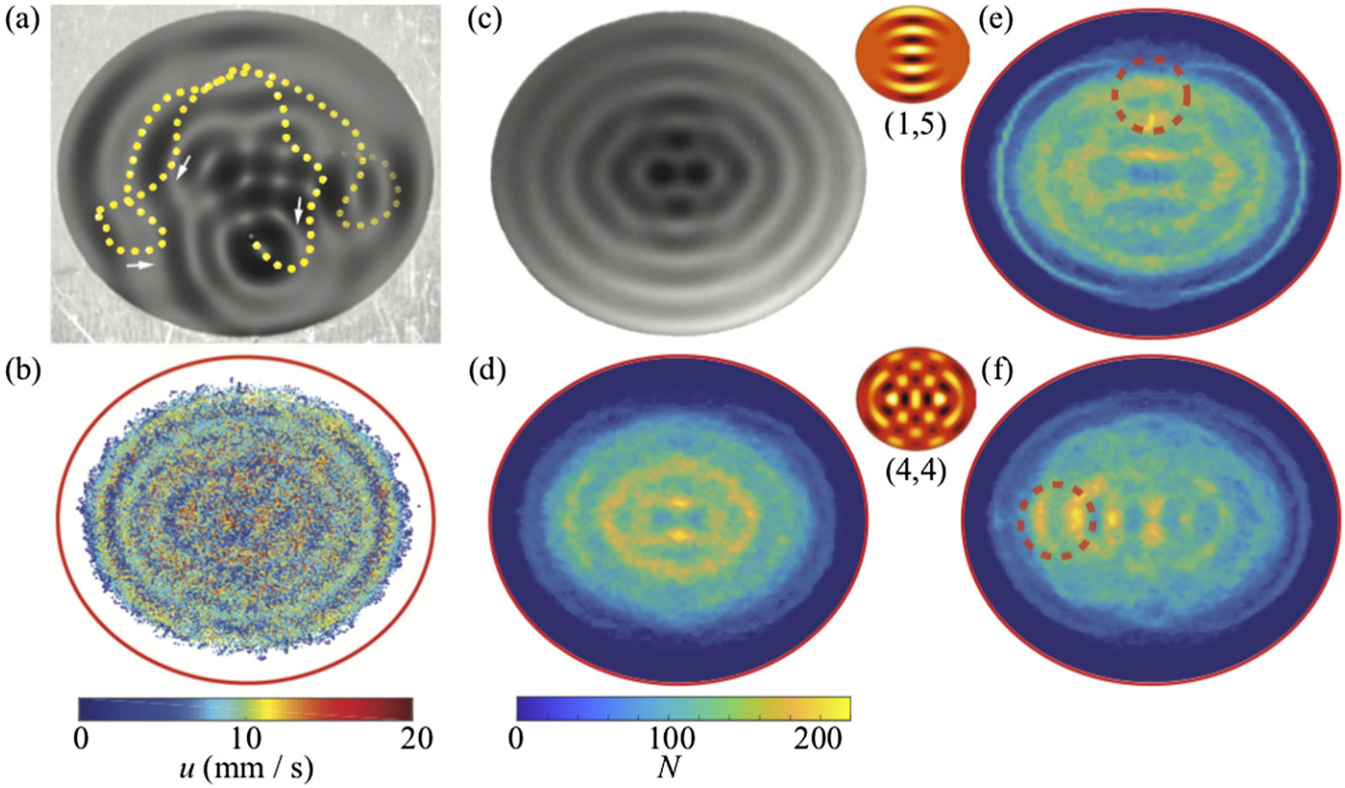

Figure 11. Walkers in an elliptical corral [13]. (a) The instantaneous wave field excited by the drop's trajectory (dashed yellow curve). (b) The chaotic trajectory is colored according to the instantaneous drop speed, revealing a correlation between position and speed. (c) Mean pilot-wave obtained by time-averaging the wave field over 30 min. The wave field is described by the superposition of two cavity modes, specifically, the odd (1, 5) and even (4, 4) elliptical eigenfunctions (insets) of the Helmholtz equation with Dirichlet boundary conditions. (d) Histogram of the walker position, deduced from the trajectory in (b). (e) Placing a submerged circular well at the midpoint of the upper semi-minor axis leads to a localized disturbance. (f) When the well is placed at the left focus, amplification of the (4, 4) mode leads to the projection of a high-density region toward the empty focus, an analog of the quantum mirage [265]. Reprinted by permission from Springer Nature Customer Service Centre GmbH: Nature Physics. [13] © 2018.

however, when placed at one focus of the ellipse, it favored one mode over the other (figure 11(f)), and so induced a signal at the other focus, a nonlocal statistical projection effect reminiscent of the quantum mirage [265].

7.3. The nonlocal mean-pilot-wave potential

The observed correlation between the histogram of a droplet walking in an elliptical corral and the mean wave field [13] led Durey *et al* [35] to an important theoretical result. They proved that, for a walker executing perfectly periodic impacts in an unbounded domain, the time-averaged pilot-wave field $\bar{h}(\boldsymbol{x})$ may be expressed as the convolution of the walker position probability distribution $\rho(\boldsymbol{x})$ and the wave field of a bouncer, $h_{\mathrm{B}}(\boldsymbol{x})$:

$$\bar{h}(\boldsymbol{x}) = \rho(\boldsymbol{x}) * h_{\mathrm{B}}(\boldsymbol{x}). \tag{24}$$

This result holds for both periodic and chaotic walker motion. For circular motion along an orbit of radius r_0, the walker distribution is $\rho(\boldsymbol{x}) = \delta(|\boldsymbol{x}| - r_0)/2\pi r_0$, so the mean wave field is given by $\bar{h}(r) = \frac{AT_{\mathrm{M}}}{T_{\mathrm{F}}} J_0(k_{\mathrm{F}} r_0) J_0(k_{\mathrm{F}}|\boldsymbol{x}|)$ [29, 266]: it has a Bessel form, and an amplitude prescribed by the orbital radius. Notably, this result indicates that the mean wave field vanishes identically when the walker orbits along zeros of $J_0(k_{\mathrm{F}}|\boldsymbol{x}|)$. The prevalence of such circular orbits has been noted in several experimental and theoretical investigations of orbital pilot-wave dynamics [15–17, 26, 29, 31, 207, 219, 220], and would seem to suggest an energetic rationale for orbital quantization. The convolution result (24) was generalized to the case of variable bottom topography by Durey *et al* [207].

Another key insight from the study of Durey *et al* [35] was that, in the high-memory limit, the instantaneous wave field converges to its time-averaged form. This convergence, as demonstrated in their simulations of one-dimensional walker motion in a simple harmonic potential, underscores the importance of the mean wave field in the walker dynamics. In particular, it indicates that the mean pilot-wave plays the role of a self-induced nonlocal potential that the walker navigates, reminiscent of the quantum potential in Bohmian mechanics (section 2.3). Efforts are currently being made to assess the extent to which such a physical picture describes the walker dynamics in other settings. Notably, while the mean-pilot-wave potential may be simply characterized in two dimensional corrals (e.g. figure 11(c)), the convergence of the instantaneous pilot-wave field to the mean was not evident, even at the highest memory, owing to the influence of viscous wave damping.

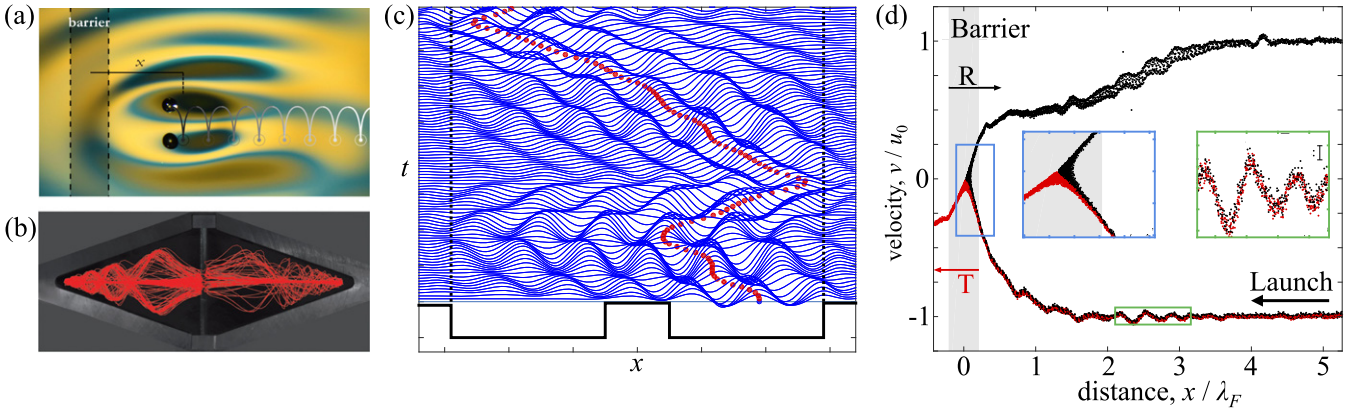

Figure 12. Walker tunneling. (a) The walker approaches a submerged barrier [9]. (b) Experimental trajectories (red) reported by Eddi *et al* [52]: the walker crossed the obstacle 14 times in 110 attempts. (c) Simulations of walker tunneling between two cavities when the walker is confined to a line [8]. A space-time plot of the walker (red) and pilot wave (blue) captures a tunneling event. (d) Trajectories measured in the experiments of Tadrist *et al* [9], displayed in position-velocity phase space. Reflected and transmitted trajectories are indicated in black and red, respectively. Points indicate the location of each impact. Green inset: incoming velocity fluctuations, with a characteristic error bar shown. Blue inset: the separation point between reflected and transmitted trajectories. (a), (d) Reproduced figure with permission from [9], Copyright (2020) by the American Physical Society. (b) Reproduced figure with permission from [6], Copyright (2009) by the American Physical Society. (c) Reproduced figure with permission from [8], Copyright (2017) by the American Physical Society.

8. Walker-boundary interactions

When a walker interacts with submerged topography, its pilot-wave is altered, its motion disturbed. Recent studies of walker-boundary interactions have led to a number of intriguing analogs of optical and quantum systems.

8.1. Tunneling

Eddi *et al*'s [6] experimental investigation of a walker impinging normal to a submerged barrier demonstrated that walkers exhibit features of quantum tunneling on a macroscopic scale (figures 12(a) and (b)). The authors demonstrate that the reflection or transmission of a walker over a submerged barrier is unpredictable; moreover, the crossing probability decreases exponentially with increasing barrier width, as in the case of quantum tunneling [267, 268]. Walker tunneling was revisited theoretically by Hubert *et al* [7], who used the Rayleigh oscillator model of Labousse and Perrard [232] (section 4.6) to capture the observed crossing statistics.

Nachbin *et al* [8] used their two-dimensional, variable-topography model (section 4.7) to simulate walker tunneling across a shallow region separating two relatively deep cavities (figure 12(c)). Simulation of the chaotic dynamics arising at high memory showed that the probability of walker tunneling across a shallow region decreases exponentially with barrier width, as in the original experiments of Eddi *et al* [6]. Moreover, for a fixed barrier width, the tunneling probability was a non-monotonic function of the forcing acceleration, attaining a maximum for a critical value of γ: the forcing acceleration needed to be high enough for the local pilot-wave to permit tunneling, but not so large as to generate large-amplitude standing waves in the target cavity that prevent it.

Tadrist *et al* [9] revisited walker tunneling experimentally with a view to assessing whether resolution of the fast bouncing dynamics would render the apparently unpredictable behavior predictable. In a parameter regime where there was a 50% chance of tunneling, they determined the conditions for tunneling. They applied the technique of Tadrist *et al* [49] for inferring the precise point and time of drop impact. They thus deduced that that the spatial dependence of the bouncing phase is not determinant in walker tunneling. Rather, their study shows that the tunneling is determined by minute variations in the drop's horizontal momentum at a distance of approximately three barrier widths from the barrier: faster drops cross the barrier, slower drops do not (figure 12(d)).

8.2. Reflection, refraction and optical analogs

A walker approaching a discrete step in bottom topography at an angle of incidence θ_i may either be reflected by the step, or cross onto the shallow layer above the step and continue to walk. Pucci *et al* [203] examined walker reflection from a submerged planar barrier. Their experiments showed that droplets exhibit non-specular reflection. A small range of reflection angles ($60^\circ < \theta_r < 80^\circ$) arises, and the precise value of θ_r depends only weakly on the system parameters, including θ_i, the walker speed and size, the step size and the memory. The observed behavior was captured theoretically with simulations based on the model of Faria [22] (section 4.7). The non-specular reflection indicates that momentum is not conserved in the direction parallel to the boundary, that a wave-mediated net tangential force is applied to the drop during its interaction with the step, an effect rationalized in the theoretical developments of Turton [233].

Bragg diffraction was first observed in patterns of x-rays scattered off crystalline solids. The Bragg condition is met for certain wavelengths and incident angles, and is associated with a sharp decrease in the reflected radiation [269]. Vandewalle *et al* [57] considered walker motion in a circular annular channel with periodically varying bottom topography consisting of submerged walls aligned perpendicular to the channel. They demonstrated that an analog Bragg condition exists: when the spacing of the walls is $\lambda_F/2$, the time-averaged droplet speed

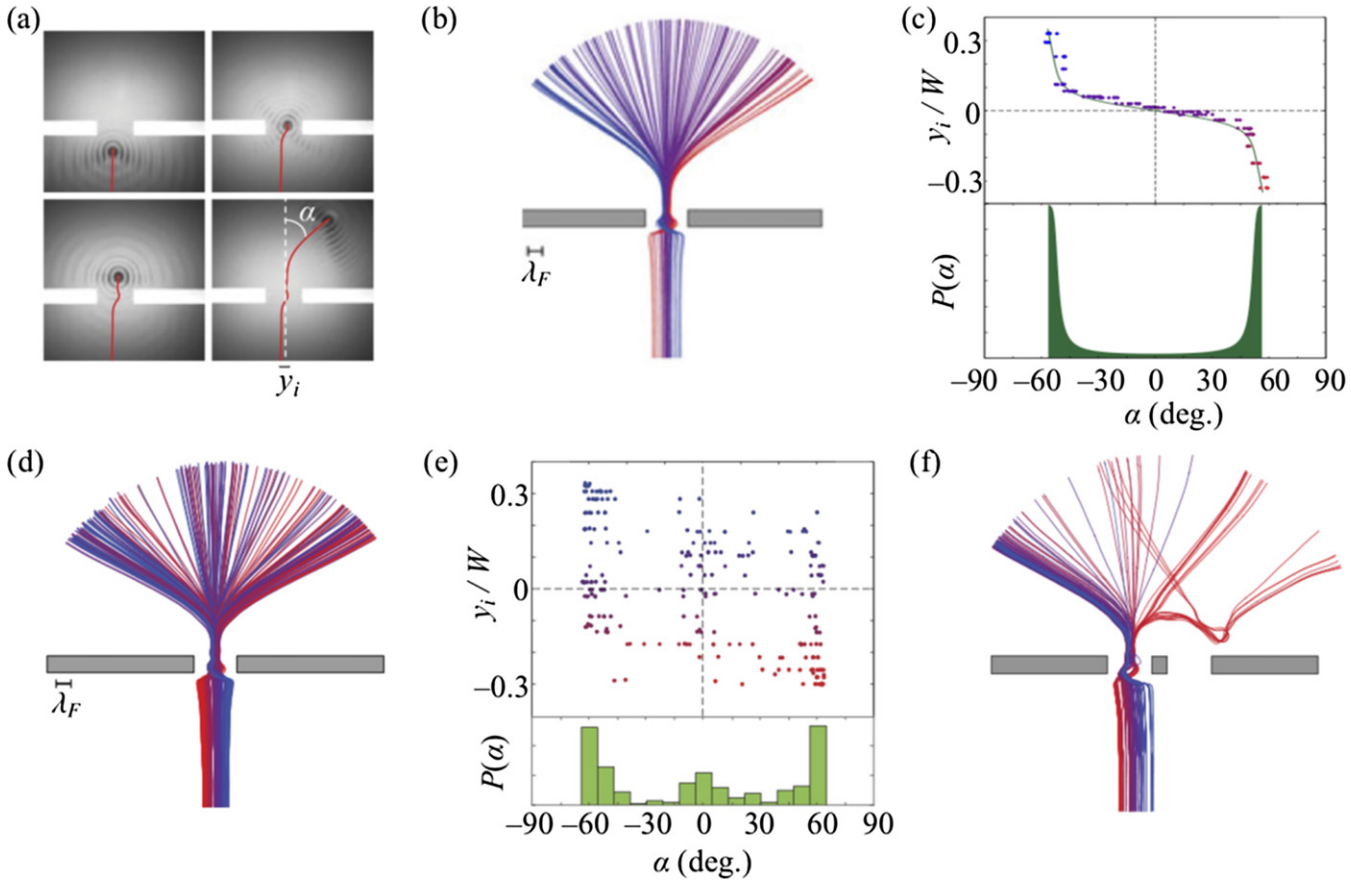

Figure 13. Scattering of walkers through single and double slits, as reported in the experiments of Pucci *et al* [23]. (a) A walker with impact parameter y_i passes through a single slit of width $W = 14.7$ mm $= 3.1\lambda_F$ and is deflected by an angle α. (b) Trajectories in the deterministic regime, $\gamma/\gamma_F = 0.985 \pm 0.002$. (c) Top panel: the dependence of the deflection angle α on the impact parameter y_i for the trajectories in panel (b). Bottom panel: the corresponding probability density function $P(\alpha)$ of the deflection angle. (d) Trajectories in the chaotic regime, $\gamma/\gamma_F = 0.998 \pm 0.002$, where the deflection angle α is independent of the impact parameter y_i, as evident in (e). (f) Trajectories of a walker passing through one slit of a double-slit arrangement in the chaotic regime, $\gamma/\gamma_F = 0.998 \pm 0.002$. Note the marked difference from the trajectories in (d), which indicates the influence of the second slit. Adapted with permission from [23]. © Cambridge University Press.

decreases sharply. Filoux *et al* [56] investigated the dynamics of a walker confined to long rectangular corrals of different widths d. They found that the walker's longitudinal (v_y) and transverse (v_x) velocities both increase with d, with the ratio $\langle v_y^2\rangle/\langle v_x^2\rangle$ being maximized for $d/\lambda_F \approx 1.5$–2, as defines the optimal wave guide.

The Talbot effect arises in optics when monochromatic light is shone through a diffraction grating [270]. The intensity pattern of light at the grating recurs at integer multiples of the Talbot length, as is defined in terms of the wavelength of incident light, λ, and the spacing of the grating, d, through $Z_T = \frac{\lambda}{2}\left(1 - \sqrt{1-(\lambda/d)^2}\right)^{-1}$ [271]. Sungar *et al* [59] demonstrated an analogous effect with the Faraday system excited just above threshold when there is a linear array of partially submerged pillars spaced at $2\lambda_F$. The images of these pillars are projected by distances corresponding to integer multiples of the Faraday–Talbot length, which has precisely the form of the Talbot length, but with λ_F in place of λ. They further demonstrated that the projected images could trap bouncers and walkers, thus providing a hydrodynamic analog of optical trapping with the Talbot effect. Sungar *et al* [60] showed that by spacing the pillars a distance $3\lambda_F/2$ apart, they could capture effects analogous to those of alternating grating phase in optics. They also considered circular arrays of pillars, which allowed for tuning of the magnification of the projected images.

8.3. Diffraction from slits

The possibility of the walking droplet system as a hydrodynamic quantum analogue was launched by the seminal study of Couder and Fort [2], who reported that walkers exhibit single-particle diffraction and interference when passing through apertures between submerged barriers. They sent single walkers toward a submerged barrier with openings on the scale of the guiding wavelength (figure 13(a)). As the drop passed through the slit, its trajectory was deviated owing to the distortion of its pilot wave, a form of macroscopic particle diffraction. The impact parameter y_i, defined as the location of the incident trajectory of the walker relative to the centreline of the slit, was varied so as to uniformly span the slit, in order to best approximate an incident plane wave.

The principal inferences of Couder and Fort's [2] study were threefold. First, the deflection angle α was independent

of the impact parameter y_i. Second, the emerging statistical pattern corresponded roughly to the amplitude of the Fraunhofer diffraction pattern of a monochromatic plane wave impinging on the slits. Third, in the double-slit arrangement, the wave interacts with both slits; thus, the trajectory of the walker is altered by the presence of the second slit, an indication of single-particle interference on the macroscale. Their experimental results in the single-slit geometry were roughly reproduced by numerical simulations in which the walls were modeled by periodically spaced secondary wave sources that locally damp the walker wave field [117].

The results of Couder and Fort [2] were contested on statistical grounds by Bohr and co-workers [19, 20], who pointed out that in the double-slit arrangement, the limited amount of data (75 independent trajectories) was insufficient to conclude that an interference pattern emerged. Specifically, the fit with a Gaussian distribution was as good as that with the amplitude of the inferred Fraunhofer diffraction pattern. The experimental results of Andersen *et al* [19] were also at odds with those of Couder and Fort [2], in that they observed a strong correlation between the diffraction angle and the impact parameter y_i. Moreover, no coherent diffraction pattern was apparent in their experiments. Subsequently, Rode *et al* [24] reported direct measurements of the wave fields in the vicinity of the slits, which they found were only weakly altered by the presence of the second slit.

Pucci *et al* [23] revisited the single and double-slit experiments of Couder and Fort [2] with a refined experimental set-up that allowed for a systematic characterization of the dependence of the walker behavior on drop size and memory. Notably, their study made clear the importance of shielding the system from air currents, a precaution not taken in previous experiments [2, 19, 272]. As the drop size and memory were not reported in the original experiments of Couder and Fort [2], it was not possible to reexamine the parameter regime originally considered. In the bulk of the experiments reported by Pucci *et al* [23], there was a strong correlation between deflection angle and impact parameter (figures 13(b) and (c)). This correlation vanished only at the highest memory considered, $\gamma/\gamma_F = 0.998$, in a small-drop parameter regime characterized by chaotic walking and unpredictable trajectories (figures 13(d) and (e)).

In all cases considered, the system behavior was dominated by the tendency for a drop to follow a path with a fixed angle relative to the plane of the slits, the same angle arising in nonspecular reflection from a submerged barrier [203]. The three dominant central peaks apparent in the diffraction patterns of Couder and Fort [2] were thus evident in the majority of the parameter regimes considered by Pucci *et al* [23]; however, the dependence of the number of peaks on the slit width apparent in Fraunhofer diffraction was not evident. Nevertheless, in the double-slit geometry, a key quantum feature contested by Bohr and co-workers [19, 20, 24] was recovered: the droplet is influenced by both slits by virtue of the spatial extent and persistence of its guiding wave field (figure 13(f)). The experimental behavior was well captured by the model of Faria [22] (section 4.7): discrepancy between simulation and experiment arose only at the very highest memories, where the droplet bouncing becomes chaotic, so the walker dynamics cannot be expected to be adequately described by a model based on the assumption of periodic bouncing. Walker diffraction by single and double slits was recently revisited by Ellegaard and Levinsen [25], who undertook the most comprehensive exploration of parameter space to date. Their experimental results were largely consistent with those reported by Pucci *et al* [23], but also revealed new, relatively rich diffraction behavior in the double-slit arrangement.

Diffraction is a feature of waves, both on macroscopic and microscopic scales. Due to the association of a particle with a wave in quantum mechanics, single-particle diffraction has generally been thought to be exclusive to the quantum realm. However, diffraction may also be a feature of classical objects, provided they have an associated wave component. For example, Schiebel *et al* [273] have shown that snakes slithering through an array of posts exhibit a form of diffraction. One should not find it surprising that the walker diffraction pattern is different from that arising in single-electron diffraction. First, there is little reason to believe that the walker's pilot wave has a form similar to that of an electron. Second, the geometries are markedly different: in electron diffraction, the characteristic gap width is typically a thousand de Broglie wavelengths, while in the walker system, the gap width is comparable to a single Faraday wavelength. Third, the influence of the hydrodynamic pilot wave is limited by viscous damping.

Nevertheless, the mechanisms for both single-particle diffraction and interference in the hydrodynamic system are clear. Diffraction arises owing to the distortion of the drop's guiding wave by the slit arrangement. Interference by the second slit may arise through its acting to alter the global wave field, specifically that beneath the walker. Both mechanisms rely explicitly on the hereditary nature of the walker system and the spatial delocalization of the walker associated with its pilot-wave field; moreover, both are limited by viscous wave damping. Recent developments in pilot-wave hydrodynamics suggest the manner in which one might find richer diffraction behavior in a generalized pilot-wave framework (see section 9). Notably, in the special case considered in hydrodynamic quantum field theory (HQFT) [88], to be detailed in section 9.3, the pilot-wave field in the vicinity of the particle takes the form of a plane wave with the de Broglie wavelength [89].

8.4. Walker scattering from pillars and wells

Harris *et al* [172] examined the interaction of walking droplets with a submerged circular pillar. At low memory, simple scattering events, characterized by a relatively rapid deflection by some angle, are the norm. However, at high memory the drop departs the pillar along a path corresponding to a logarithmic spiral (figures 14(a)–(d)). The form of the spiral is independent of the droplet's impact parameter: there is a universal spiral emerging for a given drop size, pillar size and memory. The pitch angle increases with vibrational forcing: the trajectory approached but never reached a circular orbit in the high-memory limit (figure 14(e)). Because the drop speed remains equal to the free walking speed along the spiral, and

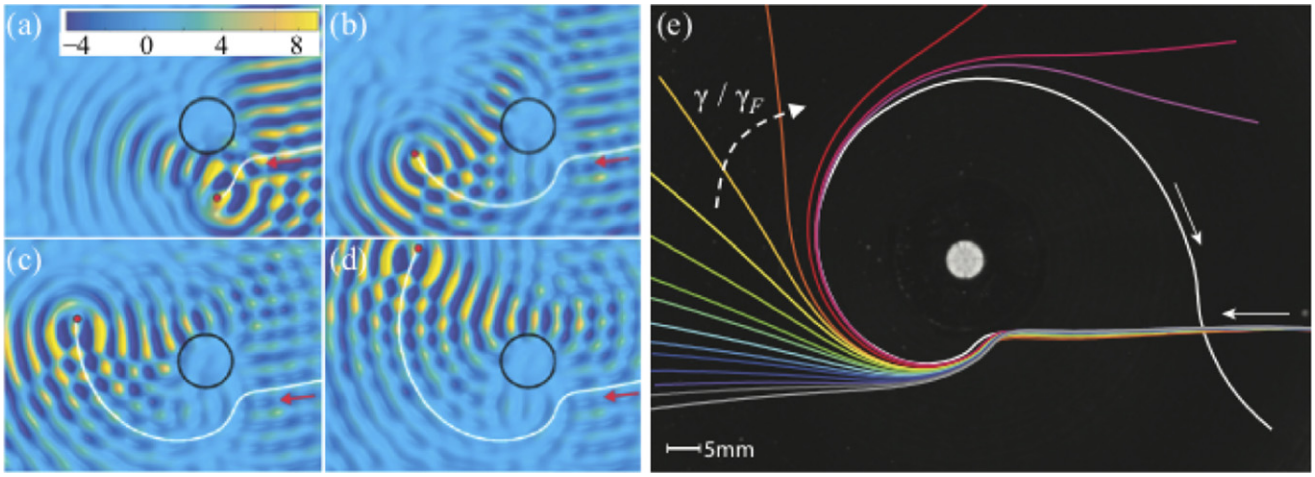

Figure 14. Walker scattering [172]. (a)–(d) Surface topography measurements of a walker interacting with a submerged pillar of radius 5 mm (black circle) [204]. The white curve indicates the walker's trajectory: a rectilinear approach path transitions to an outgoing logarithmic spiral. The color bar indicates the wave amplitude in microns. (e) A droplet spirals about a pillar with radius 2.5 mm. As γ/γ_F increases from 0.97 to 0.99, the drop spends more time on a spiral path. Adapted from [172], with the permission of AIP Publishing.

the drop accelerates slowly along the spiral, the system was ideally suited to application of the boost model (equation (21), [229]). An effective force due to the presence of the pillar was inferred, and found to be a lift force, $\boldsymbol{F}_p = m_w\,\boldsymbol{\Omega} \times \dot{\boldsymbol{x}}_p$, proportional to the boosted walker mass, m_w and the cross product of the drop's velocity $\dot{\boldsymbol{x}}_p$ and instantaneous angular velocity about the post, $\boldsymbol{\Omega}$. When the equivalent form of the Coriolis and Lorentz forces is considered, this memory-induced lift force is seen to be suggestive of self-induction: the drop moves as would an electric charge in the magnetic field generated by its own current. This system presents a clear macroscopic example of pilot-wave-mediated forces giving rise to apparent action at a distance.

Sáenz *et al* [18] considered a droplet walking in a shallow bath, interacting with a deep circular well (figure 15). Here, the walker was drawn inwards along an Archimedean spiral toward the well center. At high memory, the inferred well-induced force once again takes the form of a non-local lift force. After the drop crosses the well center, it moves radially outwards, with speed oscillations arising over a lengthscale corresponding to the Faraday wavelength. A superposition of an ensemble of incident trajectories (figure 15(b)) reveals that these speed oscillations leave a circularly symmetric statistical signature with the Faraday wavelength (figure 15(c)). This arrangement provides a hydrodynamic analog of Friedel oscillations, the statistical signature of electrons on a metallic surface scattering off an impurity [274, 275]. While walker speed oscillations have been reported elsewhere in both experiments [10, 13, 168, 215] and simulations [215, 276], their role in the emergent statistical behavior of walking droplets had not previously been noted and may be more prevalent than previously believed. Indeed, the origins of the statistical form emerging in the large corrals [10, 13] may be rooted in such speed oscillations induced by boundary collisions [208], in conjunction with the walker reflection laws [203]. These in-line speed oscillations represent a new paradigm for the emergence of a statistical signature with the wavelength of the pilot wave, one that does not rely on the presence of chaos.

9. Generalized pilot-wave framework

We have detailed the three key features responsible for emergent quantum-like behavior in the hydrodynamic pilot-wave system. First, the pilot-wave must be generated by the particle; a free particle thus responds only to its own field. Second, there must be a memory of the particle path recorded in the pilot-wave field, which renders the particle dynamics hereditary. Third, there must be resonance between the particle and wave field, which ensures that the pilot wave field be quasi-monochromatic. Having established these essential features of the hydrodynamic pilot-wave system, one may define a new class of dynamical systems with these features, and dispense with other nonessential details, including peculiarities of the hydrodynamic pilot-wave system, with a view to broadening the range of classical pilot-wave dynamics and to capturing new quantum analogs.

9.1. Parametric generalizations

The exploration of a simple parametric generalization of the hydrodynamic pilot-wave system was proposed by Bush [3], and has been profitably explored by a number of investigators [27, 36, 48, 266, 276]. The constant-phase stroboscopic model (12) discussed in section 4.3 may be non-dimensionalized to yield

$$\kappa_0(1-\Gamma)\ddot{\boldsymbol{x}}_p + \dot{\boldsymbol{x}}_p = -\frac{2}{(1-\Gamma)^2}\nabla\tilde{h}(\boldsymbol{x}_p, t),$$
$$\tilde{h}(\boldsymbol{x}, t) = \int_{-\infty}^{t} J_0(|\boldsymbol{x} - \boldsymbol{x}_p(s)|)\mathrm{e}^{-(t-s)}\,\mathrm{d}s, \qquad (25)$$

where $\kappa_0 = k_F\sqrt{m^3gA/2D^3T_F}$ is the dimensionless mass and $\Gamma = (\gamma - \gamma_W)/(\gamma_F - \gamma_W)$ the dimensionless forcing acceleration, that assumes the value $\Gamma = 0$ at the walking threshold $\gamma = \gamma_W$ and $\Gamma = 1$ at the Faraday threshold $\gamma = \gamma_F$ [3]. The dimensionless mass κ_0 varies over the limited range 0.9–2.2 for the parameter regimes explored to date in the

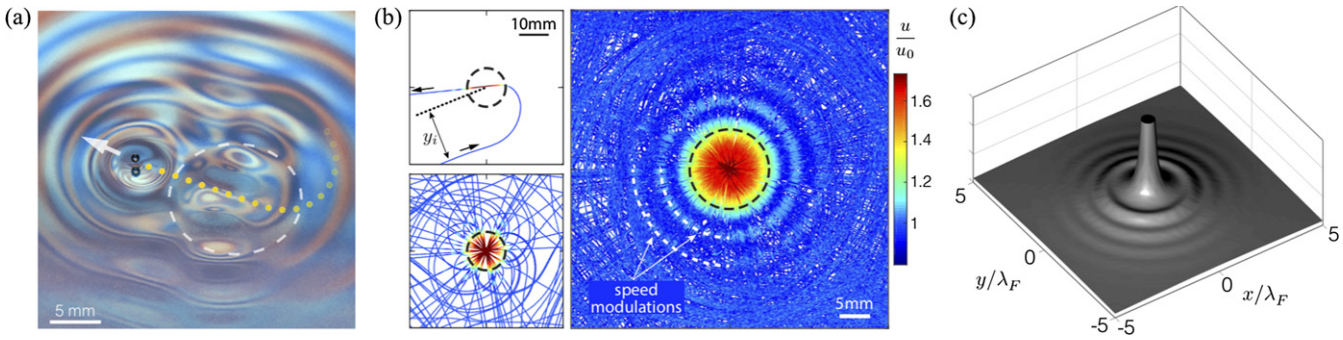

Figure 15. Hydrodynamic analogue of Friedel oscillations [18]. (a) Oblique view of a droplet trajectory (yellow dots) passing over a submerged circular well (dashed white circle). (b) The drop spirals inward toward the well along an Archimedean spiral, then exits the well radially. Color coding the trajectories according to the drop speed, u/u_0, indicates speed oscillations in the outgoing phase. The right panel shows an ensemble of 449 droplet trajectories in the high-memory limit, $\gamma/\gamma_F = 0.99$. (c) The radial speed modulations give rise to a Friedel-like signature in the histogram of the droplet position. From [18]. Adapted with permission from AAAS.

hydrodynamic pilot-wave system, but may be assigned any value in this generalized framework.

Oza *et al* [17] and Labousse *et al* [26] explored theoretically the possibility of hydrodynamic spin states, wherein the walker executes a circular orbit despite the absence of an external force. While it was previously shown [17] that, without external confinement [26], spin states are unstable in the laboratory, Oza *et al* [27] assessed the stability of spin state solutions to equation (25) for all values of κ_0 and Γ. They showed that the spin states of radius $r_0 \approx \lambda_F/2$ could be stabilized for sufficiently small values of the dimensionless mass, $0 \leqslant \kappa_0 \lesssim 0.2$, for a range of forcing accelerations.

Tambasco and Bush [266] examined a walker interacting with a spatially oscillating radial potential of Bessel form using numerical simulations of equation (25). By suitable choice of κ_0 and Γ, they were able to find a parameter regime in which the walker switched intermittently between weakly unstable circular orbits, and settled into a statistically steady state but never a stable orbit. They also deduced that, in this setting, the timescale of statistical convergence was an order of magnitude greater than the memory time. Valani and Slim [48] used a variant of equation (25) as the basis for numerical simulations of two identical in-phase walkers. In addition to the orbiting and promenading modes observed in walker experiments (section 5.1), they discovered a variety of exotic trajectories (figure 16).

In the Hong–Ou–Mandel (HOM) interference experiment [277], two photons arrive at a beam splitter, and two detectors far from the splitter record the arrival of the photons. As the distance between the photon source and detectors is varied continuously, the probability that a photon is detected by both detectors exhibits a dip and eventually vanishes, which is the so-called HOM effect. Valani *et al* [36] conducted a numerical study of two walkers launched toward a common point of intersection. For a parameter regime (κ_0, Γ) comparable to that of the walkers, they deduced the probability that the pair forms bound states (either orbiting, promenading or drafting). Such binding events correspond to a dip in the probability of the pair continuing unperturbed, so give rise to a statistical signature akin to the HOM effect.

Finally, equation (25) was adapted by Durey *et al* [276] to examine the prevalence of in-line oscillations for one-dimensional motion in this generalized pilot-wave framework. They delineated distinct parameter regimes characterized by underdamped oscillations, of the form reported by Sáenz *et al* [18] in their study of analog Friedel oscillations, periodic speed oscillations of the form reported by Wind-Willassen *et al* [168] and Bacot *et al* [215], and periodic and aperiodic jittering modes. In the jittering modes, the droplet bounces in place until its pilot wave grows sufficiently to propel it into a nearby wave trough. The process may result in either rectilinear periodic motion, or aperiodic motion characterized by irregular reversals in direction. The latter results in a random-walk-like dynamics and emergent quantum-like statistics reminiscent of those reported for particle motion along a line in the presence of a spring force [35]. Moreover, it leads to a characteristic diffusivity $D \sim u_0\lambda_F$, a result that evokes Nelson's stochastic dynamics [83, 84] (section 2.5). A similar random-walk-like behavior was observed theoretically in simulations of the path-memory model (6) by Hubert *et al* [216], who found that, at high memory, a walker's motion is ballistic over short timescales, sub-diffusive over intermediate timescales and diffusive over long timescales. Finally, in-line oscillations were also prevalent in the simulations of Durey [278], who reduced the equations for one-dimensional pilot-wave dynamics to a form similar to the Lorenz system [279].

9.2. *Further generalizations*

Further generalizations of the pilot-wave framework (25) will yield additional insights into the viability of pilot-wave mechanics as a classical dynamical underpinning of quantum statistics. An obvious possibility is altering the kernel in the wave force, as prescribes both the wave form and its spatio-temporal damping. One could also relax the assumption of perfect particle-wave resonance, and so include a richer dynamics of the form explored in the variable-phase stroboscopic model [50]. Another possibility is the inclusion of a stochastic background field, which would in principle allow for one to encompass pilot-wave dynamics and stochastic mechanics in a single theoretical framework. Extensions to

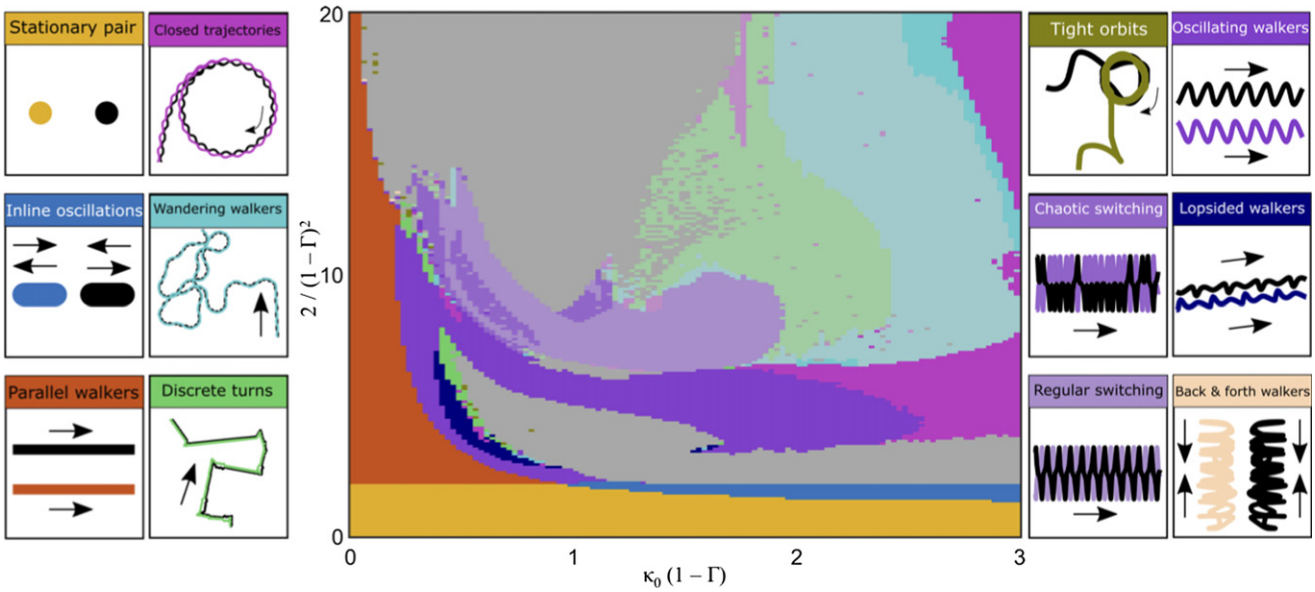

Figure 16. Simulations indicate the rich behavior of identical in-phase particle pairs accessible within the generalized pilot-wave framework (section 9.1) [48]. In gray regions, the pair becomes unbound. Colored regions correspond to the bound states depicted in the legend. Adapted from [48], with the permission of AIP Publishing.

three-dimensions, while not difficult conceptually, have thus far met with limited success.

There is little reason to believe that walker-boundary interactions are closely related to those arising at a microscopic scale; thus, various possibilities for boundary conditions in pilot-wave dynamics should also be explored. Dubertrand *et al* [21] presented a model of single-slit diffraction [2, 19, 20, 23, 24] in which walkers are scattered by a pair of nearby submerged barriers. They time-averaged the trajectory equation (8) over the bouncing period, and considered a wave field h of the form

$$h(\boldsymbol{x}, t_n) = -A \sum_{k=-\infty}^{n-1} \mathrm{Im}[G(\boldsymbol{x}, \boldsymbol{x}_k)] \mathrm{e}^{-(n-k)T_\mathrm{F}/T_\mathrm{M}}. \qquad (26)$$

Here, G is the Green's function for the Helmholtz equation $(\Delta + k_\mathrm{F}^2)G(\boldsymbol{x}, \boldsymbol{x}_0) = \delta(\boldsymbol{x} - \boldsymbol{x}_0)$ with Neumann boundary conditions on the obstacles and outgoing radiation boundary conditions at infinity. Their numerical simulations show that, while the walker does indeed scatter when passing through the slit, the deflection angles are substantially smaller than those reported in the walker system [2, 19, 20, 23, 24].

Devauchelle *et al* [280] developed a similar pilot-wave model, but replaced the δ-function in the Helmholtz equation by different functional forms to account for the particle's finite size. They neglected the particle inertia, and posited that the particle's velocity is proportional to the local surface wave gradient. Their combined analytical and numerical approach enabled them to demonstrate the existence of a self-propelling state resembling rectilinear walking; moreover, particle interaction with boundaries lead to in-line oscillations.

Broadening the scope of pilot-wave dynamics even further, Fort and Couder [281] proposed a theoretical model for a so-called 'inertial walker' which consists of a self-propelling particle that generates waves that continue to propagate in the particle's inertial frame at the time of emission, the result being an interference pattern different from that in the walker system. The authors show that the wave field generated by the circular motion of an inertial walker along an orbit of radius r_0 admits resonant wave modes when the orbital perimeter $2\pi r_0$ is an integer multiple of the Faraday wavelength λ_F, a condition analogous to the Bohr–Sommerfeld quantization rule [282].

9.3. Hydrodynamically-inspired quantum field theory

Several authors have attempted to formulate a form of quantum dynamics based on insights gained from the walker system. Andersen *et al* [19] explored the behavior of a dynamical system in which a particle locally excites a waveform satisfying Schrödinger's equation, then moves in response to gradients of the phase of that field. Orbital quantization was shown to arise naturally, along with an analog to the Bohr–Sommerfeld quantization rule; however, they concluded that their model was not capable of giving rise to behavior analogous to that arising in the quantum double-slit experiment. Borghesi [87] proposed an elastic pilot-wave model wherein a point particle moves within a non-dissipative elastic substrate. The coupled dynamics of the particle and elastic medium are governed by a modified Klein–Gordon equation. When the particle speed is small relative to the elastic wave speed, it is proportional to the gradient of the phase of the wave, a result that evokes de Broglie's guidance equation. Shinbrot [283] examined the Klein–Gordon equation with an oscillatory potential as a model for a quantum particle emitting and absorbing pilot waves. He concluded that bound state solutions with half-integer spin exist provided the particle rest mass oscillates in time, another result evocative of de Broglie's physical picture [130]. Most recently, Drezet *et al* [284] presented a mechanical analog of quantum bradyons and tachyons

Table 3. Different pilot-wave theories put into the general framework of equations (27) and (28). The pilot-wave phase S is defined through the equation $u = |u|e^{iS/\hbar}$, where u is ϕ (for de Broglie's double-solution theory [80]) or ψ (for Andersen *et al* [19]).

Model	Trajectory equation	$\boldsymbol{u}$	$\boldsymbol{\mathcal{L}}$	$\boldsymbol{f}(\boldsymbol{x},t)$
Stroboscopic (12) Oza *et al* [205]	$m\ddot{\boldsymbol{x}}_\mathrm{p} + D\dot{\boldsymbol{x}}_\mathrm{p} = -F\boldsymbol{\nabla}h(\boldsymbol{x}_\mathrm{p},t)$	h	$-1/T_\mathrm{M}$	$J_0(k_\mathrm{F}\lvert\boldsymbol{x}\rvert)$
Faraday waves (13)–(15) Milewski *et al* [44]	$m\ddot{\boldsymbol{x}}_\mathrm{p} + D\dot{\boldsymbol{x}}_\mathrm{p} = -F(t)\boldsymbol{\nabla}h(\boldsymbol{x}_\mathrm{p},t)$	$\begin{pmatrix} h \\ \phi \end{pmatrix}$	$\begin{pmatrix} 2\nu\Delta & \mathcal{D} \\ \frac{\sigma}{\rho}\Delta - g(t) & 2\nu\Delta \end{pmatrix}$	$\begin{pmatrix} 0 \\ -P_\mathrm{D}(\lvert\boldsymbol{x}\rvert,t)/\rho \end{pmatrix}$
Bohmian mechanics [81, 82]	$m\ddot{\boldsymbol{x}}_\mathrm{p} = -\boldsymbol{\nabla}\left(-\frac{\hbar^2}{2m}\frac{\Delta\lvert\psi(\boldsymbol{x}_\mathrm{p},t)\rvert}{\lvert\psi(\boldsymbol{x}_\mathrm{p},t)\rvert}\right)$	ψ	Schrödinger equation $\frac{i\hbar}{2m}\Delta$	0
Schrödinger particle Andersen *et al* [19]	$\dot{\boldsymbol{x}}_\mathrm{p} = \frac{\boldsymbol{\nabla}S(\boldsymbol{x}_\mathrm{p},t)}{m}$	ψ	Schrödinger equation	$-\frac{i}{\hbar}A(t)\delta(\boldsymbol{x})$
de Broglie's double solution [80]	$\dot{\boldsymbol{x}}_\mathrm{p} = -c^2\frac{\boldsymbol{\nabla}S}{\partial S/\partial t}$	$\begin{pmatrix} \phi \\ \phi_t \end{pmatrix}$	Klein–Gordon equation $\begin{pmatrix} 0 & 1 \\ c^2\Delta - \omega_\mathrm{c}^2 & 0 \end{pmatrix}$	Unspecified
Hydrodynamic QFT [88]	$\dot{\boldsymbol{x}}_\mathrm{p} = -\alpha\boldsymbol{\nabla}\phi(\boldsymbol{x}_\mathrm{p},t)$	$\begin{pmatrix} \phi \\ \phi_t \end{pmatrix}$	Klein–Gordon equation	$-\epsilon_\mathrm{p}\sin(2\omega_\mathrm{c}t)\delta_a(\boldsymbol{x})$

through consideration of a vibrating particle propelling itself along a frictionless string.

Dagan and Bush [88] have extended de Broglie's double-solution mathematical program through positing the form of the dynamic interactions of waves and particles on the Compton scale, including the mechanism for particle-induced wave generation. They model the particle as a localized periodic disturbance in the Klein–Gordon field at twice the Compton frequency (table 3). As in pilot-wave hydrodynamics, the particle is propelled by gradients in the amplitude of its pilot-wave field. Resonance is achieved between the particle and its pilot wave, leading to self-excited motion of the particle. Like the hydrodynamic bouncing state above the walking threshold, the stationary state gives way to a dynamic state characterized by quasi-steady self-propulsion of the particle. Notably, the mean speed rapidly converges to a value consistent with the de Broglie relation, $p = \gamma_\mathrm{L} m_0 v = \hbar k_\mathrm{B}$. Moreover, the particle motion is characterized by relativistic in-line oscillations with frequency ck_B and wavelength λ_B, reminiscent of the Zitterbewegung featured in early models of quantum dynamics [143, 145]. Their results suggest a new trajectory-based interpretation of the quantum dispersion relation, $\omega^2 = \omega_\mathrm{c}^2 + c^2k_\mathrm{B}^2$: the first term corresponds to the energy of internal vibration and wave generation, the second to the kinetic energy associated with in-line oscillations. The hydrodynamic pilot-wave system has made clear that in-line oscillations provide a mechanism for a statistical signature with the oscillation wavelength [18]. One can thus readily imagine how statistical signatures with the de Broglie wavelength might emerge on the quantum scale.

Analysis of this HQFT [89] has revealed that there is a critical wave–particle coupling constant beyond which self-propulsion ensues, the analog of the walking threshold. In two dimensions, when strobed at the Compton frequency, the pilot-wave form in the vicinity of the particle takes the form of a plane wave with the de Broglie wavelength. Consequently, the local gradient of the wave amplitude is proportional to that of the wave phase, indicating that the wave–particle coupling considered in HQFT is consistent with that proposed by de Broglie [80] (table 3). In the relativistic limit, the de Broglie wavelength approaches the Compton wavelength, suggesting the possibility of quantization and structure on the Compton scale. For example, spin states in HQFT might correspond to the classical model of the electron [144]. HQFT thus promises the possibility of accounting for the emergence of quantization and a statistical signature on the de Broglie wavelength for non-relativistic mechanics, and structure on the Compton scale for relativistic mechanics. Further explorations of two-dimensional HQFT, extensions to three-dimensions, and coupling to the ensemble interpretation of quantum mechanics [103], will determine its viability as a trajectory-based description of quantum systems.

9.4. General particle-wave framework

The bulk of the pilot-wave models reviewed herein, both hydrodynamic and quantum, have the form

$$\mathcal{D}_t[\boldsymbol{x}_\mathrm{p}] = \boldsymbol{G}\left(\boldsymbol{u}(\boldsymbol{x}_\mathrm{p},t), \boldsymbol{u}_t(\boldsymbol{x}_\mathrm{p},t), \boldsymbol{\nabla}\boldsymbol{u}(\boldsymbol{x}_\mathrm{p},t), \Delta\boldsymbol{u}(\boldsymbol{x}_\mathrm{p},t), \dots\right), \tag{27}$$

$$\boldsymbol{u}_t = \boldsymbol{\mathcal{L}}\boldsymbol{u} + \boldsymbol{f}(\boldsymbol{x} - \boldsymbol{x}_\mathrm{p}, t), \quad \boldsymbol{u} = (h, \phi, \dots). \tag{28}$$

The particle trajectory is described by equation (27), the pilot-wave evolution by (28). In the trajectory equation, the time-derivative operator $\mathcal{D}_t$ acts on the particle position $\boldsymbol{x}_\mathrm{p}$, giving rise to time-derivative terms that must be balanced by some function $\boldsymbol{G}$ of the set of variables $\boldsymbol{u}$ characterizing the pilot-wave field, evaluated at the particle position. For hydrodynamic pilot-wave theory, these variables $\boldsymbol{u}$ include the wave height h and possibly other quantities, for example the velocity potential ϕ of the liquid bath in the formulation of Milewski *et al* [44]. In the evolution equation (28) for $\boldsymbol{u}$, the wave variables, $\boldsymbol{f}$ denotes the localized particle-induced forcing and $\boldsymbol{\mathcal{L}}$ is a linear differential operator. We note that Duhamel's principle, which states that the solution to an inhomogeneous linear

evolution equation such as equation (28) may be expressed as a time-integral over the history of the forcing $\boldsymbol{f}$, necessarily implies that the memory of the particle's trajectory $\boldsymbol{x}_{\rm p}(t)$ is encoded in the wave variables $\boldsymbol{u}$.

Table 3 shows how several of the hydrodynamic and quantum pilot-wave models may be put into this general pilot-wave framework. The hydrodynamic pilot-wave theories describe a balance between particle inertia, drag and the propulsive wave force, so $\mathcal{D}_t[\boldsymbol{x}_{\rm p}] = m\ddot{\boldsymbol{x}}_{\rm p} + D\dot{\boldsymbol{x}}_{\rm p}$. In the stroboscopic model (12), $\boldsymbol{u} = h$, $\boldsymbol{f}(\boldsymbol{x}, t) = J_0(k_{\rm F}|\boldsymbol{x}|)$ and $\boldsymbol{\mathcal{L}} = -1/T_{\rm M}$. In the Faraday pilot-wave model, (13)–(15), $\boldsymbol{u} = (h, \phi)$ and $\boldsymbol{f}(r, t) = (0, -P_{\rm D}(r, t)/\rho)$ is the localized particle-induced forcing. The linear operator $\boldsymbol{\mathcal{L}}$ contains the Dirichlet-to-Neumann map for the velocity potential ϕ, $\mathcal{D}[\phi|_{z=0}] = \phi_z|_{z=0}$, which reduces the partial differential equations (13)–(15) on the domain $z \leqslant 0$ to the free surface $z = 0$.

In Bohmian mechanics [81, 82], there is no drag: the particle inertia is balanced by the gradient of the quantum potential, whose form depends on the wave function ψ that evolves according to Schrödinger's equation. Notably, the Schrödinger equation is not forced by the particle, so $\boldsymbol{f} = 0$; that is, particles are driven by the wave function, but the origins of this wave function are not specified [284]. This deficit was also a feature of de Broglie's double solution theory [80], where the functional form of the particle-induced wave forcing $\boldsymbol{f}$ was not specified. HQFT [88, 89] specifies this wave forcing in a manner informed by the hydrodynamic system.

10. Discussion and future directions

The walking droplets represent a macroscopic example of a particle moving in synchrony with its own wave field, one in which the particle-wave interaction is both visible and resolved theoretically. Growing evidence suggests that its range as a quantum analog is limited by the viscous damping of the pilot-wave field, and by the influence of drop inertia, features of the walker system that may be sidestepped within a generalized pilot-wave framework. If microscopic particles are indeed characterized by a high-frequency vibration at the Compton frequency, the theoretical description of walking droplets may yield insight into their dynamics. For example, it raises the possibility that the runaway solutions in the Lorentz-Abraham-Dirac equation may result from an unresolved dynamics on the Compton scale [233, 286, 287].

10.1. The emerging physical picture

Three features of pilot-wave hydrodynamics are critical to the emergence of its quantum-like features. The first is the association of the particle with a self-propelling wave source. The second is the resonance between the particle and wave, which results in the highly structured wave field whose form is responsible for the emergence of quantum-like features. The third is path memory, the ability of the drop to store information on the bath surface, the feature responsible for the temporal non-locality of the drop dynamics that may result in the misinference of spatial nonlocality. The first two are explicitly features of de Broglie's double solution theory: the droplet bouncing plays the role of the particle vibration in de Broglie's theory, and the wave-droplet resonance that of the harmony of phases in de Broglie's mechanics [3]. The third is not explicit in de Broglie's mechanics, but is a feature of the hereditary particle-wave interactions considered by Brillouin [288], who showed that for the case of a particle moving faster than its wave field, orbital quantization may naturally emerge.

Three paradigms have now been established for the emergence of quantum-like statistics from pilot-wave dynamics of the form engendered in the walker system. The first relies on the chaotic switching between weakly unstable quantized periodic dynamical states, the second on in-line oscillations of the walker speed, the third on the droplet's random-walk-like motion across its pilot-wave field. The first two are evident in the walker system, the third in theoretical models thereof. All three rely on the highly structured, quasi-monochromatic form of the pilot-wave field, and so depend critically on the resonant interaction between the droplet and its guiding wave.

The first paradigm arose from studies of walkers in closed environments, their motion confined by either boundaries or imposed forces. Examples include the small corral experiments [10, 14], where the walker range is prescribed by the corral radius; walker motion in a simple harmonic potential [29, 30, 32, 33, 220], where the drop range is prescribed by the effective applied spring constant, $L \sim u_0\sqrt{m/k}$; and walker motion in a rotating frame [15–17, 219], where the effective range is prescribed by the radius of the inertial orbit, $L \sim u_0/2\Omega$. The quantized orbital states emerge in these systems owing to the dynamic constraint imposed on the droplet by its pilot wave, when the crossing time, $T_{\rm C} \sim L/u_0$, is less than the memory time, $T_{\rm M} \sim T_{\rm d}/(1 - \gamma/\gamma_{\rm F})$ [32]. This criterion implies that in crossing its domain, a walker is always navigating a background potential of its own making. In the high-memory limit, the quantized periodic orbital states destabilize, and chaotic switching between these weakly unstable states leads to the emergence of multimodal, quantum-like statistics.

The second paradigm for the emergence of quantum-like statistics was identified in the hydrodynamic quantum analog of Friedel oscillations [18]. A number of prior studies identified the walkers' tendency to execute in-line speed oscillations with a wavelength comparable to the Faraday wavelength. Specifically, such oscillations were first reported in the experiments of Wind-Willassen *et al* [168], and are also apparent in the drop speed maps reported in the corral experiments [10, 13] (figures 10(b) and 11(b)). In-line speed oscillations were characterized experimentally and numerically by Bacot *et al* [215], whose simulations suggest that they arise in a relatively broad region of parameter space. The statistical signature associated with such oscillations is readily apparent in the analog Friedel oscillations [18], but may also play a role in other settings, including wall reflection [203, 208], tunneling [9] and large corrals [10, 13]. The prevalence of in-line oscillations in the context of a generalized pilot-wave theory has recently been examined by Durey *et al* [276]. Finally, in-line oscillations with the de Broglie wavelength and the Compton frequency, reminiscent of the Zitterbewegung motion of early models of quantum dynamics [143, 145] are a robust feature

of HQFT [88, 89], suggesting the possibility of an analogous dynamical feature on the microscopic scale.

The third such paradigm relies on the droplet interacting with its wave field in such a way as to execute a random walk with a step length comparable to λ_F, resulting in an effective diffusivity $D \sim U\lambda_F$, where U is the mean walker speed. This type of diffusive motion was first identified, in simulations of walkers in a corral, by Gilet [11, 12], who noted the similarity to the behavior of quantum particles in Nelson's stochastic mechanics [83]. Such motion has since been captured in high-memory simulations of free walkers [216] and one-dimensional walker motion in the presence of a confining spring force [35]. Such episodic motion has also been reported in experimental investigations of walkers above the Faraday threshold [157], and for subcritical two-frequency vibrational forcing [200]. The emergent diffusive behavior was also seen to accompany the chaotic 'jittering' mode captured theoretically by Durey *et al* [276] in their exploration of the generalized pilot-wave framework, and similar dynamics were reported by Dagan and Bush [88] in their simulations of HQFT.

The hydrodynamic pilot-wave system is extraordinarily rich, characterized by many disparate timescales ranging from a fraction of a second to hours, all of them accessible in the laboratory. First, the Faraday period T_F is the timescale of wave generation, twice the bath's driving period. Second, the memory time T_M prescribes the longevity of the pilot wave. Third, there is the translation timescale, $T_H = \lambda_F/u_0$; fourth, that of the drop's horizontal acceleration, T_A. For closed systems of extent L, there are three additional timescales: the crossing time $T_C = L/u_0$, the timescale of establishment of the mean pilot-wave field, and the timescale of statistical relaxation, beyond which the system has converged to a statistically steady state. These last two both scale with the memory time, but the latter is typically an order of magnitude larger than the former [266]. One can also define a recurrence time T_R, the time taken for a particle to cross its own path. While $T_R/T_C = 1$ for one-dimensional motion, it will increase dramatically in two and three dimensions. One can well imagine that $T_R \leqslant T_M$ is a requirement for quantum behavior, one that will be progressively more difficult to satisfy in higher dimensions. Note that various theoretical models have emerged in the limits where there is a disparity between these various timescales. For example, the stroboscopic model (12) [205] is based on the assumption that $T_F \ll T_H$, the boost equation (21) [229] that $T_M \ll T_A$ and the Rayleigh oscillator model [232] that $T_M \ll (T_A, T_H)$. Notably, the great majority of these timescales are absent from the standard quantum mechanical description of microscopic systems, where particle dynamics is not described. The exploration of the various asymptotic limits in the context of a generalized pilot-wave framework poses a substantial mathematical challenge.

The limitations of the hydrodynamic system are associated with two physical effects that are not features of de Broglie's pilot-wave theory, specifically, pilot-wave damping and particle inertia. The limiting influence of viscosity is immediately clear from the fact that the quantum phenomena invariably arise in the high-memory limit, when the pilot wave is most persistent. The limitation imposed by finite droplet inertia is suggested by the stability of spin states [27] and the instability to in-line oscillations [276] being enhanced in the small-inertia limit. The inviscid, low inertia limit is currently being explored in the walker-inspired HQFT [88, 89].

10.2. Reinterpretation

Hydrodynamic quantum analogs has provided a perspective that allows for a classical reinterpretation of at least some of the quantum language. The walker system represents a classical realization of wave–particle duality as envisaged by de Broglie, wherein a real object has both wave and particle components. In the walker system, this duality is the root of both the emergent quantized dynamical states and the structured statistical forms. The superposition of statistical states reflects the coexistence of several weakly unstable periodic dynamical states [16, 29], a notion that is also prevalent in periodic orbit theory [257, 258]. Statistical projection effects may be induced by favoring one dynamical state over another [13].

There is no intrinsic uncertainty in the walker system: it is a classical system that evolves according to deterministic laws. Nevertheless, in many settings, the dynamics is chaotic, so predictability is lost. de Broglie's interpretation of the quantum uncertainty relations is that they are an expression of an unresolved dynamics on the Compton scale [138]. Tadrist *et al* [49] proposed that the lack of predictability in the walker system may likewise be rooted in uncertainty in the fast timescale of droplet bouncing. However, such indeterminacy is not a prerequisite for chaos, which is also apparent in simulations of the stroboscopic model [219, 221, 255], where vertical dynamics are not explicitly treated. We note further that uncertainty in the walker system can be introduced artificially through suitably intrusive measurement. Couder and Fort [2] pointed out that the deflection of a walker passing through a slit could be interpreted in terms of an effective position–momentum uncertainty relation for the walkers: when a walker is confined spatially, the momentum in the direction of confinement becomes uncertain due to walker deflection prompted by the distortion of its pilot wave. The emergent physical picture is thus that uncertainty is not intrinsic to the walker system, but may emerge as an expression of its chaotic dynamics, or in response to intrusive measurement. In the absence of intrinsic uncertainty in this coupled wave–particle system, the notion of complementarity may be seen as an unnecessary conceit.

The corral studies place in stark relief the non-problem of wave-function collapse as it pertains to the walker system. If the histogram presented in figure 10(c) were indeed a complete description of the system, then the act of observation revealing the droplet to be at a specific point would cause the spatially extended wave function to collapse instantaneously to a point. Acknowledgment of an underlying dynamics obviates the need to fret over the superluminal nature of wave-function collapse. Indeed, in this particular instance, the analog of quantum nonlocality might more sensibly be termed statistical nonlocality [289].

The walker system has also provided a number of examples where wave-mediated forces give rise to apparent action at a distance. Through their subtle influence on the pilot wave field, topographic anomalies such as submerged circular pillars [172] and wells [18] were seen in section 8.4 to give rise to nonlocal lift forces that caused the drops to follow spiral paths. In the walker double-slit experiment [2], the presence of the second slit was seen to have an influence on droplets passing through the first [23]. Without awareness of the dynamical significance of the pilot-wave field and the itinerant hereditary droplet dynamics, such forces appear to be spatially nonlocal. Richard Feynman insisted on the impossibility of understanding how an electron's path can be altered by the presence of a slit through which it does not pass [289]. The plausibility of the answer proposed some 60 years earlier by de Broglie has received support from the bouncing droplet system. The electron would interact with both slits if it were dressed by a wave field that spans and is influenced by both slits.

Another means of misinferring a spatially nonlocal dynamics in the walker system was illustrated by Durey *et al* [35], who demonstrated the nonlocal form of the mean-pilot-wave potential. Specifically, they showed that for 1D walker motion in the presence of a central spring force, in the high-memory limit the instantaneous pilot-wave field converges to its mean, whose form depends on the walker's statistical distribution. Thus, in this instance, local wave-mediated forces engender an effect on the walking droplets analogous to the quantum potential in Bohmian mechanics. However, because the instantaneous wave-field differs from the mean, the drop is also subjected to an additional force that sidesteps the nonlocality of Bohmian mechanics while simultaneously precluding the need to invoke a stochastic background forcing. This reasoning would seem to lend further credence to the view that Bohmian mechanics describes a mean quantum dynamics, an inference supported by the agreement between Bohmian descriptions of slit diffraction [120] and recent experiments on weak measurement [121].

Taken as a collective, studies of bouncer and walker lattices [38, 39, 50–55, 234, 240, 242] forge new connections between the walker system and the field of crystal vibrations, connections to be clarified and deepened through analysis of different crystal arrangements. Studies of one-dimensional coupled walker oscillators [234] and two-dimensional spin lattices [55] have revealed the possibility of wave-mediated forces giving rise to long-range synchronization and collective order. The precise relation between classical correlation, statistical indistinguishability [234] and entanglement in the walker system is the subject of ongoing investigation. Particular attention will be given to the notion that, just as nonlocality may be an expression of hereditary pilot-wave dynamics, entanglement may result from two particles having a common memory of a wave-mediated interaction that synchronized their internal clocks.

10.3. Philosophy

The walker system reminds us that much of the inscrutability of quantum mechanics and its paradoxes are forced upon us only if we insist that the statistical description of quantum particles is complete. The walker system suggests a physical picture that is compatible with the ensemble interpretations of quantum mechanics [102, 103]; however, it extends beyond the realm of interpretation in suggesting a form for the underlying dynamics of individual particles. Comparison of the walker system with Bohmian mechanics and de Broglie's original mechanics indicates that its dynamical richness renders it closer to the latter than the former. However, pilot-wave hydrodynamics has buttressed de Broglie's conception by providing a tangible example of a vibrating particle creating a quasi-monochromatic pilot-wave field, and being guided by that wave in such a way as to generate quantum-like statistics. The physical picture suggested by pilot-wave hydrodynamics, as engendered in HQFT [88, 89], comes replete with a mechanism for particle-induced wave generation, and sidesteps the need to invoke either a nonlocal potential or a stochastic background field.

While one remains free to consider the statistical description of quantum mechanics to be sufficient, it is becoming increasingly evident that this description is not incompatible with the notion of microscopic particles following trajectories. An argument against the development of a complex theory of quantum dynamics of the form suggested by the walker system is that it is not worth the effort. Occam's razor is often invoked: Why complicate the simple statistical theory of quantum mechanics with a dynamical theory that will undoubtedly be complicated and difficult to implement? One does well to remember that such an effort would be supported by an analogous philosophical Occam's razor: the development of a rational quantum dynamics would allow us to dispense with the very notion of quantum interpretation, and restore a rational view of the microscopic world.

Acknowledgments

J W M B gratefully acknowledges the financial support of the National Science Foundation (NSF) through grant CMMI-1727565. A O acknowledges the support of the Simons Foundation through the Collaboration Grant for Mathematics No. 587006.

ORCID iDs

John W M Bush https://orcid.org/0000-0002-7936-7256
Anand U Oza https://orcid.org/0000-0002-9079-9172

References

[1] Couder Y, Protière S, Fort E and Boudaoud A 2005 Walking and orbiting droplets *Nature* **437** 208
[2] Couder Y and Fort E 2006 Single particle diffraction and interference at a macroscopic scale *Phys. Rev. Lett.* **97** 154101
[3] Bush J W M 2015 Pilot-wave hydrodynamics *Annu. Rev. Fluid Mech.* **47** 269–92
[4] Bush J W M 2015 The new wave of pilot-wave theory *Phys. Today* **68** 47–53

[5] Bush J W M, Couder Y, Gilet T, Milewski P A and Nachbin A 2018 Introduction to focus issue on hydrodynamic quantum analogs *Chaos* **28** 096001

[6] Eddi A, Fort E, Moisy F and Couder Y 2009 Unpredictable tunneling of a classical wave–particle association *Phys. Rev. Lett.* **102** 240401

[7] Hubert M, Labousse M and Perrard S 2017 Self-propulsion and crossing statistics under random initial conditions *Phys. Rev.* E **95** 062607

[8] Nachbin A, Milewski P A and Bush J W M 2017 Tunneling with a hydrodynamic pilot-wave model *Phys. Rev. Fluids* **2** 034801

[9] Tadrist L, Gilet T, Schlagheck P and Bush J W M 2020 Predictability in a hydrodynamic pilot-wave system: resolution of walker tunneling *Phys. Rev.* E **102** 013104

[10] Harris D M, Moukhtar J, Fort E, Couder Y and Bush J W M 2013 Wavelike statistics from pilot-wave dynamics in a circular corral *Phys. Rev.* E **88** 011001

[11] Gilet T 2014 Dynamics and statistics of wave–particle interactions in a confined geometry *Phys. Rev.* E **90** 052917

[12] Gilet T 2016 Quantumlike statistics of deterministic wave–particle interactions in a circular cavity *Phys. Rev.* E **93** 042202

[13] Sáenz P J, Cristea-Platon T and Bush J W M 2018 Statistical projection effects in a hydrodynamic pilot-wave system *Nat. Phys.* **14** 315–9

[14] Cristea-Platon T, Sáenz P J and Bush J W M 2018 Walking droplets in a circular corral: quantisation and chaos *Chaos* **28** 096116

[15] Fort E, Eddi A, Boudaoud A, Moukhtar J and Couder Y 2010 Path-memory induced quantization of classical orbits *Proc. Natl Acad. Sci. USA* **107** 17515–20

[16] Harris D M and Bush J W M 2014 Droplets walking in a rotating frame: from quantized orbits to multimodal statistics *J. Fluid Mech.* **739** 444–64

[17] Oza A U, Harris D M, Rosales R R and Bush J W M 2014 Pilot-wave dynamics in a rotating frame: on the emergence of orbital quantization *J. Fluid Mech.* **744** 404–29

[18] Sáenz P J, Cristea-Platon T and Bush J W M 2020 A hydrodynamic analog of Friedel oscillations *Sci. Adv.* **6** 20

[19] Andersen A, Madsen J, Reichelt C, Ahl S R, Lautrup B, Ellegaard C, Levinsen M T and Bohr T 2015 Double-slit experiment with single wave-driven particles and its relation to quantum mechanics *Phys. Rev.* E **92** 013006

[20] Bohr T, Andersen A and Lautrup B 2016 Bouncing droplets, pilot-waves, and quantum mechanics *Recent Advances in Fluid Dynamics with Environmental Applications* ed J Klapp, L D G Sigalotti, A Medina, A López and G Ruiz-Chavarría (Switzerland: Springer) pp 335–49

[21] Dubertrand R, Hubert M, Schlagheck P, Vandewalle N, Bastin T and Martin J 2016 Scattering theory of walking droplets in the presence of obstacles *New J. Phys.* **18** 113037

[22] Faria L M 2017 A model for Faraday pilot waves over variable topography *J. Fluid Mech.* **811** 51–66

[23] Pucci G, Harris D M, Faria L M and Bush J W M 2018 Walking droplets interacting with single and double slits *J. Fluid Mech.* **835** 1136–56

[24] Rode M, Madsen J and Andersen A 2019 Wave fields in double-slit experiments with wave-driven droplets *Phys. Rev. Fluids* **4** 104801

[25] Ellegaard C and Levinsen M T 2020 Interaction of wave-driven particles with slit structures *Phys. Rev.* E **102** 023115

[26] Labousse M, Perrard S, Couder Y and Fort E 2016 Self-attraction into spinning eigenstates of a mobile wave source by its emission back-reaction *Phys. Rev.* E **94** 042224

[27] Oza A U, Rosales R R and Bush J W M 2018 Hydrodynamic spin states *Chaos* **28** 096106

[28] Eddi A, Moukhtar J, Perrard S, Fort E and Couder Y 2012 Level splitting at a macroscopic scale *Phys. Rev. Lett.* **108** 264503

[29] Perrard S, Labousse M, Miskin M, Fort E and Couder Y 2014 Self-organization into quantized eigenstates of a classical wave-driven particle *Nat. Commun.* **5** 3219

[30] Perrard S, Labousse M, Fort E and Couder Y 2014 Chaos driven by interfering memory *Phys. Rev. Lett.* **113** 104101

[31] Labousse M, Perrard S, Couder Y and Fort E 2014 Build-up of macroscopic eigenstates in a memory-based constrained system *New J. Phys.* **16** 113027

[32] Kurianski K M, Oza A U and Bush J W M 2017 Simulations of pilot-wave dynamics in a simple harmonic potential *Phys. Rev. Fluids* **2** 113602

[33] Durey M and Milewski P A 2017 Faraday wave-droplet dynamics: discrete-time analysis *J. Fluid Mech.* **821** 296–329

[34] Perrard S and Labousse M 2018 Transition to chaos in wave memory dynamics in a harmonic well: deterministic and noise-driven behavior *Chaos* **28** 096109

[35] Durey M, Milewski P A and Bush J W M 2018 Dynamics, emergent statistics, and the mean-pilot-wave potential of walking droplets *Chaos* **28** 096108

[36] Valani R N, Slim A C and Simula T 2018 Hong–Ou–Mandel-like two-droplet correlations *Chaos* **28** 096104

[37] Protière S, Couder Y, Fort E and Boudaoud A 2005 The self-organization of capillary wave sources *J. Phys.: Condens. Matter* **17** 3529

[38] Protière S, Boudaoud A and Couder Y 2006 Particle-wave association on a fluid interface *J. Fluid Mech.* **554** 85–108

[39] Lieber S I, Hendershott M C, Pattanaporkratana A and Maclennan J E 2007 Self-organization of bouncing oil drops: two dimensional lattices and spinning clusters *Phys. Rev.* E **75** 56308

[40] Protière S, Bohn S and Couder Y 2008 Exotic orbits of two interacting wave sources *Phys. Rev.* E **78** 036204

[41] Eddi A, Terwagne D, Fort E and Couder Y 2008 Wave propelled ratchets and drifting rafts *Europhys. Lett.* **82** 44001

[42] Borghesi C, Moukhtar J, Labousse M, Eddi A, Fort E and Couder Y 2014 Interaction of two walkers: wave-mediated energy and force *Phys. Rev.* E **90** 063017

[43] Filoux B, Hubert M and Vandewalle N 2015 Strings of droplets propelled by coherent waves *Phys. Rev.* E **92** 041004(R)

[44] Milewski P A, Galeano-Rios C A, Nachbin A and Bush J W M 2015 Faraday pilot-wave dynamics: modelling and computation *J. Fluid Mech.* **778** 361–88

[45] Oza A U, Siéfert E, Harris D M, Moláček J and Bush J W M 2017 Orbiting pairs of walking droplets: dynamics and stability *Phys. Rev. Fluids* **2** 053601

[46] Arbelaiz J, Oza A U and Bush J W M 2018 Promenading pairs of walking droplets: dynamics and stability *Phys. Rev. Fluids* **3** 013604

[47] Galeano-Rios C A, Couchman M M P, Caldairou P and Bush J W M 2018 Ratcheting droplet pairs *Chaos* **28** 096112

[48] Valani R N and Slim A C 2018 Pilot-wave dynamics of two identical, in-phase bouncing droplets *Chaos* **28** 096114

[49] Tadrist L, Sampara N, Schlagheck P and Gilet T 2018 Interaction of two walkers: perturbed vertical dynamics as a source of chaos *Chaos* **28** 096113

[50] Couchman M M P, Turton S E and Bush J W M 2019 Bouncing phase variations in pilot-wave hydrodynamics and the stability of droplet pairs *J. Fluid Mech.* **871** 212–43

[51] Eddi A, Decelle A, Fort E and Couder Y 2009 Archimedean lattices in the bound states of wave interacting particles *Europhys. Lett.* **87** 56002

[52] Eddi A, Boudaoud A and Couder Y 2011 Oscillating instability in bouncing droplet crystals *Europhys. Lett.* **94** 20004

[53] Thomson S J, Couchman M M P and Bush J W M 2020 Collective vibrations of confined levitating droplets *Phys. Rev. Fluids* **5** 083601

[54] Sáenz P J, Pucci G, Goujon A, Cristea-Platon T, Dunkel J and Bush J W M 2018 Spin lattices of walking droplets *Phys. Rev. Fluids* **3** 100508

[55] Sáenz P J, Pucci G, Turton S E, Goujon A, Rosales R R, Dunkel J and Bush J W M 2020 Emergent order in hydrodynamic spin lattices (under review)

[56] Filoux B, Hubert M, Schlagheck P and Vandewalle N 2017 Walking droplets in linear channels *Phys. Rev. Fluids* **2** 013601

[57] Vandewalle N, Filoux B and Hubert M 2019 Bragg's reflection for walking droplets in 1D crystals (arXiv:1904.05778v1)

[58] Tang J, Zhao X and Liu J 2020 Quantized orbital-chasing liquid metal heterodimers directed by an integrated pilot-wave field *Phys. Rev. Fluids* **5** 053603

[59] Sungar N, Tambasco L D, Pucci G, Sáenz P J and Bush J W M 2017 Hydrodynamic analog of particle trapping with the Talbot effect *Phys. Rev. Fluids* **2** 103602

[60] Sungar N, Sharpe J P, Pilgram J J, Bernard J and Tambasco L D 2018 Faraday–Talbot effect: alternating phase and circular arrays *Chaos* **28** 096101

[61] Chu H-Y and Fei H-T 2014 Vortex-mediated bouncing drops on an oscillating liquid *Phys. Rev.* E **89** 063011

[62] Cetto A M, de la Peña L and Valdés-Hernández A 2015 Specificity of the Schrödinger equation *Quantum Stud.: Math. Found.* **2** 275–87

[63] Grössing G, Fussy S, Mesa Pascasio J and Schwabl H 2015 Implications of a deeper level explanation of the deBroglie-Bohm version of quantum mechanics *Quantum Stud.: Math. Found.* **2** 133–40

[64] Grössing G, Fussy S, Mesa Pascasio J and Schwabl H 2018 Vacuum landscaping: cause of nonlocal influences without signaling *Entropy* **20** 458

[65] Vervoort L and Gingras Y 2016 Macroscopic oil droplets mimicking quantum behaviour: how far can we push an analogy? *Int. Stud. Philos. Sci.* **29** 271–94

[66] Vervoort L 2016 No-go theorems face background-based theories for quantum mechanics *Found. Phys.* **46** 458–72

[67] Vervoort L 2018 Are hidden-variable theories for pilot-wave systems possible? *Found. Phys.* **48** 803–26

[68] Colin S, Durt T, Willox R and de L 2017 Broglie's double solution program: 90 years later *Ann. Fond. Louis Broglie* **42** 19–71

[69] Sbitnev V I 2018 Hydrodynamics of superfluid quantum space: de Broglie interpretation of the quantum mechanics *Quantum Stud.: Math. Found.* **5** 257–71

[70] Hatifi M, Willox R, Colin S and Durt T 2018 Bouncing oil droplets, de Broglie's quantum thermostat, and convergence to equilibrium *Entropy* **20** 780

[71] Walleczek J, Grössing G, Pylkkänen P and Hiley B 2019 Emergent quantum mechanics: David Bohm centennial perspectives *Entropy* **21** 113

[72] Volterra V 1913 L'applicazione del calcolo ai fenomeni di eredità *Opere Matematiche* **3** 554–68

[73] Boltzmann L 1874 *Zur Theorie der Elastischen Nachwirkung* (*Wiener Berichte*) vol 70 pp 275–306

[74] Grabec I 2017 Vibration driven random walk in a Chladni experiment *Phys. Lett.* A **381** 59–64

[75] Eddi A, Sultan E, Moukhtar J, Fort E, Rossi M and Couder Y 2011 Information stored in Faraday waves: the origin of a path memory *J. Fluid Mech.* **674** 433–63

[76] Turton S E, Couchman M M P and Bush J W M 2018 A review of the theoretical modeling of walking droplets: toward a generalized pilot-wave framework *Chaos* **28** 096111

[77] de Broglie L 1923 Ondes et quanta *Comptes Rendus* **177** 507–10

[78] de Broglie L 1926 *Ondes et Mouvements* (Paris: Gautier Villars)

[79] de Broglie L 1956 *Une Tentative d'interprétation Causale et Nonlinéaire de la Mécanique Ondulatoire: la Théorie de la Double Solution* (Paris: Gautier-Villars)

[80] de Broglie L 1987 Interpretation of quantum mechanics by the double solution theory *Ann. Fond. Louis Broglie* **12** 1–23

[81] Bohm D 1952 A suggested interpretation of the quantum theory in terms of hidden variables. I *Phys. Rev.* **85** 66–179

[82] Bohm D 1952 A suggested interpretation of the quantum theory in terms of hidden variables. II *Phys. Rev.* **85** 180–93

[83] Nelson E 1966 Derivation of the Schrödinger equation from Newtonian mechanics *Phys. Rev.* **150** 1079–85

[84] Nelson E 1966 Review of stochastic mechanics *J. Phys.: Conf. Ser.* **361** 012011

[85] de la Peña L and Cetto A M 1996 *The Quantum Dice: An Introduction to Stochastic Electrodynamics* (Dordrecht: Kluwer Academic)

[86] de la Peña L, Cetto A M and Valdés-Hernández A 2015 *The Emerging Quantum: The Physics Behind Quantum Mechanics* (Switzerland: Springer)

[87] Borghesi C 2017 Equivalent quantum equations in a system inspired by bouncing droplets experiments *Found. Phys.* **47** 933–58

[88] Dagan Y and Bush J W M 2020 Hydrodynamic quantum field theory: the free particle *C. R. Mec.* (accepted)

[89] Durey M and Bush J W M 2020 Hydrodynamic quantum field theory: the onset of particle motion and the form of the pilot wave *Front. Phys.* **8** 300

[90] Newton I 1704 *Opticks: Or, A Treatise of the Reflections, Refractions, Inflections and Colours of Light* (London: Dover) (https://doi.org/10.5479/sil.302475.39088000644674)

[91] Thomson W 1867 On vortex atoms *London Edinburgh Dublin Philos. Mag. J. Sci* **34** 15–24

[92] Young T 1804 The Bakerian Lecture: experiments and calculations relative to physical optics *Phil. Trans. R. Soc.* **94** 1–16

[93] Berry M V, Chambers R G, Large M D, Upstill C and Walmsley J C 1980 Wavefront dislocations in the Aharonov-Bohm effect and its water wave analogue *Eur. J. Phys.* **1** 154–62

[94] Denardo B C, Puda J J and Larraza A 2009 A water wave analog of the Casimir effect *Am. J. Phys.* **77** 1095–101

[95] Steen P H, Chang C-T and Bostwick J B 2019 Droplet motions fill a periodic table *Proc. Natl Acad. Sci. USA* **116** 4849–54

[96] Dürr D, Goldstein S and Zanghì N 2013 *Quantum Physics Without Quantum Philosophy* (Berlin: Springer)

[97] Bub J 1997 *Interpreting the Quantum World* (Cambridge: Cambridge University Press)

[98] Bricmont J 2017 History of quantum mechanics or the comedy of errors *Int. J. Quant. Found.* **3** 31–64

[99] Bricmont J 2016 *Making Sense of Quantum Mechanics* (Berlin: Springer)

[100] Bassi A and Ghirardi G 2003 Dynamical reduction models *Phys. Rep.* **379** 257–426

[101] Everett H 1957 Relative state formulation of quantum mechanics *Rev. Mod. Phys.* **29** 454–62

[102] Born M 1926 Quantenmechanik der Stoßvorgänge *Z. Phys.* **38** 803–27

[103] Ballentine L E 1970 The statistical interpretation of quantum mechanics *Rev. Mod. Phys.* **42** 358–81

[104] Griffiths R B 1984 Consistent histories and the interpretation of quantum mechanics *J. Stat. Phys.* **36** 219–72

[105] Bell J S 1964 On the Einstein Podolsky Rosen paradox *Physics* **1** 195–200

[106] Aspect A, Grangier P and Roger G 1981 Experimental tests of realistic local theories via Bell's theorem *Phys. Rev. Lett.* **47** 460

[107] Aspect A, Grangier P and Roger G 1982 Experimental realization of Einstein–Podolsky–Rosen–BohmGedanken experiment: a new violation of Bell's inequalities *Phys. Rev. Lett.* **49** 91

[108] Aspect A, Dalibard J and Roger G 1982 Experimental test of Bell's inequalities using time-varying analyzers *Phys. Rev. Lett.* **49** 1804

[109] Zeilinger A 1999 Experiment and the foundations of quantum physics *Rev. Mod. Phys.* **71** S288–97

[110] Bell J S 1987 *Speakable and Unspeakable in Quantum Mechanics* (Cambridge: Cambridge University Press)

[111] Morgan P 2006 Bell inequalities for random fields *J. Phys. A: Math. Gen.* **39** 7441–55

[112] Davies P C W and Brown J R 1993 *The Ghost in the Atom: An Interview with John Bell* (Cambridge: Cambridge University Press)

[113] Madelung E 1926 Quantentheorie in hydrodynamischen form *Z. Phys.* **40** 322–6

[114] Spiegel E A 1980 Fluid dynamical form of the linear and nonlinear Schrödinger equations *Phys.* D **1** 236–40

[115] Bühler O 2010 Wave-vortex interactions in fluids and superfluids *Annu. Rev. Fluid Mech.* **42** 205–28

[116] Pitaevskii L and Stringari S 2003 *Bose–Einstein Condensation* (Oxford: Oxford University Press)

[117] Couder Y and Fort E 2012 Probabilities and trajectories in a classical wave–particle duality *J. Phys.: Conf. Ser.* **361** 012001

[118] Myrvold W C 2003 On some early objections to Bohm's theory *Int. Stud. Philos. Sci.* **17** 7–24

[119] Bohm D and Vigier J P 1954 Model of the causal interpretation of quantum theory in terms of a fluid with irregular fluctuations *Phys. Rev.* **96** 208–16

[120] Philippidis C, Dewdney C and Hiley B J 1979 Quantum interference and the quantum potential *Nuovo Cimento* B **52** 15–28

[121] Kocsis S, Braverman B, Ravets S, Stevens M J, Mirin R P, Shalm L K and Steinberg A M 2011 Observing the average trajectories of single photons in a two-slit interferometer *Science* **332** 1170–3

[122] Yu S, Piao X and Park N 2018 Bohmian photonics for independent control of the phase and amplitude of waves *Phys. Rev. Lett.* **120** 193902

[123] Sanz Á 2018 Atom-diffraction from surfaces with defects: a Fermatian, Newtonian and Bohmian joint view *Entropy* **20** 451

[124] Larder B, Gericke D O, Richardson S, Mabey P, White T G and Gregori G 2018 Fast nonadiabatic dynamics of many-body quantum systems *Sci. Adv.* **5** eaaw1634

[125] Holland P R 1993 *The Quantum Theory of Motion: An Account of the de Broglie–Bohm Causal Interpretation of Quantum Mechanics* (Cambridge: Cambridge University Press)

[126] Dürr D and Teufel S 2009 *Bohmian Mechanics: The Physics and Mathematics of Quantum Theory* (Berlin: Springer)

[127] Oriols X and Mompart J 2019 *Applied Bohmian Mechanics: From Nanoscale Systems to Cosmology* (Singapore: Jenny Stanford Publishing)

[128] Nassar A B and Miret-Artés S 2017 *Bohmian Mechanics, Open Quantum Systems and Continuous Measurements* (Berlin: Springer)

[129] de Broglie L 1930 *An Introduction to the Study of Wave Mechanics* (London: Methuen Co)

[130] de Broglie L 1970 The reinterpretation of wave mechanics *Found. Phys.* **1** 5–15

[131] Davisson C and Germer L H 1927 The scattering of electrons by a single crystal of nickel *Nature* **119** 558–60

[132] Davisson C J and Germer L H 1928 Reflection of electrons by a crystal of nickel *Proc. Natl Acad. Sci.* **14** 317–22

[133] Wilczek F 2010 *The Lightness of Being: Mass, Ether, and the Unification of Forces* (New York: Basic Books)

[134] de Broglie L 1924 Recherches sur la théorie des quanta *PhD Thesis* Migration—université en cours d'affectation

[135] de Broglie L 1927 La mécanique ondulatoire et la structure atomique de la matière et du rayonnement *J. Phys. Radium* **8** 225–41

[136] Chebotarev L 2000 Introduction: the de Broglie–Bohm–Vigier approach in quantum mechanics *Jean-Pierre Vigier and the Stochastic Interpretation of Quantum Mechanics* ed S Jeffers, B Lehnert, N Abramson and L Chebotarev (Montreal: Apeiron) pp 1–18

[137] Bacchiagaluppi G and Valentini A 2009 *Quantum Theory at the Crossroads: Reconsidering the 1927 Solvay Conf.* (Cambridge: Cambridge University Press)

[138] de Broglie L 1969 Sur l'interprétation des relations d'incertitude *C. R. Acad. Sci.* **268** 277

[139] Kragh H 2019 Equation with the many fathers. the Klein–Gordon equation in 1926 *Am. J. Phys.* **52** 1024–33

[140] Gilder L 2009 *The Age of Entanglement: When Quantum Physics was Reborn* 1st edn (New York: Vintage Book)

[141] Milonni P W 1994 *The Quantum Vacuum: An Introduction to Quantum Electrodynamics* (New York: Academic)

[142] Sakurai J J and Napolitano J 2011 *Modern Quantum Mechanics* 2nd edn (Cambridge: Cambridge University Press)

[143] Schrödinger E 1930 About the force-free motion in relativistic quantum mechanics *Session Phys. Math.* **24** 418

[144] Burinskii A 2008 The Dirac–Kerr–Newman electron *Gravit. Cosmol.* **14** 109–22

[145] Hestenes D 1990 The Zitterbewegung interpretation of quantum mechanics *Found. Phys.* **20** 1213–32

[146] Qui C, Hamner C, Gong M, Zhang C and Engels P 2013 Observation of Zitterbewegung in a spin–orbit-coupled Bose–Einstein condensate *Phys. Rev.* A **88** 021604

[147] Gerritsma R, Kirchmair G, Zähringer F, Solano E, Blatt R and Roos C F 2010 Quantum simulation of the Dirac equation *Nature* **463** 68

[148] Boyer T H 2011 Any classical description of nature requires classical electromagnetic zero-point radiation *Am. J. Phys.* **79** 1163–7

[149] Boyer T H 2018 Stochastic electrodynamics: the closest classical approximation to quantum theory *Atoms* **7** 29

[150] Cole D C and Zou Y 2003 Quantum mechanical ground state of hydrogen obtained from classical electrodynamics *Phys. Lett.* A **317** 14–20

[151] Avendaño J and de la Peña L 2005 Reordering of the ridge patterns of a stochastic electromagnetic field by diffraction due to an ideal slit *Phys. Rev.* E **72** 066605

[152] Avendaño J and de la Peña L 2010 Matter diffraction through a double slit obtained by numerical simulation using a diffracted random electromagnetic field *Phys.* E **42** 313–6

[153] Nieuwenhuizen T M and Liska M T P 2015 Simulation of the hydrogen ground state in stochastic electrodynamics *Phys. Scr.* **T165** 014006

[154] Huang W and Batelaan H 2019 Testing quantum coherence in stochastic electrodynamics with Squeezed Schrödinger cat states *Atoms* **7** 42

[155] de la Peña L, Cetto A M and Valdés-Hernández A 2020 Connecting two stochastic theories that lead to quantum mechanics *Front. Phys.* **8** 162

[156] Moláček J and Bush J W M 2013 Drops walking on a vibrating bath: towards a hydrodynamic pilot-wave theory *J. Fluid Mech.* **727** 612–47

[157] Tambasco L D, Pilgram J J and Bush J W M 2018 Bouncing droplet dynamics above the Faraday threshold *Chaos* **28** 096107

[158] Harris D M and Bush J W M 2013 The pilot-wave dynamics of walking droplets *Phys. Fluids* **25** 091112

[159] Brun P-T, Harris D M, Prost V, Quintela J and Bush J W M 2016 Shedding light on pilot-wave phenomena *Phys. Rev. Fluids* **1** 050510

[160] Sleutel P, Dietrich E, Van der Veen J T and Van Joolingen W R 2016 Bouncing droplets: a classroom experiment to visualize wave–particle duality on the macroscopic level *Eur. J. Phys.* **37** 055706

[161] Harris D M, Quintela J, Prost V, Brun P-T and Bush J W M 2017 Visualization of hydrodynamic pilot-wave phenomena *J. Vis.* **20** 13–5

[162] Couder Y, Fort E, Gautier C-H and Boudaoud A 2005 From bouncing to floating: noncoalescence of drops on a fluid bath *Phys. Rev. Lett.* **94** 177801

[163] Goldman D I 2014 Pattern formation and fluidization in vibrated granular layers, and grain dynamics and jamming in a water fluidized bed *PhD Thesis* University of Texas, Austin

[164] Harris D M and Bush J W M 2015 Generating uniaxial vibration with an electrodynamic shaker and external air bearing *J. Sound Vib.* **334** 255–69

[165] Harris D M, Liu T and Bush J W M 2015 A low-cost, precise piezoelectric droplet-on-demand generator *Exp. Fluids* **56** 83

[166] Gilet T, Mulleners K, Lecomte J P, Vandewalle N and Dorbolo S 2007 Critical parameters for the partial coalescence of a droplet *Phys. Rev.* E **75** 36303

[167] Moláček J and Bush J W M 2013 Droplets bouncing on a vibrating fluid bath *J. Fluid Mech.* **727** 582–611

[168] Wind-Willassen Ø, Moláček J, Harris D M and Bush J W M 2013 Exotic states of bouncing and walking droplets *Phys. Fluids* **25** 082002

[169] Terwagne D 2011 Bouncing droplets, the role of deformations *PhD Thesis* Université de Liège

[170] Yang J C, Chien W, King M and Grosshandler W L 1997 A simple piezoelectric droplet generator *Exp. Fluids* **23** 445–7

[171] Ionkin N and Harris D M 2018 Note: a versatile 3D-printed droplet-on-demand generator *Rev. Sci. Instrum.* **89** 116103

[172] Harris D M, Brun P-T, Damiano A, Faria L and Bush J W M 2018 The interaction of a walking droplet and a submerged pillar: from scattering to the logarithmic spiral *Chaos* **28** 096106

[173] Faraday M 1831 On the forms and states of fluids on vibrating elastic surfaces *Phil. Trans. R. Soc.* **121** 319–40

[174] Miles J and Henderson D 1990 Parametrically forced surface waves *Annu. Rev. Fluid Mech.* **22** 143–65

[175] Douady S 1990 Experimental study of the Faraday instability *J. Fluid Mech.* **221** 383–409

[176] Edwards W S and Fauve S 1994 Patterns and quasi-patterns in the Faraday experiment *J. Fluid Mech.* **278** 123–48

[177] Stöckmann H-J 1999 *Quantum Chaos: An Introduction* (Cambridge: Cambridge University Press)

[178] Edwards W S and Fauve S 1992 Parametrically excited quasicrystalline surface waves *Phys. Rev.* E **47** R788–91

[179] Blümel R, Davidson I H, Reinhardt W P, Lin H and Sharnoff M 1992 Quasilinear ridge structures in water surface waves *Phys. Rev.* A **45** 2641

[180] Kudrolli A, Abraham M C and Gollub J P 2001 Scarred patterns in surface waves *Phys. Rev.* E **63** 026208

[181] Heller E J 1930 Bound-state eigenfunctions of classically chaotic Hamiltonian systems: scars of periodic orbits *Phys. Rev. Lett.* **53** 1515

[182] Goodridge C L, Hentschel H G E and Lathrop D P 1999 Breaking Faraday waves: critical slowing of droplet ejection rates *Phys. Rev. Lett.* **82** 3062

[183] Puthenveettil B A and Hopfinger E J 2009 Evolution and breaking of parametrically forced capillary waves in a circular cylinder *J. Fluid Mech.* **633** 355–79

[184] Rayleigh L 1879 On the capillary phenomenon of jets *Proc. R. Soc.* **29** 71–97

[185] Okumura K, Chevy F, Richard D, Quéré D and Clanet C 2003 Water spring: a model for bouncing drops *Europhys. Lett.* **62** 237

[186] Walker J 1978 The amateur scientist *Sci. Am.* **238** 151–8

[187] Terwagne D, Vandewalle N and Dorbolo S 2007 Lifetime of a bouncing droplet *Phys. Rev.* E **76** 056311

[188] Terwagne D, Gilet T, Vandewalle N and Dorbolo S 2009 Metastable bouncing droplets *Phys. Fluids* **21** 054103

[189] Gilet T, Vandewalle N and Dorbolo S 2007 Controlling the partial coalescence of a droplet on a vertically vibrated bath *Phys. Rev.* E **76** 35302

[190] Gilet T, Terwagne D, Vandewalle N and Dorbolo S 2008 Dynamics of a bouncing droplet onto a vertically vibrated interface *Phys. Rev. Lett.* **100** 167802

[191] Dorbolo S, Terwagne D, Vandewalle N and Gilet T 2008 Resonant and rolling droplet *New J. Phys.* **10** 113021

[192] Gilet T and Bush J W M 2009 The fluid trampoline: droplets bouncing on a soap film *J. Fluid Mech.* **625** 167–203

[193] Galeano-Rios C A, Milewski P A and Vanden-Broeck J-M 2019 Quasi-normal free-surface impacts, capillary rebounds and application to Faraday walkers *J. Fluid Mech.* **873** 856–88

[194] Damiano A P 2015 Surface topography measurements of the bouncing droplet experiment *Master's Thesis* École Polytechnique Fédérale de Lausanne (https://doi.org/10.1007/s00348-016-2251-4)

[195] Galeano-Rios C A, Milewski P A and Vanden-Broeck J-M 2017 Non-wetting impact of a sphere onto a bath and its application to bouncing droplets *J. Fluid Mech.* **826** 97–127

[196] Labousse M 2014 Étude d'une dynamique à mémoire de chemin: une expérimentation théorique *PhD Thesis* Université Pierre et Marie Curie UPMC Paris VI

[197] Hubert M, Filoux B, Caps H, Dorbolo S and Vandewalle N 2015 Resonant and antiresonant bouncing droplets *Phys. Rev.* E **91** 023017

[198] Zhao X, Tang J and Liu J 2018 Electrically switchable surface waves and bouncing droplets excited on a liquid metal bath *Phys. Rev. Fluids* **3** 124804

[199] Perrard S, Fort E and Couder Y 2016 Wave-based Turing machine: time reversal and information erasing *Phys. Rev. Lett.* **117** 094502

[200] Sampara N and Gilet T 2016 Two-frequency forcing of droplet rebounds on a liquid bath *Phys. Rev.* E **94** 053112

[201] Valani R, Slim A C and Simula T 2019 Superwalking droplets *Phys. Rev. Lett.* **123** 024503

[202] Moisy F, Rabaud M and Salsac K 2009 A synthetic Schlieren method for the measurement of the topography of a liquid interface *Exp. Fluids* **46** 1021–36

[203] Pucci G, Sáenz P J, Faria L M and Bush J W M 2016 Non-specular reflection of walking droplets *J. Fluid Mech.* **804** R3

[204] Damiano A P, Brun P-T, Harris D M, Galeano-Rios C A and Bush J W M 2016 Surface topography measurements of the bouncing droplet experiment *Exp. Fluids* **57** 163

[205] Oza A U, Rosales R R and Bush J W M 2013 A trajectory equation for walking droplets: hydrodynamic pilot-wave theory *J. Fluid Mech.* **737** 552–70

[206] Chu H-Y and Fei H-T 2019 Asymmetric vortexes induced traveling drop on an oscillatory liquid bath *Phys. Fluids* **31** 102102

[207] Durey M, Milewski P A and Wang Z 2020 Faraday pilot-wave dynamics in a circular corral *J. Fluid Mech.* **891** A3

[208] Cristea-Platon T 2017 On the dynamics of bouncing droplets in confined geometries *Master's Thesis* Massachusetts Institute of Technology

[209] Blanchette F 2016 Modeling the vertical motion of drops bouncing on a bounded fluid reservoir *Phys. Fluids* **28** 032104

[210] Benjamin T B and Ursell F 1954 The stability of the plane free surface of a liquid in vertical periodic motion *Proc. R. Soc.* A **225** 505–15

[211] Kumar K and Tuckerman L S 1994 Parametric instability of the interface between two fluids *J. Fluid Mech.* **279** 49–68

[212] Kumar K 1996 Linear theory of Faraday instability in viscous liquids *Proc. R. Soc.* A **452** 1113–26

[213] Müller H W, Wittmer H, Wagner C, Albers J and Knorr K 1997 Analytic stability theory for Faraday waves and the observation of the harmonic surface response *Phys. Rev. Lett.* **78** 2357–60

[214] Gilet T and Bush J W M 2009 Chaotic bouncing of a drop on a soap film *Phys. Rev. Lett.* **102** 014501

[215] Bacot V, Perrard S, Labousse M, Couder Y and Fort E 2019 Multistable free states of an active particle from a coherent memory dynamics *Phys. Rev. Lett.* **122** 104303

[216] Hubert M, Labousse M, Perrard S, Labousse M, Vandewalle N and Couder Y 2019 Tunable bimodal explorations of space from memory-driven deterministic dynamics *Phys. Rev.* E **100** 032201

[217] Tadrist L, Shim J-B, Gilet T and Schlagheck P 2018 Faraday instability and subthreshold Faraday waves: surface waves emitted by walkers *J. Fluid Mech.* **848** 906–45

[218] Terwagne D, Ludewig F, Vandewalle N and Dorbolo S 2013 The role of the droplet deformations in the bouncing droplet dynamics *Phys. Fluids* **25** 122101

[219] Oza A U, Wind-Willassen Ø, Harris D M, Rosales R R and Bush J W M 2014 Pilot-wave hydrodynamics in a rotating frame: exotic orbits *Phys. Fluids* **26** 082101

[220] Labousse M, Oza A U, Perrard S and Bush J W M 2016 Pilot-wave dynamics in a harmonic potential: quantization and stability of circular orbits *Phys. Rev.* E **93** 033122

[221] Tambasco L D, Harris D M, Oza A U, Rosales R R and Bush J W M 2016 The onset of chaos in orbital pilot-wave dynamics *Chaos* **26** 103107

[222] Raphaël E and de Gennes P-G 1996 Capillary gravity waves caused by a moving disturbance: wave resistance *Phys. Rev.* E **53** 3448

[223] Closa F, Chepelianskii A D and Raphaël E 2010 Capillary-gravity waves generated by a sudden object motion *Phys. Fluids* **22** 052107

[224] Chepelianskii A D, Schindler M, Chevy F and Raphaël E 2010 Self-consistent theory of capillary-gravity-wave generation by small moving objects *Phys. Rev.* E **91** 016306

[225] De Corato M and Garbin V 2018 Capillary interactions between dynamically forced particles adsorbed at a planar interface and on a bubble *J. Fluid Mech.* **847** 71–92

[226] Lamb H 1932 *Hydrodynamics* (Cambridge: Cambridge University Press)

[227] Dias F, Dyachenko A I and Zakharov V E 2008 Theory of weakly damped free-surface flows: a new formulation based on potential flow solutions *Phys. Lett.* A **372** 1297–302

[228] Rahman A 2018 Standard map-like models for single and multiple walkers in an annular cavity *Chaos* **28** 096102

[229] Bush J W M, Oza A U and Moláček J 2014 The wave-induced added mass of walking droplets *J. Fluid Mech.* **755** R7

[230] Haisch B and Rueda A 2000 On the relation between a zero-point-field-induced inertial effect and the Einstein–de Broglie formula *Phys. Lett.* A **268** 224–7

[231] Haisch B, Rueda A and Dobyns Y 2001 Inertial mass and the quantum vacuum fields *Ann. Phys., Lpz.* **10** 393–414

[232] Labousse M and Perrard S 2014 Non-Hamiltonian features of a classical pilot-wave dynamics *Phys. Rev.* E **90** 022913

[233] Turton S E 2020 Theoretical modeling of pilot-wave hydrodynamics *PhD Thesis* Massachusetts Institute of Technology

[234] Nachbin A 2018 Walking droplets correlated at a distance *Chaos* **28** 096110

[235] Shirokoff D 2013 Bouncing droplets on a billiard table *Chaos* **23** 013115

[236] Protière S 2007 Gouttes rebondissantes: une association onde-particule à échelle macroscopique *PhD Thesis* Université Paris-Diderot

[237] Filoux B 2017 Walking droplets above cavities *PhD Thesis* Université de Liège

[238] Sukhov S, Shalin A, Haefner D and Dogariu A 2015 Actio et reactio in optical binding *Opt. Express* **23** 247–52

[239] Yifat Y, Coursault D, Peterson C W, Parker J, Bao Y, Gray S K, Rice S A and Scherer N F 2018 Reactive optical matter: light-induced motility in electrodynamically asymmetric nanoscale scatterers *Light Sci. Appl.* **7** 1–7

[240] Couchman M M P and Bush J W M 2020 Free rings of bouncing droplets: stability and dynamics *J. Fluid Mech.* **903** A49

[241] Barnes L, Pucci G and Oza A U 2020 Resonant interactions in bouncing droplet chains *C. R. Mec.* (accepted)

[242] Thomson S J, Durey M and Rosales R R 2020 Collective vibrations of a hydrodynamic active lattice *Proc. R. Soc.* A **476** 20200155

[243] Toda M 1967 Vibration of a chain with nonlinear interaction *J. Phys. Soc. Japan* **22** 431–6

[244] Nachbin A, Couchman M M P and Bush J W M 2016 Nonlocal features of a hydrodynamic pilot-wave system *43rd Annual Meeting of the American Physical Society Division of Fluid Dynamics* http://meetings.aps.org/Meeting/DFD16/Session/L16.5

[245] Acebrón J A, Bonilla L L, Pérez Vicente C J, Ritort F and Spiller R 2005 The Kuramoto model: a simple paradigm for synchronization phenomena *Rev. Mod. Phys.* **77** 137

[246] Ashcroft N W and Mermin N D 1976 *Solid State Physics* (New York: Harcourt) ch 33 pp 704–9

[247] Durey M 2018 Faraday wave-droplet dynamics: a hydrodynamic quantum analogue *PhD Thesis* University of Bath

[248] Perrard S 2014 Une mémoire ondulatoire: etats propres, chaos et probabilités *PhD Thesis* Université Paris Diderot

[249] an der Heiden U 2002 Unfolding complexity: hereditary dynamical system—new bifurcation schemes and high dimensional chaos *Nonlinear Dynamics and Chaos: Where Do We Go From Here?* ed J Hogan, A R Krauskopf, M de Bernado, R E Wilson, H M Osinga, M E Homer and A R Champneys (Bristol: Institute of Physics Publishing) pp 55–72

[250] MacKay R S 2002 Many-body quantum mechanics *Nonlinear Dynamics and Chaos: Where Do We Go from Here?* ed J Hogan, A R Krauskopf, M de Bernado, R E Wilson, H M Osinga, M E Homer and A R Champneys (Bristol: Institute of Physics Publishing) pp 21–54

[251] Strogatz S H 2000 *Nonlinear Dynamics and Chaos: With Applications to Physics, Biology, Chemistry, and Engineering* 1st edn (Boca Raton, FL: CRC Press)

[252] Ruelle D and Takens F 1971 On the nature of turbulence *Commun. Math. Phys.* **20** 167–92

[253] Newhouse S, Ruelle D and Takens F 1978 Occurrence of strange axiom a attractors near quasi periodic flows on T^m: $m \geqslant 3$ *Commun. Math. Phys.* **64** 35–40

[254] Eckmann J-P 1981 Roads to turbulence in dissipative dynamical systems *Rev. Mod. Phys.* **53** 643

[255] Budanur N B and Fleury M 2019 State space geometry of the chaotic pilot-wave hydrodynamics *Chaos* **29** 013122

[256] Rahman A and Blackmore D 2020 Walking droplets through the lens of dynamical systems *Mod. Phys. Lett.* B (accepted)

[257] Gutzwiller M C 1971 Periodic orbits and classical quantization conditions *J. Math. Phys.* **12** 343–58

[258] Cvitanović P, Artuso R, Mainieri R, Tanner G and Vattay G 2016 *Chaos: Classical and Quantum* (Copenhagen: Niels Bohr Institute)

[259] Crommie M F, Lutz C P and Eigler D M 1993 Imaging standing waves in a two-dimensional electron gas *Nature* **363** 524–7

[260] Fiete G A and Heller E J 2003 Coll.: theory of quantum corrals and quantum mirages *Rev. Mod. Phys.* **75** 933–48

[261] Crommie M F, Lutz C P and Eigler D M 1993 Confinement of electrons to quantum corrals on a metal surface *Science* **262** 218–20
[262] Rahman A and Blackmore D 2016 Neimark–Sacker bifurcations and evidence of chaos in a discrete dynamical model of walkers *Chaos Solitons Fractals* **91** 339–49
[263] Rahman A, Joshi Y and Blackmore D 2017 Sigma map dynamics and bifurcations *Regular and Chaotic Dynamics* **22** 740–9
[264] Rahman A and Blackmore D 2020 Interesting bifurcations in walking droplet dynamics *Commun. Nonlinear Sci. Numer. Simulat.* **90** 105348
[265] Moon C R, Lutz C P and Manoharan H C 2008 Single-atom gating of quantum-state superpositions *Nat. Phys.* **4** 454–8
[266] Tambasco L D and Bush J W M 2018 Exploring orbital dynamics and trapping with a generalized pilot-wave framework *Chaos* **28** 096115
[267] Gamow G 1928 The quantum theory of nuclear disintegration *Nature* **122** 805–6
[268] Cohen-Tannoudji C, Diu B and Laloë F 1977 *Quantum Mechanics* (New York: Wiley)
[269] Bragg W H and Bragg W L 1913 The reflexion of x-rays by crystals *Proc. R. Soc. Long.* A **88** 428–38
[270] Talbot H F 1836 LXXVI. Facts relating to optical science. No. IV *Phil. Mag.* **9** 401
[271] Rayleigh. L 1881 XXV. On copying diffraction-gratings, and on some phenomena connected therewith *Phil. Mag.* **11** 196
[272] Jones E, Li A, McGregor S, Bach R and Batelaan H 2012 Oil droplet versus electron double slit diffraction *43rd Annual Meeting of the American Physical Society Division of Atomic, Molecular and Optical Physics* http://meetings.aps.org/link/BAPS.2012.DAMOP.K1.67
[273] Schiebel P E, Rieser J M, Hubbard A M, Chen L, Rocklin D Z and Goldman D I 2019 Mechanical diffraction reveals the role of passive dynamics in a slithering snake *Proc. Natl Acad. Sci.* **116** 4798–803
[274] Friedel J 1954 Electronic structure of primary solid solutions in metals *Adv. Phys.* **3** 446–507
[275] Kanisawa K, Butcher M J, Yamaguchi H and Hirayama Y 2001 Imaging of Friedel oscillation patterns of two-dimensionally accumulated electrons at epitaxially grown InAs(111)A surfaces *Phys. Rev. Lett.* **86** 3384
[276] Durey M, Turton S E and Bush J W M 2020 Speed oscillations in classical pilot-wave dynamics *Proc. R. Soc.* A **476** 20190884
[277] Hong C K, Ou Z Y and Mandel L 1987 Measurement of subpicosecond time intervals between two photons by interference *Phys. Rev. Lett.* **59** 2044
[278] Durey M 2020 Bifurcations and chaos in a Lorenz-like pilot-wave system *Chaos* **30** 103115
[279] Lorenz E N 1963 Deterministic nonperiodic flow *J. Atmos. Sci.* **20** 130–41
[280] Devauchelle O, Lajeunesse E, James F, Josserand C and Lagrée P-Y 2020 Walkers in a wave field with memory *C. R. Mec.* (accepted)
[281] Fort E and Couder Y 2013 Trajectory eigenmodes of an orbiting wave source *Europhys. Lett.* **102** 16005
[282] Messiah A 1958 *Quantum Mechanics* (New York: Dover)
[283] Shinbrot T 2019 Dynamic pilot wave bound states *Chaos* **29** 113124
[284] Drezet A, Jamet P, Bertschy D, Ralko A and Poulain C 2020 Mechanical analog of quantum bradyons and tachyons *Phys. Rev.* E **102** 052206
[285] Holland P R 1995 *The Quantum Theory of Motion: An Account of the de Broglie–Bohm Causal Interpretation of Quantum Mechanics* (Cambridge: Cambridge University Press)
[286] Hammond R T 2010 Relativistic particle motion and radiation reaction in electrodynamics *Electron. J. Theor. Phys.* **7** 221–58
[287] Templin J D 1999 Radiation reaction and runaway solutions in acoustics *Am. J. Phys.* **67** 407
[288] Brillouin M 1919 Actions mécaniques à hérédite discontinue par propagation; essai de théorie dynamique de l'atome à quanta *Comptes-Rendus de l'Académie des Sciences* **168** 1318–20
[289] Vervoort L 2012 The instrumentalist aspects of quantum mechanics stem from probability theory *AIP Conf. Proc.* **1424** 348–53
[290] Feynman R P 1964 *The Feynman Lectures on Physics* (Reading, MA: Addison-Wesley)

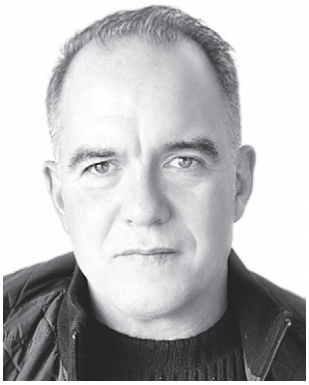

John W M Bush is a Professor of Applied Mathematics in MIT's Department of Mathematics. He received his BSc and MSc degrees in physics from the University of Toronto, his PhD in geophysics from Harvard University. Following postdoctoral research at DAMTP, University of Cambridge, he joined the MIT faculty MIT in 1998. His research concerns the discovery and exploration of physical phenomena arising in either natural or laboratory settings, and their elucidation via the application of mathematics. His work typically has both experimental and theoretical components, and is rooted in MIT's Applied Math Laboratory. He is a fluid mechanician whose research began in geophysics, but then shifted to interfacial flows and their appearance in biology. For the past decade, his research has been focused on hydrodynamic quantum analogs.

Anand U Oza is an Assistant Professor in the Department of Mathematical Sciences at the New Jersey Institute of Technology (NJIT). He received his bachelor's degree from Princeton University, master's degree at DAMTP, University of Cambridge, and PhD in mathematics from MIT. He was an NSF postdoctoral fellow at the Courant Institute, New York University, and then joined the NJIT faculty in 2017. His research is concerned with physical applied mathematics, with a focus on fluid mechanics and soft matter physics. His work uses a combination of mathematical modeling, asymptotic analysis, and numerical simulation, and is typically motivated by laboratory experiments.